# CHARACTERIZATION OF THERMO-MECHANICAL AND LONG-TERM BEHAVIORS OF MULTI-LAYERED COMPOSITE MATERIALS

A Thesis

by

ARAVIND R. NAIR

Submitted to the Office of Graduate Studies of
Texas A&M University
in partial fulfillment of the requirements for the degree of

MASTER OF SCIENCE

August 2006

Major Subject: Mechanical Engineering

# CHARACTERIZATION OF THERMO-MECHANICAL AND LONG-TERM BEHAVIORS OF MULTI-LAYERED COMPOSITE MATERIALS

A Thesis

by

ARAVIND R. NAIR

Submitted to the Office of Graduate Studies of
Texas A&M University
in partial fulfillment of the requirements for the degree of

MASTER OF SCIENCE

Approved by:

Chair of Committee, Anastasia Muliana
Committee Members, Harry Hogan
Eyad Masad
Head of Department, Dennis L. O'Neal

August 2006

Major Subject: Mechanical Engineering

# ABSTRACT

Characterization of Thermo-mechanical and Long-term Behaviors of
Multi-layered Composite Materials. (August 2006)
Aravind R. Nair, B.E, University of Madras, India
Chair of Advisory Committee: Dr. Anastasia Muliana

This study presents characterization of thermo-mechanical viscoelastic and long-term behaviors of thick-section multi-layered fiber reinforced polymer composite materials. The studied multi-layered systems belong to a class of thermo-rheologically complex materials, in which both stress and temperature affect the time-dependent material response. The multi-layered composites consist of alternating layers of unidirectional fiber (roving) and randomly oriented continuous filament mat. Isothermal creep-recovery tests at various stresses and temperatures are performed on E-glass/vinylester and E-glass/polyester off-axis specimens. Analytical representation of a nonlinear single integral equation is applied to model the thermo-mechanical viscoelastic responses for each off-axis specimen. Long-term material behaviors are then obtained through vertical and horizontal time shifting using analytical and graphical shifting procedures. Linear extrapolation of transient creep compliance is used to extend the material responses for longer times. The extended long-term creep strains of the uniaxial E-glass/vinylester specimens are verified with the long-term experimental data of Scott and Zureick (1998). A sensitivity analyses is then conducted to examine the impact of error in material parameter characterizations to the overall long-term material behaviors. Finally, the calibrated long-term material parameters are used to study the long-term behavior of multi-layered composite structures. For this purpose, an integrated micromechanical material and finite element structural analyses is employed. Previously developed viscoelastic micromodels of multi-layered composites are used to generate the effective nonlinear viscoelastic responses of the studied composite systems and then implemented as a material subroutine in Abaqus finite element code. Several long-term composite structures are analyzed, that is; I-shaped columns and flat panels under axial

compression, and a sandwich beam under the point bending and transmission tower under lateral forces. It is shown that the integrated micromechanical-finite element model is capable of predicting the long-term behavior of the multilayered composite structures.

# ACKNOWLEDGMENTS

I am grateful to my mentor and committee chair, Dr. Anastasia Muliana, for her continuous guidance and encouragement through out this project. Her support means a great deal to me. I would like to extend my gratitude to Dr. Harry Hogan and Dr. Eyad Masad for their helpful comments on the work.

I would also like to acknowledge Mr. Inmon Rodney, Department of Aerospace Engineering for providing me with insights on the various aspects of creep testing and to Mr. Jeffrey Perry, Department of Civil Engineering for providing the facility for testing.

# TABLE OF CONTENTS

CHAPTER Page

# LIST OF FIGURES

FIGURE Page

FIGURE Page

FIGURE Page

# LIST OF TABLES

TABLE Page

# CHAPTER I
# INTRODUCTION

Fiber reinforced polymer (FRP) composite materials are widely used in current structural applications such as transmission towers, structural components for off-shore drilling platform, aircrafts, bridges, fluid conveying pipes and many others. These applications require to use thin and thick-section multi-layered composite systems. The multi-layered composites combine different forms of reinforcements such as unidirectional fiber, randomly oriented filament, woven fabric, or braided preforms made of the same or different materials. The combined reinforcements are often repeated through the cross-sectional thickness and embedded in a matrix system. Matrix systems are commonly made of vinylester or polyester resin with additive materials such as glass microsphere and clay particles, while fibers are often made of carbon or glass. The multi-layered FRP systems exhibit pronounced time dependent behaviors due to the flow of soft polymeric matrix. Elevated temperatures and moisture contents intensify the deformation and deterioration of the internal microstructures that lead to material failure. The low fiber volume fraction in the FRP multi-layered composites strengthens their viscoelastic responses. However, the effects of combined time-stress-temperature-moisture on the overall performance of FRP multi-layered systems have not been sufficiently investigated and accounted for. In addition, their long-term behaviors under thermo-hygro-mechanical loadings have not been fully explored.

This chapter presents a literature review of analytical, numerical, and experimental works on thermo-viscoelastic behaviors of FRP composites. The objectives and outlines of the present study will be described.

---

This thesis follows the style of Composite Science and Technology.

## 1.1 CURRENT WORKS IN THERMO-VISCOELASTIC BEHAVIORS OF COMPOSITE MATERIALS AND STRUCTURES

### 1.1.1 Analytical and numerical studies on thermo-viscoelastic behaviors of composite materials

Analytical and numerical modeling approaches on the thermo-mechanical viscoelastic behaviors have been developed mainly on laminated FRP composites having unidirectional fiber reinforcements. Although composite systems exhibit material and geometric heterogeneities, to avoid complexity in characterizing their mechanical properties, composite systems are often modeled as anisotropic homogeneous media. Schapery [1] derived effective anisotropic viscoelastic modulus and thermal expansion coefficient of laminated composites having unidirectional fiber reinforcements based on each constituent property. The correspondence principle was used to formulate the effective viscoelastic moduli from the elastic constitutive properties. The inverse transforms from the Laplace domain is solved using two approximation methods namely collocation and direct methods. Another method of analysis, the quasi static method, was also discussed, where a viscoelastic solution was approximated from an elastic solution with the elastic constants being replaced by time-dependent relaxation moduli. Tuttle et al. [2] and Pasricha et al. [3] used the classical laminated theory (CLT) with combined nonlinear viscoelastic, viscoplastic, and thermal effects to analyze laminated plates subjected to a repeated number of creep-recovery intervals at different temperatures and stress levels. Prony series was used to model linear creep compliance. The combined CLT with viscoelastic/viscoplastic constitutive models predicted creep responses of different laminates with various stacking sequences. The ability of the model to make long term prediction for cyclic thermo-mechanical model was considered. It is noted that reasonable agreements between measured and predicted strains were obtained for all laminates for the six months testing period. Taouti and Cederbaum [4] presented a numerical scheme for stress-relaxation analysis of orthotropic laminated plates. The Schapery nonlinear viscoelastic model was used. Their method transformed the

nonlinear convolution integral into a system of first-order differential equations. The stress relaxation for a given strain level is obtained by solving these equations. Yi et al. [5-7] used a strain-based Schapery integral relation and developed a FE integration procedure to analyze nonlinear viscoelastic response in laminated composites subjected to mechanical and hygrothermal loading. Different nonlinear viscoelastic problems in laminated composites were solved using this FE method, such as interlaminar stress, bending and twisting of laminated composites.

### 1.1.2 Thermo-mechanical viscoelastic experimental works on FRP composites

Experimental studies have been conducted to characterize nonlinear thermo-mechanical viscoelastic behaviors of laminated composite materials with unidirectional fiber reinforcements. Creep-recovery tests under various temperatures (at isothermal condition) and stresses are performed. Mohan and Adams [8] conducted one-hour creep followed by one-hour recovery tests under tensile and compression loadings for neat epoxy resin, graphite/epoxy amnd glass/epoxy materials. The tests were carried out at various temperatures ranging from 20 to 125°C and relative humidity of 55, 57 and 100%. The Schapery integral model was applied for the creep-recovery behaviors. It was shown that temperature and moisture content affected the nonlinear viscoelastic parameters in the Schapery equation. Sternstein et al. [9] conducted three point bending stress relaxation tests for 10,000 seconds and recovery tests of 30,000 seconds on polysulphone neat resin and T300/polysulphone laminates. Viscoelastic behaviors of neat resins, which depend on the magnitude of stress and temperature, were less pronounced than that of the laminated composites. This was due to the existence of void and fiber-matrix shearing that may accelerate the relaxation in composite systems. Greenwood [10], performed four point creep bending test for 5000 hours to determine the time-dependent behaviors of carbon fiber reinforced resin plastic (CFRP) composite at 180°, 190° and 200°C and at stress levels of 53% and 67% of the ultimate strength. It was observed that at the end of the test, the outer fiber creep strains in the central section of the laminated specimens, increased by 20% of the initial elastic strain. It was noted

that the boundary between the lamination plates, which is the resin rich area, significantly influenced creep deformations. The soft resin led to crack formation along the interlaminar components. Howard and Holloway [11] conducted 300-700 hour creep and 1000 hour recovery tests on FRP composites under different stress levels ranging from 10 to 40% of the ultimate composite strength. The studied FRP system consisted of randomly oriented glass fiber and polyester matrix. The stress-dependent nonlinear viscoelastic parameters in Schapery equation were adequately calibrated from the creep and recovery tests. Katouzian et al. [12] performed 10 hours creep tests on neat epoxy resin (thermoset), PEEK polymer (thermoplastic), carbon/PEEK and carbon/epoxy composites under several stress levels at different temperatures: 23$^{o}$C, 100$^{o}$C and 140$^{o}$C. Schapery's single integral constitutive equation was used to characterize the nonlinear parameters. They mentioned that the nonlinear viscoelastic responses were more pronounced by increasing the temperature for both polymers and $[45_4]_s$ laminated systems. While for $[90_4]_s$ laminates, the linear viscoelastic responses were exhibited. Violette and Schapery [13] studied time and temperature behaviors of unidirectional carbon/epoxy composites under compression. The specimens were tested at different temperatures: 24$^{o}$C, 50$^{o}$C, and 60$^{o}$C and constant loading rates. Two constitutive models were used to characterize the elastic and viscoelastic material properties. The first model was a homogenized orthotropic plane stress. The second model consisted of alternating fiber and matrix layers. It was shown that the relationship between failure stress and time followed a power law function. Jain et al. [14] studied the environmental effects on creep behaviors of glass/polyester FRP laminated plates. The FRP laminates were tested at various temperatures and humidity under creep bending load ranging from 7 to 35% of the plate short term flexural strength. The creep tests were performed for 2 years. Linear creep behaviors were exhibited in all tested laminates up to 10,000 hours. A sudden increase in deformation was shown beyond 10,000 hours. This is due to abruptly changes in temperature and humidity under seasonal change from winter to summer.

### 1.1.3 Accelerated methods for long term material predictions

Accelerated creep tests at several elevated temperatures have been conducted and used to create a master curve for predicting long-term behaviors of laminated composites. A time-shifting method has been developed to create the master curve from a series of short-term creep tests at elevated temperatures. This method is known as the time temperature superposition principle (TTSP). For a class of thermo-rheologically simple materials (TSM), horizontal shifting in logarithmic time scale is sufficient to create a smooth master curve that represents a long term response, while for a class of thermo-rheologically complex materials (TCM), vertical shifting is necessary prior to the horizontal shifting in order to create a master curve (Griffith et al., [15]; Tuttle, [16]; Yen and Williamson, [17]). Schwarzl and Staverman [18] formulated the conditions that must be satisfied to allow a change of temperature by a shift in the time scale and hence to be classified as a TSM. According to the authors, for a TSM, a necessary, but not sufficient condition that an arbitrary function of temperature, determined experimentally, must exist such that it decouples the time and temperature dependence of the material. Another condition that the temperature dependence of the viscous flow of the material should be identical to that of the time-dependent behavior must also be satisfied by a material to be placed under TSM. Brinson et al. [19] and Yeow et al. [20] determined the long-term (25 hours) compliances of unidirectional T300/934 graphite/epoxy materials using time-temperature superposition principle (TTSP). Short-term (15 minutes) tension creep tests were conducted for various laminates: $[10]_{8s}$, $[30]_{8s}$, $[60]_{8s}$, and $[90]_{8s}$ under temperature ranges: 20-210$^{o}$C. It was established that the same specimen could be used repeatedly. Thus, it was not necessary to perform mechanical conditioning prior to creep tests. It was also noted that the time shift factors used to create the master curve was independent of the fiber orientation. Creep tests for 25 hour period were conducted to verify the long-term responses created using the TTSP. Hiel et al. [21] employed Schapery's [22] nonlinear viscoelastic integral to study viscoelastic behavior of a T300/934 graphite/epoxy composite calibrated from short-term (100 minutes) creep tests. Two independent nonlinear integral relations were calibrated from tests for the

transverse and axial shear modes. A master curve was generated using a time-shift method in both stress and temperature scales to create long-term material responses (five days).

Tuttle and Brinson [23] coupled the Schapery's nonlinear viscoelastic model with the CLT to analyze nonlinear viscoelastic behaviors of graphite-epoxy laminates under in-plane loading. Time-temperature-stress-superposition principle (TTSSP) was used to create long-term material properties. Two different laminates $[-80/-50/40/-80]_s$ and $[20/50/-40/20]_s$ lay-ups were also tested for 69.4 days. Good long-term predictions were shown in both layups. Yen and Williamson [17] used the Findley's power law to characterize three-hour creep responses on SMC-C50 composites containing 50% glass fibers in a polyester matrix system, at various temperatures and stress levels up to 90% of the ultimate failure strength. Two master curves were then created using the time-stress-superposition principle (TSSP) and the TTSSP with reference conditions at temperature $23^oC$ and stress 10.8MPa. Vertical and horizontal shifting was performed in the TSSP and TTSSP. The instantaneous creep strain was stress-dependent and the transient creep strain was stress and temperature dependent. The TSSP and TTSSP predicted the long-term responses up to 57 and 400 days, respectively. Brinson and Dillard [24] and Brinson [25] utilized power law model (Findley et al., [26]) and the Schapery's nonlinear single integral equation to characterize long term viscoelastic properties of T300/900 graphite/epoxy materials. Ten minutes creep followed by 100 minute recovery tests were done on off-axis specimens. The TTSP was used to create long-term material responses. Good predictions were shown for $10^4$ to $10^5$ minute creep tests. Detailed studies of long-term behaviors and time-dependent failure in FRP laminated composites can be found in Brinson [27].

### 1.1.4 Viscoelastic behaviors of thick section multi-layered FRP composite systems

A relatively limited number of studies have been conducted on the viscoelastic behavior of multi-layered composites that consists of two or more different types of reinforcements. Most of the current works has been focused on testing and/or calibrating the uniaxial nonlinear viscoelastic response. Spence [28] performed tests on unidirectional glass/epoxy multi-layered specimens under compression creep for 840 hours at room temperature. The time-dependent effect was negligible for applied loads below 30% of the compressive strength. Bank and Mossalam [29] conducted long-term creep (10,000 hours) under load of 25% of the ultimate strength and short-term failure tests for E-glass/vinylester thick-section frame structures with continuous filament mat (CFM) and unidirectional (roving) layers. The frame showed nonlinear behavior at high load levels, and progressive damage occurred while increasing the load up to ultimate failure at 25 kips. Mottram [30] conducted 24 hour creep tests on an assembled multi-layered FRP beam under three point bending. The assembled FRP beam consisted of two I-shaped structural members between outer flat sheet plates, bonded with epoxy adhesive. Findley's power law model was used to characterize the creep behaviors and estimate the increase in beams mid-span deflections at longer time. It was predicted that the mid span deflections of the assembled beam increase by 20%, 60% and 100% of their initial elastic deformations in 1 week, 1 year and 10 year periods, respectively. McClure and Mohammadi [31] performed long-term creep (2500 hours) tests on FRP multilayered composites of angle sections and stubs under load of 45% of the specimen ultimate strength and initial buckling load respectively. The FRP systems consist of E-glass roving and CFM reinforcements in polyester resin. The creep stress level for the coupons corresponds to 3.3 times that used for the angle stubs. The time dependent model followed the Boltzmann superposition principle, with Findley's power law used for the compliance were used to predict the long-term behaviors. The Findley's power law was used to describe the creep behavior of a material at different stress levels. It was shown that the creep predictions using the material parameters calibrated from the coupon tests were comparable to the ones obtained using the material parameters

determined from the angle stub tests. The authors have concluded that it was not necessary to perform creep tests separately on full sized members. Scott and Zureick [32] conducted compression creep tests on a FRP material consisting of vinylester matrix reinforced with E-glass roving and CFM. The specimens were cut from the flanges and web of an I-shaped pultruded beam. Long term creep compression tests for duration of 6,000-12,000 hours were performed under three load levels of 20, 40, and 60% of the average ultimate stress (compressive). Findley's power law was used to model the overall time dependent behavior. It was noted that the Findley model was valid only if the material undergoes primary creep deformation, in which strain rate decreases with time.

Choi and Yuan [33] performed creep tests for 2500 hour duration on box type and wide flange thick-section FRP columns under fixed environmental conditions of 71°F and 50% moisture content and several stress levels of 20, 30, 40 and 50% of the material's ultimate strength. The tested column consisted of glass fibers in polyester resin. It was shown that at 2500 hours, the creep strains for box and wide flange columns have increased by 9.82 and 10.8%, respectively, from their initial elastic strain. Findley's power law model was used to estimate the creep strain from 1000 hours of experimental data. The measured and estimated values of total creep strains for both the box and wide flange columns under various load levels varied from 3 to 10% over the entire testing period. Shao and Shanmugam [34] determined the creep deformations of thick section composite panels made of E-glass rovings and CFM in an isophthalic polyester matrix. These panels were subjected to equally spaced three point bending under 25% and 50% of the maximum strength for 1 year. Findley's power law model was used for time dependent tensile and shear moduli. The panels were modeled based on Timoshenko's beam theory. The authors noted that the power exponent 'n' in the Findley model for creep tensile strain, shear strain and mid-span deflection were comparable. The creep deflection of the panels agreed well with the experimental values.

Haj-Ali and Muliana [35] and Muliana and Haj-Ali [36] conducted short-term (1 hour) creep tests on E-glass/vinylester thick-section multi-layered systems reinforced

with roving and CFM. The tests were done at fixed environmental conditions on several off-axis specimens and notched plates, in which the orientation for the roving layers was controlled. Nonlinear viscoelastic behaviors were shown for off-axis specimens under high load levels, while the uniaxial and transverse specimens showed linear viscoelastic responses. Hierarchical micromechanical models for the roving and CFM with the Schapery's nonlinear viscoelastic behaviors for the matrix were developed to model the effective nonlinear time-dependent responses and were verified with the short-term creep data.

### 1.1.5 Thermo-viscoelastic micromechanical models of layered FRP composite systems

Detailed numerical/analytical micromechanical models, which are derived based on properties, microstructure arrangement, and volume fraction of the phases, have been used to analyze linear and nonlinear time-dependent responses of FRP composites under thermo-mechanical loadings. Most of current works focus on FRP composites having single reinforcement systems. Fibers are assumed to be linear elastic and polymeric matrix is modeled either as thermo-rheologically simple materials (TSM) or thermo-rheologically complex materials (TCM). The advantage of using micromechanical models is it allows for modeling isotropic time-stess-temperature dependent materials for the in-situ polymer matrix. This can significantly reduce number of material parameters, while representing global anisotropic behaviors. Hashin et al. [37] analyzed thermoviscoelastic behaviors of unidirectional fiber composites having elastic fiber and TCM matrix system. Micromechanical models using concentric cylinder assembly (CCA) and hexagonal periodic array were used to characterize in-plane (axial, transverse, axial-shear mode) and out-of-plane (transverse shear) thermoviscoelastic properties, respectively. It is assumed that the time-temperature variations were distributed uniformly throughout the fiber/matrix phases. Numerical results were presented for creep strains under isothermal and cyclic temperature conditions. Sadkin and Aboudi [38] used a four-cell micromodel to analyze thermal effects on the

viscoelastic response of unidirectional fiber reinforced composites. The fibers were modeled as linearly elastic but could be easily generalized to viscoelastic fibers as well. The viscoelastic matrix was modeled as a TCM, in which the nonlinear parameters were temperature-dependent and not functions of stresses. The micromechanical analysis developed the relationships between average stresses and average strains in the composite system which led to the determination of the overall behavior. The viscoelastic micromodel was then verified with detailed finite element (FE) unit-cell for longitudinal and transverse creep responses of graphite/epoxy composites developed by Hashin et al [37]. For structural analysis, the cost of employing a FE model to solve complicated boundary value problem from the effective moduli generated by micromechanical model can be expensive. Yancey and Pindera [39] utilized the approximate micromechanical model developed by Aboudi [40] to predict the creep response of T300/934 graphite/epoxy composite in the linear viscoelastic range at two temperatures (72°F and 250°F). Two hour creep tests were performed to evaluate the creep compliances of the composite and bulk resin. The creep compliance of the bulk resin was then used in the micromechanical model to predict the effective compliance of the composite system. It was shown that the micromechanical model could accurately predict the creep compliance generated from the test data on the composite within linear viscoelastic range.

Haddad and Tanari [41] used a microstructural model of randomly oriented and short fiber to study the temperature-dependent creep of composite systems. Both fiber and matrix exhibited viscoelastic behaviors. The nonlinear creep response of the composite matrix is modeled using a modified form of the hereditary constitutive equation in linear viscoelasticity. The time-dependent behavior of the individual fiber-bundle is formulated as a combination of a viscoelastic matrix substance within the bundle and an ensemble of unidirectional elastic fibers. Numerical applications are shown for the case of the creep of SMC-R50 composite system within a temperature range of 28° to 75°C. Brinson and Knauss [42] used the correspondence principle of viscoelasticity to study the time-temperature behaviors of composite materials. Each phase in the composite

system is modeled as TSM with linear viscoelastic and the resulting overall composite properties are TCM. A numerical model was presented to examine the TCM behaviors of the studied composite systems. Muliana and Haj-Ali [43] derived a viscoelastic multi-scale model to analyze time-stress-temperature behaviors of graphite/epoxy laminated composite materials and structures. The experimental creep data of Hiel et al. [21] was used to verify their multi-scale model. The polymeric matrix in the FRP composite systems was modeled as TSM and the effect temperatures on the overall creep responses was carried only through the time-shift factor. An integrated multi-scale and FE models were used to analyze long-term responses of FRP lap-joint and notched plate composite structures.

## 1.2 RESEARCH OBJECTIVE

The present study deals with analysis of thermo-mechanical viscoelastic behaviors and long term performance of multi-layered FRP composites having unidirectional fiber and randomly oriented filament reinforcements. The multi-layered composites are made of E-glass roving and CFM reinforcements with vinylester and polyester resins. This study consists of three major components:

1) Short term creep tests and thermo-mechanical time-dependent material characterizations.

2) Time temperature scaling techniques for predicting long term material performances

3) Integrated micromechanical-finite element (FE) framework for analyzing long term behaviors of the multi-layered FRP structures.

The second chapter describes thermo-mechanical viscoelastic behaviors of the multi-layered systems at the macro level. Isothermal creep tests (30 minutes) under combined stresses and temperatures are performed on axial, transverse and 45° off axis specimens. The Schapery nonlinear viscoelastic single integral equation is applied for the effective thermo-mechanical creep responses for each off-axis creep test. The thermo-viscoelastic behaviors are modeled as TCM. This allows for modeling stress and temperature

variations with time. The stress and temperature nonlinear parameters in the Schapery equation are coupled in the product form, which follows characterization method of Harper and Weitsman [44] on epoxy adhesive.

The third chapter includes a time-temperature scaling technique for creating a master curve from a series of short term creep tests at several elevated temperatures to predict the long term responses. An attempt is also made to provide master curves from time-stress and time-temperature-stress shift factors. The long-term (8-16 months) predictions for the uniaxial specimens are comparable to the long-term creep tests of Scott and Zureick [32]. Sensitivity analyses of the Schapery's linear and nonlinear parameters are also performed to address the experimental data scatter, which may lead to significant error in material parameter characterizations and prediction of long-term responses.

The fourth chapter deals with implementations of micromechanical constitutive models with a general FE analysis. Previously developed micromechanical model of the multilayered systems (Haj-Ali and Muliana [35, 45]) is calibrated with the long-term material responses. FE models with 1D, 2D and 3D elements are employed. Applications of the integrated micromechanical – FE analysis are performed for time dependent collapse of composite structures and long term behaviors of composite truss and beam structures.

Conclusions and future research are given in the last chapter.

# CHAPTER II
# THERMO-MECHANICAL VISCOELASTIC BEHAVIORS OF MULTI-LAYERED COMPOSITE SYSTEMS

This chapter presents characterization of thermo-mechanical viscoelastic properties of multi-layered FRP composites. The multi-layered composites consist of alternating layers of unidirectional fibers (roving) and continuous filament mats (CFM). Two composite systems made of E-glass/vinylestsr and E-glass/polyester are tested along their axial, transverse and 45° off-axis of the roving fiber directions. The Schapery [22] single integral form is used to model each off-axis viscoelastic behaviors. Both stress and temperature dependent parameters are incorporated in the Schapery's single integral form. The time, temperature and stress dependent material parameters are calibrated from the short-term creep-recovery tests performed under several stresses and isothermal temperatures. Predictions are shown for the overall time-stress-temperature responses of the off-axis coupons that were not used in the calibration process. Finally the Poisson's effect on the thermo-mechanical viscoelasic behaviors are examined.

## 2.1 NONLINEAR THERMO-MECHANICAL VISCOELASTIC MODEL

Viscoelastic responses of a material can be represented using differential or integral forms. The Boltzmann convolution integral is widely used to represent linear viscoelastic behaviors and has been extended to model nonlinear viscoelastic responses. Findley et al. [26] used power law function for transient compliance in the convolution integral equation. Temperature and stress dependent material parameters were incorporated in the power law coefficients. Another common form for the transient compliance is using the Prony series, which consists of a series of exponential forms. Schapery [22] developed a nonlinear viscoelastic constitutive model based on a single integral equation with four nonlinear stress dependent material parameters.

This study introduces thermo-mechanical viscoelastic behaviors of composite systems that behave as thermo-rheologically complex materials (TCM). This allows for stress and temperature variation with time. The Schapery [22] integral equation is used and modified to represent the time-dependent behaviors of TCM. For a uniaxial loading under isothermal conditions, the total time-dependent strain can be expressed as:

$$\varepsilon^t = \varepsilon(t) = g_0^{\sigma^t} g_0^{T^t} D_0 \sigma^t + g_1^{\sigma^t} g_1^{T^t} \int_0^t \Delta D^{(\psi^t - \psi^\tau)} \frac{d\left(g_2^{\sigma^\tau} g_2^{T^\tau} \sigma^\tau\right)}{d\tau} d\tau + \alpha\left(T^t - T_{ref}\right) \tag{2.1}$$

Here $D_0$ and $\Delta D$ are the instantaneous elastic and transient compliances, which are assumed to be stress and temperature independent. The nonlinear stress-temperature dependences are carried through the parameters $g_0$, $g_1$ and $g_2$. The parameter $g_0$ is the nonlinear instantaneous elastic compliance which measures the reduction or increase in stiffness as a function of stress and temperature. The transient creep parameter $g_1$ measures the nonlinearity effect in the transient compliance. The parameter $g_2$ accounts for the loading rate effect on the creep response. The superscript denotes a dependent variable of this term or function. The parameters T and $T_{ref}$ are the current and reference temperatures, respectively. The coefficient of thermal expansion α a is material dependent parameter and is assumed to be constant for temperature ranges from ambient temperature to the material's service limit temperature, which is sufficiently below its glass transition temperature ($T_g$). The stress-temperature effects on the overall time-dependent responses are coupled in product forms following the characterization methods of Harper and Weitsman [44]. The parameter Ψ is the reduced-time (effective time), expressed by:

$$\psi^t \equiv \psi(t) = \int_0^t \frac{d\xi}{a^{\sigma^\xi} a^{T^\xi}} \tag{2.2}$$

At the reference environmental conditions, the nonlinear parameters are stress-dependent (the $g_j^{T^t}$ (j=0,1,2) and $a^{T^t}$ values are taken to be one). The parameters $a^{\sigma^t}$ and $a^{T^t}$ are time shift (interchange) factors in terms of stresses and non-reference temperatures, respectively. In the case when the thermal effects are carried through $a^{T^t}$ only ($g_j^{T^t}$ values are equal to one), the thermo-rheologically simple material (TSM) is exhibited.

The transient compliance is often modeled either using the Power law or Prony series exponential functions:

$$\Delta D^{\psi^t} = C\left(\psi^t\right)^n \qquad \text{or} \qquad \Delta D^{\psi^t} = \sum_{n=1}^{N} D_n\left(1-\exp[-\lambda_n \psi^t]\right) \tag{2.3}$$

The parameters C and n in the power law model are *stress-temperature-independent* material constants and measured at the reference condition (i.e., room temperature). The variable $D_n$ is the $n^{th}$ coefficient of the Prony series, and $\lambda_n$ is the $n^{th}$ reciprocal of retardation time. Both $D_n$ and $\lambda_n$ are also *stress-temperature independent*. Using the power law model for the transient compliance, the mechanical strain in Eq. (2.1) is expressed by:

$$\varepsilon^t = g_0^{\sigma^t} g_0^{T^t} D_0 \sigma^t + g_1^{\sigma^t} g_1^{T^t} C \int_0^t \left(\psi^t - \psi^\tau\right)^n \frac{d\left(g_2^{\sigma^\tau} g_2^{T^\tau} \sigma^\tau\right)}{d\tau} d\tau \tag{2.4}$$

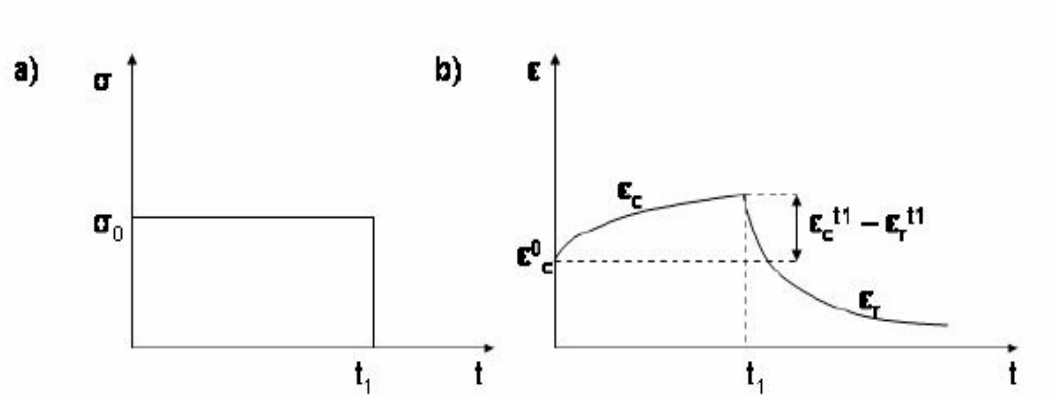


**Figure 2.1 a) Input to creep-recovery tests b) Creep-recovery response**

Creep-recovery test, illustrated in figure (2.1 a.), is often performed to characterize the time-stress-temperature dependent material parameters in the Schapery equation. A compressive or tensile step load is applied to the specimen and maintained for a duration of time ($t=t_1$) and then the load is removed. The stress history for creep-recovery test is given in equation 2.5. Since it is not possible to apply an instantaneous loading, a ramping load is performed, following the ASTM testing procedure (ASTMD3410 and ASTM D3039 [46, 47]).

Lou and Schapery [48] characterized the nonlinear stress-dependent material parameters in the Schapery's integral model of glass/epoxy laminated composites using graphical shifting of creep-recovery strain data. This study follows characterization method of Lou and Schapery [48] for the time-stress-temperature parameters in the studied multi-layered composites. Stress history during creep-recovery tests under isothermal conditions is expressed as:

$$\sigma^t = \sigma_0[H(t) - H(t - t_1)] \tag{2.5}$$

Where H(t) is the Heaviside function and the loading rate in Eq (2.4) is expressed as:

$$\frac{d\left(g_2^{\sigma_0} g_2^T \sigma^\tau\right)}{d\tau} = g_2^{\sigma_0} g_2^T \sigma_0 \left[\delta(t) - \delta(t - t_1)\right] \tag{2.6}$$

Substituting Eq. (2.6) into Eq. (2.4) give the following creep and recovery strains, which is illustrated in figure 2.1b,

$$\varepsilon_c^t = \left[ g_0^{\sigma_0} g_0^T D_0 + g_1^{\sigma_0} g_1^T g_2^{\sigma_0} g_2^T C\left(\frac{t}{a^{\sigma_0} a^T}\right)^n \right]\sigma_0 \qquad 0 < t \le t_1 \tag{2.7}$$

$$\varepsilon_r^t = g_1^T g_2^{\sigma_0} g_2^T C\left[ \left(\frac{t_1}{a^{\sigma_0} a^T} + \frac{t - t_1}{a^T}\right)^n - \left(\frac{t - t_1}{a^T}\right)^n \right]\sigma_0 \qquad t \ge t_1 \tag{2.8}$$

During the recovery stage, the recovery strain ($\varepsilon_r^t$) will reduce to its initial unloaded state, provided the material does not undergo plastic deformation or damage. The material parameters in the Schapery equations can be characterized by fitting Eqs. (2.7) and (2.8) into linear and nonlinear creep-recovery responses at several stresses and temperatures. The material characterization process is described in the following steps:

1) Linear material parameters: Do, C, and n are calibrated from a linear creep response at the reference condition ( $g_j^{\sigma^t}$ (j=0,1,2), $a^{\sigma^t}$, $g_j^{T^t}$, and $a^{T^t}$ are equal to one). The initial compliance is computed using $D_0 = \frac{\varepsilon_c^0}{\sigma_0}$, where $\varepsilon_c^0$ represents an instantaneous elastic strain. The time-dependent transient creep strain is given by $\varepsilon_c^t - \varepsilon_c^0$. The parameters C and n are determined by fitting the transient compliance $\Delta D^t = \frac{\varepsilon_c^t - \varepsilon_c^0}{\sigma_0} = Ct^n$ in a logarithmic scale, which is expressed as:

$$\log \Delta D^t = \log C + n \log(t) \tag{2.9}$$

2) Stress-dependent material parameters are then characterized using creep-recovery responses, in Eqs. (2.7) and (2.8), from several stress levels at the reference temperature ($g_j^{T^t}$ and $a^{T^t}$ are equal to one). The Schapery equation involves the instantaneous change in strain following the removal of creep load at time $t_1$. The creep strain at the instant of load removal ($t=t_1$) is given by $\varepsilon_c^{t_1}$. The load removal also results in an instantaneous recovery strain given by $\varepsilon_r^{t_1}$. The amount of the instantaneous change in strain due to creep load removal at time $t_1$, illustrated in figure 2.1b, is:

$$\varepsilon_c^{t_1} - \varepsilon_r^{t_1} = \left[ g_0^{\sigma_0} D_0 + (g_1^{\sigma_0} - 1) g_2^{\sigma_0} C \left( \frac{t_1}{a^{\sigma_0}} \right)^n \right] \sigma_0 \tag{2.10}$$

If the material follows a linear viscoelastic response the elastic recovery strain ($\varepsilon_c^{t_1} - \varepsilon_r^{t_1}$) will be equal to the instantaneous elastic strain ($\varepsilon_c^0$). Equation (2.10) also shows that the instantaneous change in strain due to creep load removal at time $t_1$ equals to the instantaneous elastic strain at time $t=0$ ($\varepsilon_c^0$) only if the material exhibits linear response during creep ($g_1^{\sigma_0} = 1$).

Creep, recovery, and transient creep strains at time $t_1$, shown in figure 2.1b, are:

$$\varepsilon_c^{t_1} = \left[ g_0^{\sigma_0} D_0 + g_1^{\sigma_0} g_2^{\sigma_0} C \left( \frac{t_1}{a^{\sigma_0}} \right)^n \right] \sigma_0 \tag{2.11-1}$$

$$\varepsilon_r^{t_1} = \left[ g_2^{\sigma_0} C \left( \frac{t_1}{a^{\sigma_0}} \right)^n \right] \sigma_0 \tag{2.11-2}$$

$$\Delta \varepsilon_c^{t_1} = \varepsilon_c^{t_1} - \varepsilon_c^o = \left[ g_1^{\sigma_0} g_2^{\sigma_0} C \left( \frac{t_1}{a^{\sigma_0}} \right)^n \right] \sigma_0 \tag{2.11-3}$$

At this point, the parameters $g_0^{\sigma_0}$ and $g_1^{\sigma_0}$ are ready to be determined from the instantaneous responses and creep-recovery behaviors at time $t_1$ (Eq. (2.11-1, 2, and 3)):

$$g_o^{\sigma_0} = \frac{\varepsilon_c^o}{D_o \sigma_o} \tag{2.12}$$

$$g_1^{\sigma_0} = \frac{\Delta\varepsilon_c^{t_1}}{\Delta\varepsilon_c^{t_1} - \left(\varepsilon_c^{t_1} - \varepsilon_r^{t_1}\right) + \varepsilon_c^o} \tag{2.13}$$

Next, using the calibrated $g_1^{\sigma_0}$, C, and n, the parameters $g_2^{\sigma_0}$ and $a^{\sigma_0}$ are then characterized by fitting the transient creep compliance in the logarithmic scale as:

$$\log\left[\frac{\varepsilon_c^t - \varepsilon_c^o}{\sigma_o}\right] = \log g_1^{\sigma_0} + \log g_2^{\sigma_0} + \log C + n\left[\log t - \log a^{\sigma_0}\right] \tag{2.14}$$

3) The temperature dependent material parameters ($g_j^{T^t}$ and $a^{T^t}$) are determined from creep responses at several elevated temperatures. For this purpose, it would be easier to pick the stress-independent responses since the values of $g_j^{\sigma^t}$ and $a^{\sigma^t}$ are equal to one. In this study, the recovery tests were performed with load removal only without releasing the current temperature back to the reference condition ($T_o$), which will be discussed later in the experimental part. Therefore, it is only possible to characterize the product of $g_1^T g_2^T$ and $a^T$ using the logarithmic form of the transient compliance in Eq. (2.14), while the parameter $g_0^T$ is easily calibrated using Eq. (2.12).

## 2.2 CREEP-RECOVERY TEST ON OFF-AXIS MULTI-LAYERED SYSTEMS

The thermo mechanical viscoelastic behavior in the Eq. (2.1) is applied for the FRP multi-layered composites. The studied multi-layered composites consist of repeating layers of unidirectional fiber (roving) and continuous filament mat (CFM). The time-stress-temperature dependent material parameters are characterized from the creep recovery tests performed under several load levels and isothermal temperatures. Predictions are made using the creep responses of off-axis coupons that were not used in the calibration.

The MTS-810 test frame having 22 kips capacity is used to conduct creep-recovery tests. An environmental chamber placed around the test frame, shown in figure 2.2, is used to control the testing temperatures. The specimen is gripped to the jaws. The strains are recorded using an on-board data acquisition system.

The strains were measured using CEA series gages, from Micro-Measurements placed on the front and back faces of the specimens. The normal temperature range of this type of gage is -100 to +350F (-75 to +175°C), which is adequate for the temperature range considered for this experimental investigation. The strain gages were bonded to the specimens using M-bond 200 adhesives.


**Figure 2.2 MTS-810 test frame with environmental chamber.**

Two different multi-layered composites manufactured by Creative Pultrusion Inc. are studied. The first system consists of 4 roving and 5 CFM layers of E-glass fiber and vinylester resin. The second system is made of 2 roving and 3 CFM layers of E-glass fiber and polyester resin. The two FRP systems are illustrated in figure 2.3. Compression and tension creep tests are performed on the E-glass/vinylester and E-glass/polyester composites, respectively. The compression and tension tests are carried out in accordance with the ASTM D3410 [46] and ASTM D3039 [47], respectively. The dimensions of the compression coupons are 6 x 1.25 x 0.5 inches and the ones of tension coupons are 10 x 1.25 x 0.25 inches. The specimens are gripped along 2 inches at both edges. Axial strains are monitored using strain gages that are attached at the center on both sides of the specimens. Transverse strain is also recorded from a strain gage mounted on one side of the specimens.

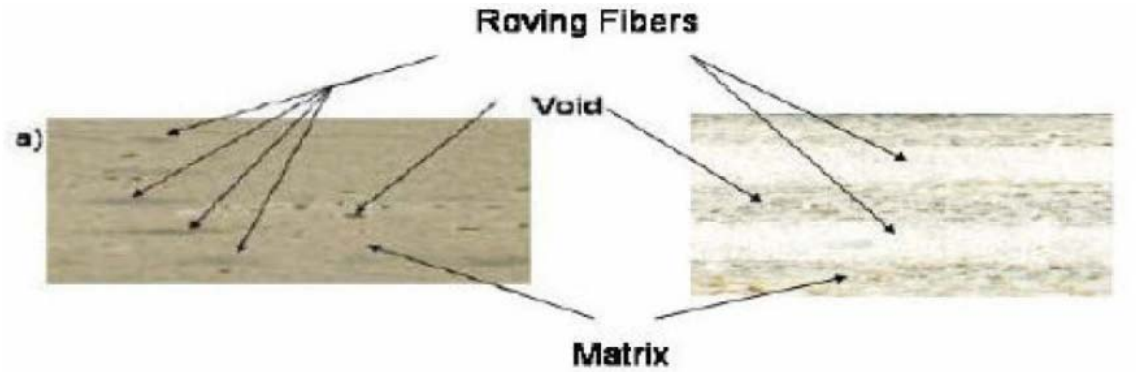


**Figure 2.3 Cross section of the two studied multi-layered FRP systems a) E-glass/vinylester system b) E-glass/polyester system.**

Axial, transverse, and 45$^{o}$ off-axis coupons are cut from the thick unidirectional E-glass/vinylester and E-glass/polyester composite plates such that the orientation of the roving layers is controlled. This allows testing under multi-axial in-plane stress states. Fiber volume fraction (FVF), effective elastic modulus, and ultimate compression strength for the E-glass/vinylester system are taken from the study by Haj-Ali and Kilic

[45], given in Table (2.1). Static tensile tests are first performed to determine the effective elastic properties and ultimate strength for the E-glass/polyester system, shown in Table (2.2). For the static tests, axial load is applied with a constant displacement rate of 0.02 in/min, following the ASTM standard. To determine the ultimate strength, the loads at which the specimens fail are noted. Error estimates of strain measurements in off-axis creep tests due to the misalignment of the material symmetry were given by Haj-Ali and Kilic [45]. They found that the maximum error from the strain was about 1% in the center of the coupon, where the strain was measured. The added shear stress in tension was reduced by using longer coupons (12"). In addition, the relatively larger section area (0.625 $in^2$) reduced the added shear stress magnitude due to misalignment.

**Table 2.1 Effective compressive material properties for E-glass/vinylester system with FVF 34% measured at T=75°F (Haj-Ali and Kilic, [45]).**

| Off-axis angle (θ) | 0° | 45° | 90° |
|---|---|---|---|
| Young Modulus, ksi | 2779 | 1727 | 1727 |
| (GPa) | (19) | (12) | (12) |
| $\sigma_c^{ult}$ ksi | 40 | 24 | 24 |
| (MPa) | (276) | (165) | (165) |

**Table 2.2 Effective tensile material properties for E-glass/polyester system with FVF 34% measured at T=75°F.**

| Off-axis angle (θ) | 0° | 45° | 90° |
|---|---|---|---|
| Young Modulus ksi | 1902 | 1359 | 1273 |
| (GPa) | (13) | (9) | (9) |
| $\sigma_t^{ult}$ ksi | 32 | 12 | 9 |
| (MPa) | (221) | (83) | (62) |

Thirty minute creep followed by ten minute recovery tests are conducted under isothermal conditions. The tests are carried out at several stress levels: 0.2-0.6 of the material ultimate strength and temperatures 75°F-150°F. The specimens are soaked in the environmental chamber at the tested temperature for at least 30 minutes prior to each creep test. To measure temperature's equilibrium in the tested specimens, a dummy coupon is placed in the environmental chamber and the temperature distribution inside the specimen is monitored using a thermocouple. Axial and transverse strain gages are also placed in the dummy coupons to record thermal strains. Figure (2.4) shows averaged time required to achieve equilibrium tested temperatures along with the thermal strains for the axial and 45° off-axis specimens.

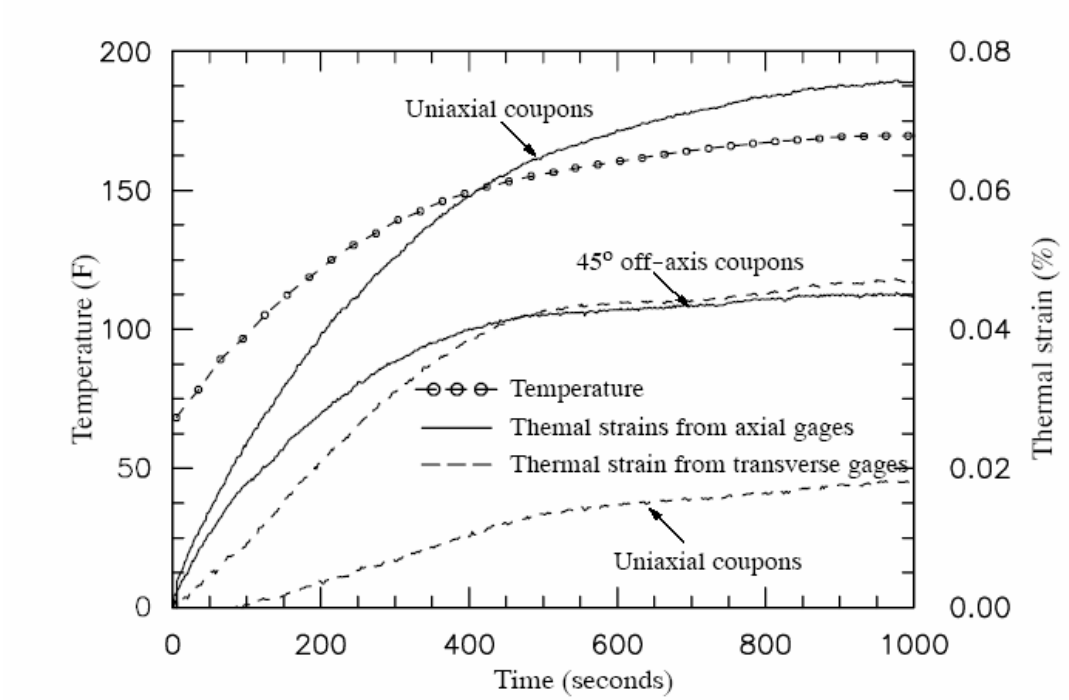


**Figure 2.4 Time required to heat the 0.5 inch E-glass/vinylester up to several elevated temperatures and thermal strains for the uniaxial and 45° off-axis coupons.**

It is seen from Fig. (2.4) that it requires more than 100 seconds for each specimen to reach equilibrium at the tested temperatures from the reference condition (75$^{o}$F). Therefore, at these particular short-term creep tests, it is impractical to conduct temperature recovery tests. The recovery tests are conducted by removing the stresses only. During the tests, temperatures have fluctuated around ±1$^{o}$F and loads have varied around ±0.5% of the applied loads.

E-glass/vinylester coupons with off-axis angles: 0$^{o}$, 45$^{o}$, and 90$^{o}$ are prepared for creep compression tests. A single coupon is used for multiple creep tests under combined stress levels 0.2, 0.4, and 0.6 of the specimen's ultimate strength and temperatures 75$^{o}$F, 100$^{o}$F, 125$^{o}$F, and 150$^{o}$F. Yeow et al. [20] had established that same specimen can be used for multiple creep tests without significantly altering the mechanical properties. Testing starts with the lowest temperature and stress level (75°F and 0.2 of ultimate strength respectively) and consecutively ends with the highest

temperature (150°F) and stress level (0.6 of ultimate). Table (2.3) lists an array of off-axis creep compression tests. The coupons subjected to multiple creep tests are given at least 24 hours recovery duration between the consecutive tests. Creep tests at the highest temperature for every stress level are repeated using different coupons, except for the transverse (90°) specimen, in which the repeated creep tests are performed using the same coupon. The repeated tests are used to examine possible accumulated residual strain and damage occurred during the creep tests using a single coupon. Time-dependent failure has occurred on the uniaxial specimen at load ratio 0.6 and temperatures 125°F and 150°F. The failure time recorded from a single test is presented in Table (2.4). Experimental tests, listed in Table (2.3), are repeated twice using different sets of specimens. Maximum recorded strain difference from two different coupons in the repeated tests is 3%.

**Table 2.3 Creep tests with different off-axis E-glass/vinylester coupons subjected to various fractions of their ultimate compressive strength and temperatures.**

Cx − y − z ≡ Compression-off-axis angle - coupon number - loading ratio - temperature

| 0° | 45° | 90° |
|---|---|---|
| C0-1-02-075 * | C45-1-02-075 * | C90-1-02-075 * |
| C0-1-02-100 ** | C45-1-02-100 ** | C90-1-02-100 ** |
| C0-1-02-125 ** | C45-1-02-125 ** | C90-1-02-125 ** |
| C0-1-02-150 ** | C45-1-02-150 ** | C90-1-02-150 ** |
| C0-2-02-150 | | |
| C0-1-04-075 * | C45-1-04-075 * | C90-1-04-075 * |
| C0-1-04-100 | C45-1-04-100 | C90-1-04-100 |
| C0-1-04-125 | C45-1-04-125 | C90-1-04-125 |
| C0-1-04-150 | C45-1-04-150 | C90-1-04-150 |
| C0-2-04-150 | C45-2-04-150 | C90-1-04-150r |
| C0-1-06-075 * | C45-1-06-075 * | C90-1-06-075 * |
| C0-1-06-100 | C45-1-06-100 | C90-1-06-100 |
| | C45-1-06-125 | C90-1-06-125 |
| | C45-1-06-150 | C90-1-06-150 |
| | C45-2-06-150 | C90-1-06-150r |

* Experimental data used for stress-dependent calibration

** Experimental data used for temperature-dependent calibration

**Table 2.4 Time-stress-temperature dependent failure.**

| Specimens | Fiber orientation | Stress ratio | Temperature °F | Failure time seconds |
|---|---|---|---|---|
| E-glass/vinylester (compression) | 0 | 0.6 | 125 | 182 |
| | 0 | 0.6 | 150 | 100 |
| E-glass/polyester (tension) | 45 | 0.6 | 125 | 3730 |
| | 45 | 0.6 | 150 | 426 |

Next, six and three E-glass/polyester tensile coupons are prepared for the 45° and 90° off-axis angle respectively. Each coupon is used for multiple creep tests under fixed load levels and several temperatures: 75°F, 100°F, 125°F, and 150°F. The creep tests started with the lowest temperatures and stress levels, as listed in Table (2.5). Repeated creep tests are performed at the highest temperature using the same coupon. Tensile creep tests on the uniaxial coupon are not performed due to the immediate failure occurred during creep tests at high temperature (150°F) even for load ratio 0.2. Failure has occurred during creep tests on the 45° off-axis specimens at load level 0.6 and the failure time is given in Table (2.4). In order to examine repeatability and obtain example of statistical interpretation of the experimental data, creep tests for the 45° off-axis angle at load ratio 0.4 and temperatures 75°F-150°F are repeated using tensile specimen numbers 5, 6, and 7 (shown in Table 2.5). Each coupon is also used for multiple creep tests at several temperatures. The 45° off-axis specimen under load ratio 0.4 is chosen for the repeated tests due to the highly material nonlinearity exhibited at elevated temperatures without specimen failure. Table 2.6 presents average and standard deviation values for compliances measured at 1800 seconds. Maximum compliance variability with respect to the average compliances from 4-5 repeated tests is 6.6%.

**Table 2.5 Creep tests with different off-axis E-glass/polyester coupons subjected to various fractions of their ultimate tensile strength and temperatures.**

Tx − y − z ≡ Tension-off-axis angle - coupon number - loading ratio - temperature

| 45° | | | | 90° |
|---|---|---|---|---|
| T45-1-02-075 * | | | | T90-1-02-075 * |
| T45-1-02-100 ** | | | | T90-1-02-100 ** |
| T45-1-02-125 ** | | | | T90-1-02-125 ** |
| T45-1-02-150 ** | | | | T90-1-02-150 ** |
| T45-1-02-150r | | | | T90-1-02-150r |
| T45-2-04-075 * | T45-5-04-075 | T45-6-04-075 | T45-7-04-075 | T90-2-04-075 * |
| T45-4-04-100 | T45-5-04-100 | T45-6-04-100 | T45-7-04-100 | T90-2-04-100 |
| T45-4-04-125 | T45-5-04-125 | T45-6-04-125 | T45-7-04-125 | T90-2-04-125 |
| T45-4-04-150 | T45-5-04-150 | T45-6-04-150 | T45-7-04-150 | T90-2-04-150 |
| T45-4-04-150r | | | | T90-2-04-150r |
| T45-3-06-075 * | | | | T90-3-06-075 * |
| T45-3-06-100 | | | | T90-3-06-100 |
| T45-3-06-125 | | | | T90-3-06-125 |
| | | | | T90-3-06-150 |
| | | | | T90-3-06-150r |

* Experimental data used for stress-dependent calibration

** Experimental data used for temperature-dependent calibration

**Table 2.6 Statistical interpretation of time dependent compliance of E-glass/polyester 45° off-axis coupons**

| Temperature (F) | D(t) x $10^{-4}$ 1/ksi (1/MPa) at t=1800 seconds | | |
|---|---|---|---|
| | Average | Standard Deviation | % Deviation |
| 75 | 7.99 (1.16) | 0.27 (0.04) | 3.4 |
| 100 | 11.25 (1.63) | 0.62 (0.09) | 5.5 |
| 125 | 14.57 (2.11) | 0.96 (0.14) | 6.6 |
| 150 | 16.63 (2.41) | 0.81 (0.12) | 4.9 |

Note: the values are obtained from 4–5 data points

## 2.3 MATERIAL CHARACTERIZATION AND PREDICTION OF THERMO-MECHANICAL VISCOELASTIC BEHAVIOR

Time-stress-temperature dependent material parameters in Eq. (2.1) are determined for each off-axis specimen using creep-recovery data under isothermal conditions. Characterization methods in Eqs. (2.9)- (2.14) are followed. The experimental data marked by (*) in Tables 2.3 and 2.5 are used for stress-dependent parameter calibration, while, the (**) indicates test data used for temperature-dependent parameter calibration. The rest of the test data are reserved for predictions. The linear viscoelastic parameters in the Schapery equation are calibrated from creep responses performed under a relatively low magnitude of applied stress (0.2 of ultimate failure load) and at the reference temperature ($75^{o}$F). Figure 2.5 shows creep strains of $45^{o}$ off-axis E-glass/vinylester specimens under compression loads at $75^{o}$F. Average strains from two axial gages are reported for stress levels 0.2-0.6 and are used for material calibrations. The responses from the lowest load level (0.2) at temperature 75°F are then used to

calibrate the parameters Do, C, and n by matching the overall responses with the experimental data. The calibrated linear parameters are given in table 2.7.

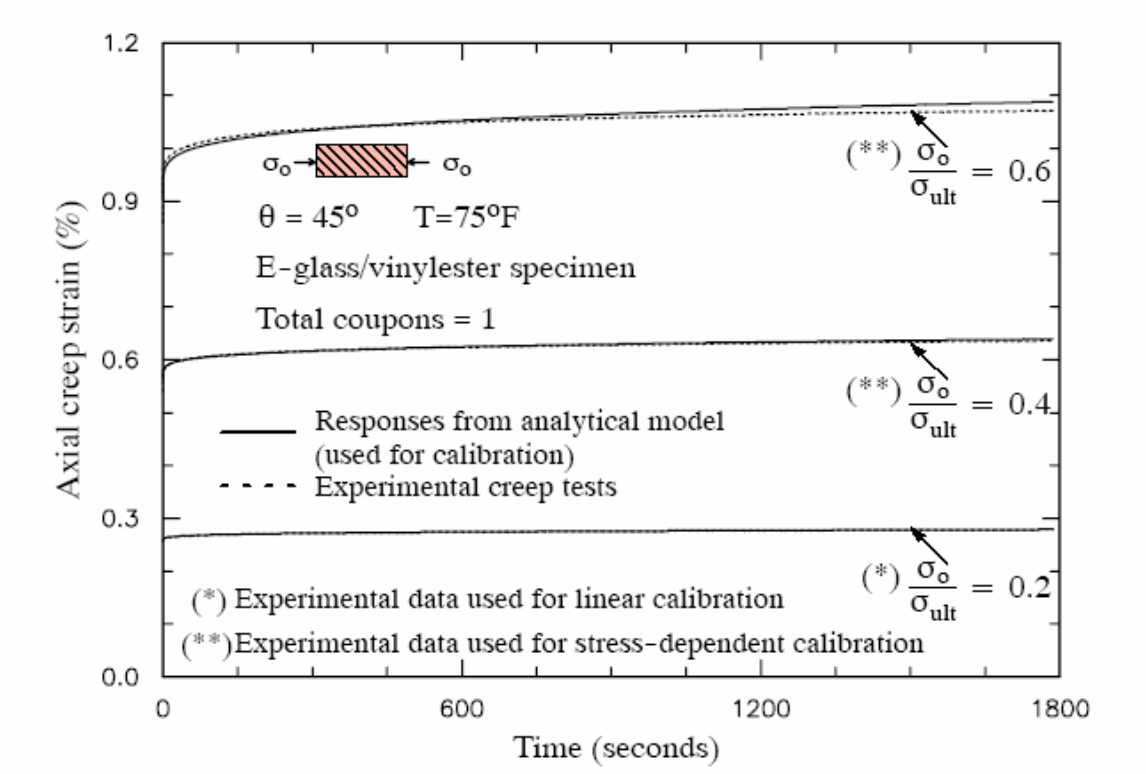


**Figure 2.5 Creep compression responses for 45° off-axis specimens at T=75°F (experimental data used for stress-dependent parameter calibrations).**

**Table 2.7 Linear viscoelastic parameters for E-glass/vinylester and E-glass/polyester coupons.**

| Specimen | E-glass/vinylester | | | E-glass/polyester | |
|---|---|---|---|---|---|
| Off-axis angle (θ) | 45° | 90° | 0° | 45° | 90° |
| Do x $10^{-4}$ 1/ksi (1/MPa) | 5.44 (0.79) | 5.58 (0.81) | 3.66 (0.53) | 8.01 (1.16) | 7.17 (1.04) |
| C x $10^{-5}$ 1/ksi (1/MPa) | 1.1 (0.16) | 9.32 (1.35) | 2.19 (0.32) | 2.25 (0.33) | 1.94 (0.28) |
| n | 0.200 | 0.189 | 0.160 | 0.270 | 0.177 |

The nonlinear viscoelastic parameters $g_0$, $g_1$, $g_2$ and a, are held equal to one during this calibration stage. Next, the responses from the higher load levels at the same temperature are used to calibrate the stress-dependent material parameters. For this purpose, the non-linear temperature dependent parameters are held equal to one. The recovery strains of 45° off-axis E-glass/vinylester specimens at different load ratios are given in Figure 2.6. The small strain magnitudes, which are less than 0.03% after 600 minute recovery time, will eventually lead to complete recovery at sufficiently longer time. The complete recovery curves for E-glass/ vinylester and E-glass/polyester specimens are provided in Appendix A.

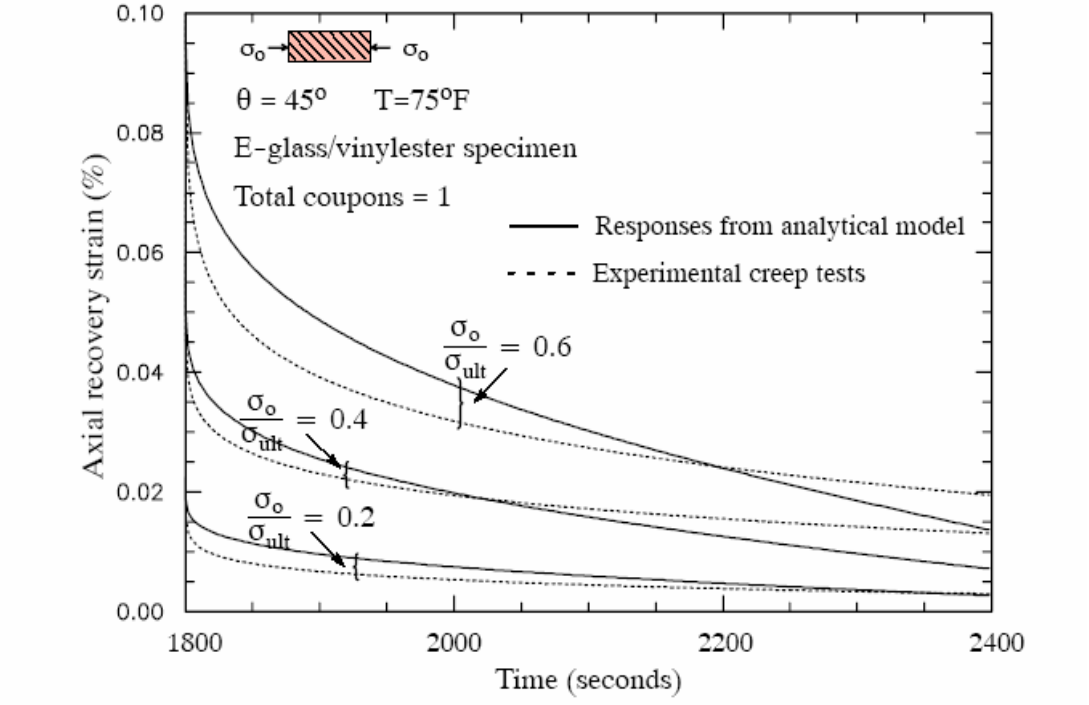


**Figure 2.6 Recovery responses for 45° off-axis specimens at T=75°F (the magnitude of the strain after 10 minute recovery is less than 0.03%, which indicates fully recovered).**

For characterizing the temperature dependent material parameters, the creep responses at the lowest load level and elevated temperatures are used. Thus the temperature-dependent parameters are characterized using the creep responses at the lowest load level (0.2) and several elevated temperatures (75-150°F), as illustrated in Figure 2.7. At the lowest temperature and load level, all the nonlinear material parameters will be equal to one. At elevated temperatures and the lowest load level (0.2), the stress dependent nonlinear parameters are held equal to one. Figures 2.8(a) and (c) present the stress and temperature dependent material parameters for the $45^o$ off-axis E-glass/vinylester specimens under compression loads. Similar calibration procedure is also performed to characterize material parameters for the uniaxial and transverse specimens. Table 2.7 presents the calibrated linear viscoelastic parameters for the E-

glass/vinylester specimens. The higher values of the parameters C and n imply that time-dependent behaviors are more pronounced for the off-axis specimens. This is due to the matrix dominated and added shear mode in the off-axis specimens. The transient compliance can also be expressed using Prony series in Eq. 2.3. Thus, another linear time-dependent calibration is performed to characterize the Prony coefficients. Table 2.8 presents the Prony coefficients from 1800 second creep data in a second unit time.

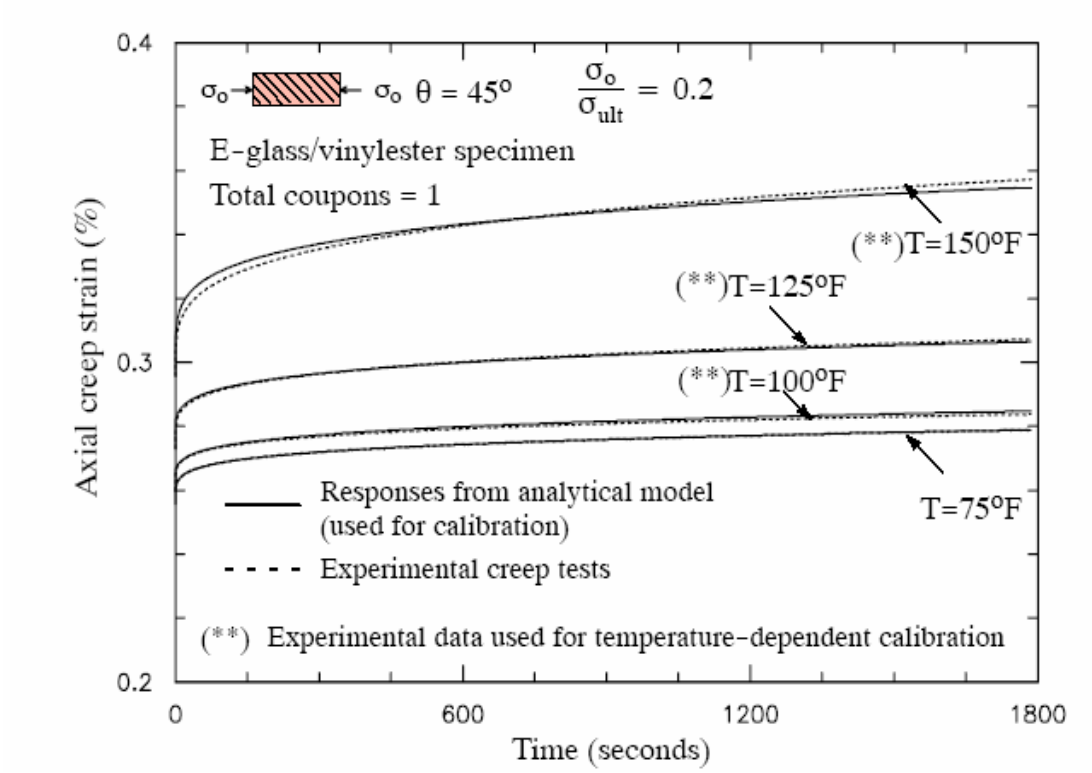


**Figure 2.7 Creep compression responses for 45° off-axis specimens at load ratio 0.2 (experimental data used for temperature dependent parameter calibration).**

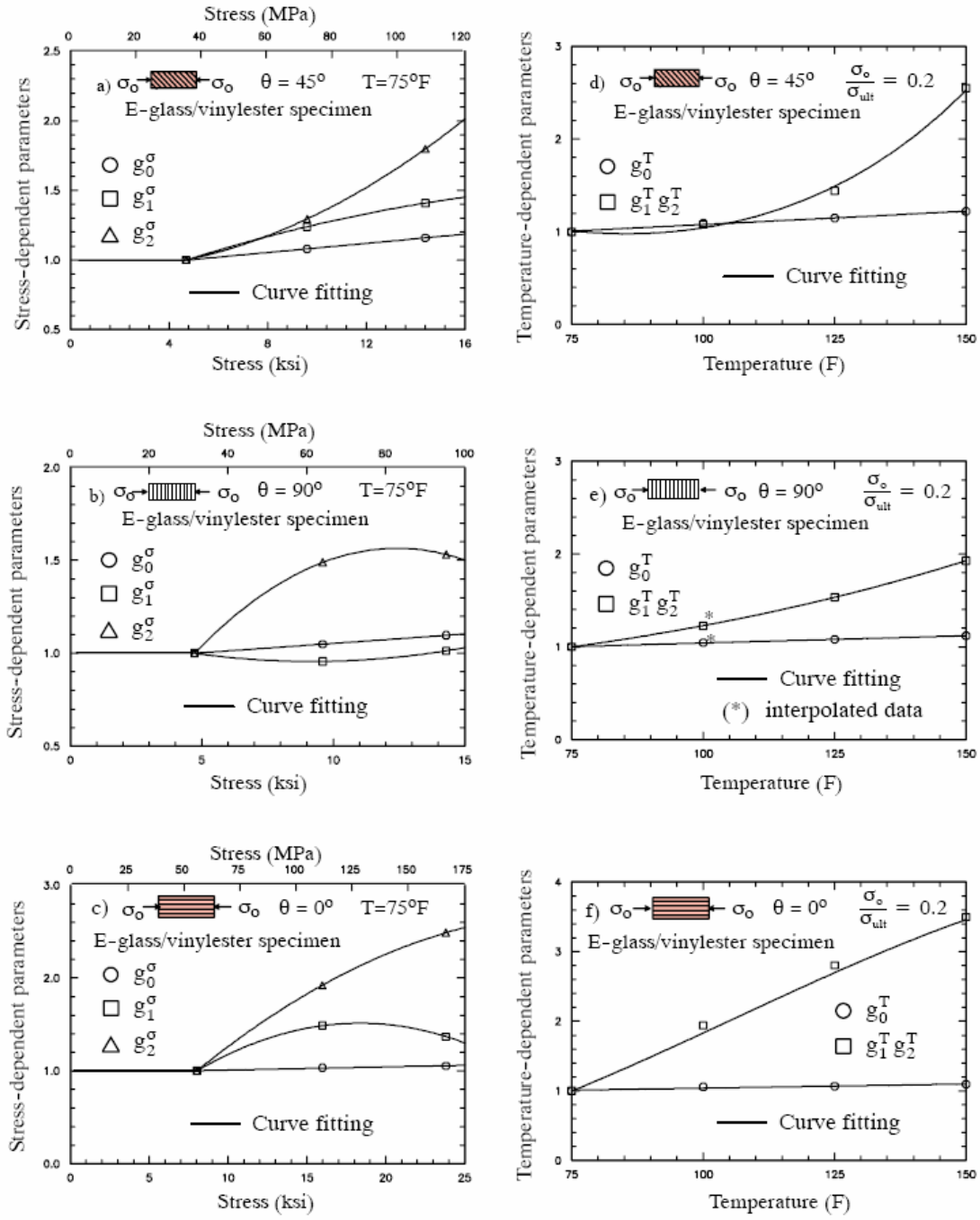


**Figure 2.8 Nonlinear parameters for E-glass/vinylester specimens under compression loads. (a-c) Stress-dependent; (d-f) Temperature dependent.**

**Table 2.8 Prony series coefficients for E-glass/vinylester and E-glass/polyester specimens from 30 minute calibration.**

| n | λn (1/sec) | Dn x10$^{-6}$ 1/ksi (1/MPa) | | | | |
|---|---|---|---|---|---|---|
| | | E-glass/vinylester | | | E-glass/polyester | |
| | | 45° | 90° | 0° | 45° | 90° |
| 1 | 1 | 16.23 (2.36) | 13.15 (1.91) | 3.06 (0.44) | 24.47 (3.55) | 35.00 (5.08) |
| 2 | $10^{-1}$ | 0.97 (0.14) | 2.27 (0.33) | 0.19 (0.03) | 20.87 (3.03) | 18.90 (2.74) |
| 3 | $10^{-2}$ | 13.21 (1.92) | 7.65 (1.11) | 1.31 (0.19) | 36.85 (5.35) | 16.00 (2.32) |
| 4 | $10^{-3}$ | 13.34 (1.94) | 16.04 (2.33) | 2.58 (0.37) | 84.41 (12.25) | 22.00 (3.19) |
| 5 | $10^{-4}$ | 42.18 (6.12) | - | - | 104.87 (15.22) | 20.00 (2.92) |

The calibrated stress and temperature dependent parameters for the 45° off-axis, transverse, and uniaxial E-glass/vinylester specimens are given in Fig. 2.8 (a-f). At the stresses lower than 20% of the ultimate strength, all nonlinear stress-dependent parameters in Eq. (2.4) are set to be one. The stress-dependent parameters are exactly calibrated for stress levels 40% and 60% of the ultimate strength. The temperature dependent parameters are calibrated at 100°F, 125°F, and 150°F. Polynomial functions are used to fit the calibrated stress and temperature parameters. The accuracy of these polynomial functions is within these calibrated stresses and temperatures; beyond these calibrated limits, the polynomial function may not represent the actual material behaviors. During the creep tests for the transverse specimen at load level 0.2 and temperature 100°F, the strain gages have failed in recording the creep strain data. Thus, the temperature parameters are calibrated only at 75°F, 125°F, and 150°F. The polynomial fitted functions are then used to interpolate the temperature parameters at 100°F, illustrated in Figure 2.8e. As mentioned earlier, the creep-recovery tests at the isothermal conditions allow for calibrating only the product of $g_1^T g_2^T$. This is because

during the recovery cycle only the stresses were removed. To separate the parameters $g_1^T$ and $g_2^T$, the temperature recovery tests are required, which are discussed by Harper and Weitsman [44].

Next, predictions of the overall nonlinear time-stress-temperature dependent responses of the off-axis coupon tests that were not used in the calibration process are presented. Figures 2.9 and 2.10 are predictions of compression creep strains at load levels 0.4 and 0.6 and elevated temperatures for the E-glass/vinylester 45$^o$ off-axis and transverse specimens, respectively. Overall good predictions are shown. This validates the assumption that stress and temperature effects on the time-dependent behaviors of multi-layered composites can be coupled in the product form. More pronounced nonlinearity is exhibited for the 45$^o$ off-axis (shear) specimens. Creep tests at 150$^o$F are repeated twice using the same specimens that were previously tested at the same temperature. The purpose is to monitor possible damage accumulation during the nonlinear creep tests. No damages or permanent deformations exist during the creep compression tests on the 45$^o$ off-axis and transverse specimens. Some deviation in creep strain prediction is shown for the 45$^o$ off-axis specimen at the highest load and temperature. It is seen in Figure 2.10 that both creep responses at load ratio 0.4 and 0.6 under T=100$^o$F encounter the same amount of experimental and prediction data mismatch. This is due to the interpolated temperature dependent parameters at this specific temperature. Nevertheless, the predicted responses are comparable with the creep test data. Experimental data scatter due to material variability with maximum difference 3% are shown from the repeated tests using different specimens, as previously mentioned. More accurate material parameter calibrations can be done by using averaged responses of several repeated tests with more stress and temperature intervals. However, the main goal of this study is to perform time-stress-temperature material characterization technique of TCM under multi-axial loading. The compression creep tests on the axial specimens for load ratio 0.2 and 0.4 are given in figure 2.11. Failure has occurred on the specimens tested at load ratio 0.6 and temperatures 125$^o$F and 150$^o$F.

Failure time is given in table 2.4. This is due to the combined high stresses and elevated temperatures, which accelerate the nonlinear deformations in the materials.

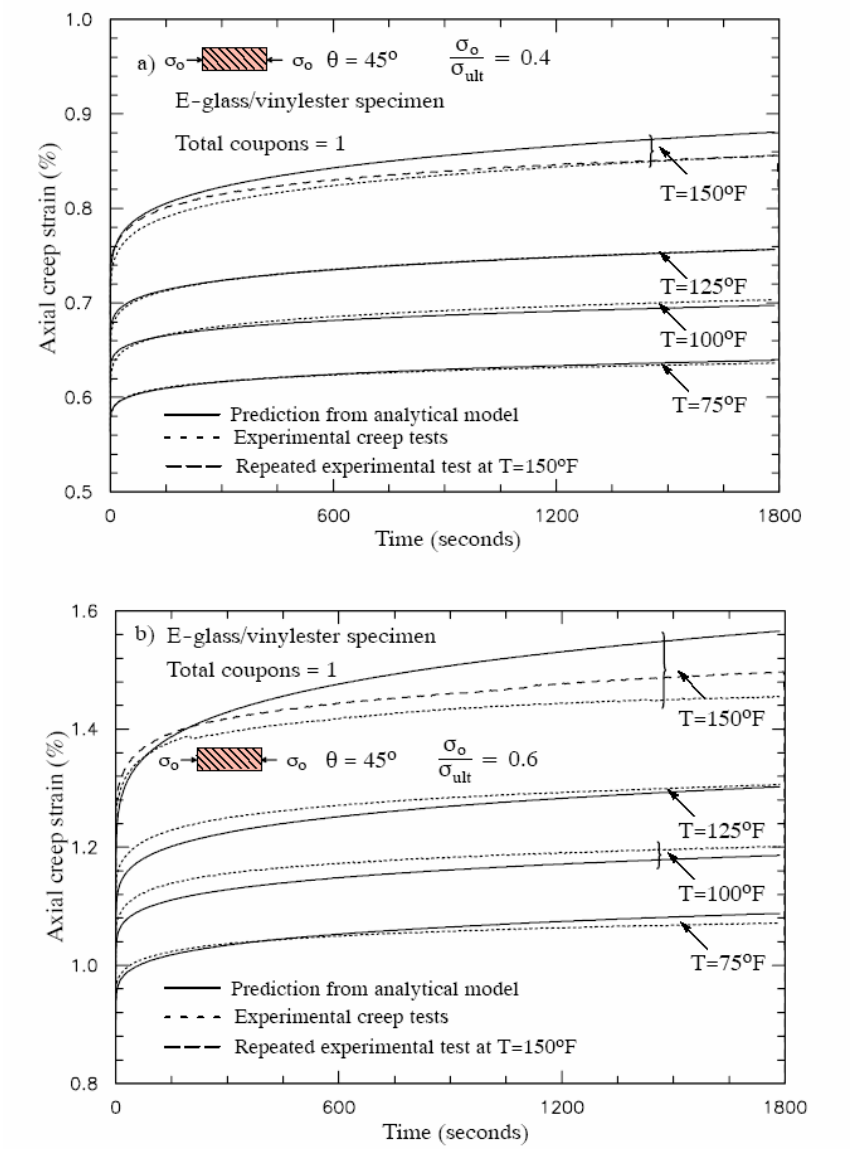


**Figure 2.9 Creep compression responses for 45° off-axis specimens at load ratio a) 0.4 and b) 0.6**

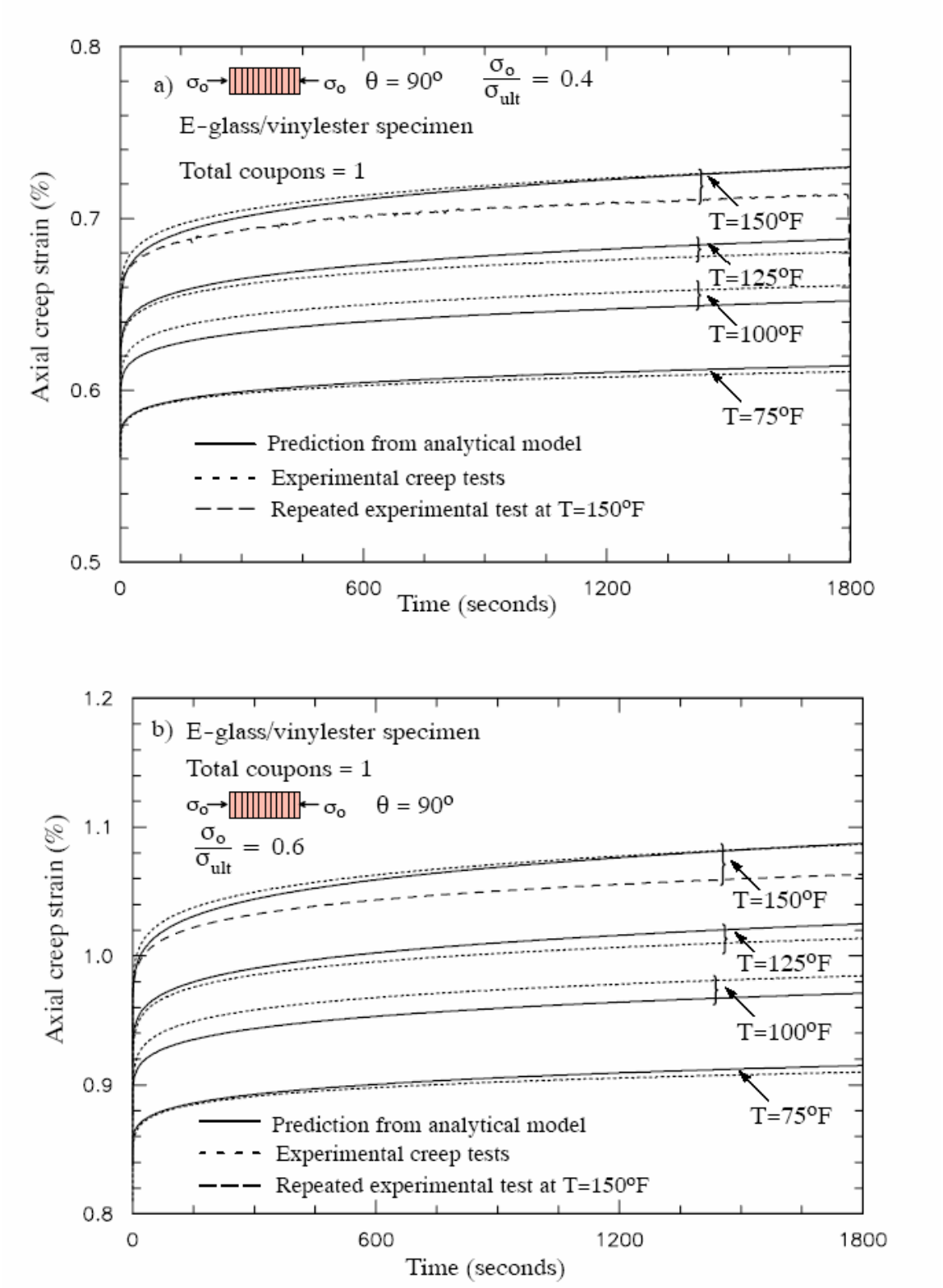


**Figure 2.10 Creep compression responses for transverse specimens at load ratio a) 0.4 and b) 0.6**

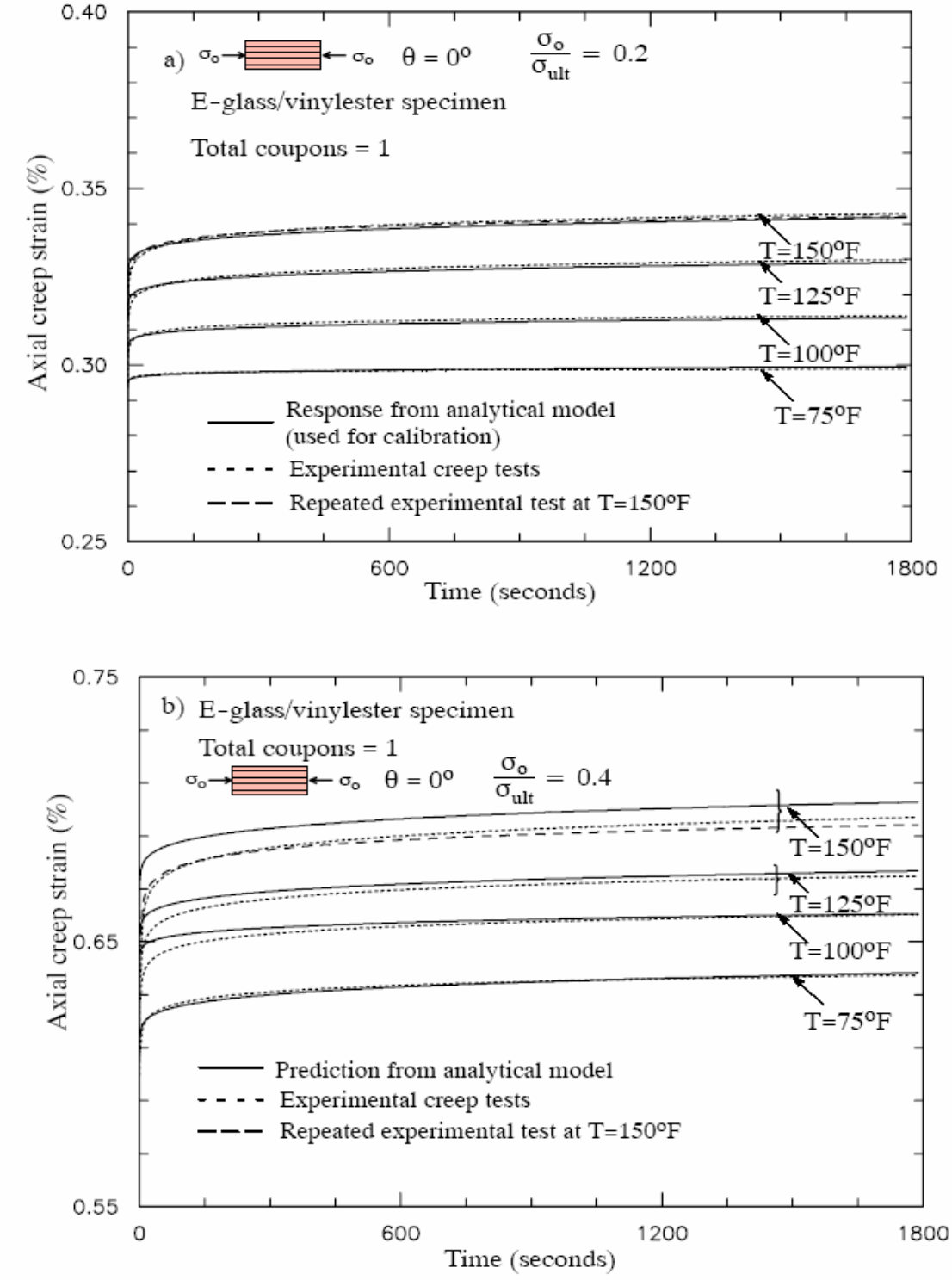


**Figure 2.11 Creep compression responses for uniaxial specimens at load ratio a) 0.4 and b) 0.6**

Linear and nonlinear time-dependent material calibrations are also performed for E-glass/polyester 45$^{o}$ off-axis and transverse specimens under tensile loads. The calibrated linear material parameters are given in table 2.6 and the calibrated nonlinear stress and temperature dependent parameters are illustrated in Figure 2.12 (a-d). Figures 2.13 and 2.14 show predictions of tensile creep tests under combined high load levels and elevated temperatures for the 45$^{o}$ off-axis and transverse specimens, respectively. Repeated creep tests for the 45$^{o}$ off-axis angle are done under load ratio 0.4 and several temperatures. Total of five coupons are used for this purpose. The repeated responses are also shown in Fig. 2.13a. Time-dependent failures have occurred on creep tests of the 45$^{o}$ off-axis specimens at stress level 0.6 and temperatures 125$^{o}$F and 150$^{o}$F. The failure time is reported in table 2.4. Creep tests are not performed on the uniaxial specimens due to the time-dependent failure occurred during testing at elevated temperature even at low load levels. Specimens tested under tensile load are weaker and fail at earlier time compared to the ones tested under compression. This is due to the existence of voids in the samples from the manufacturing defect and the tension load tends to open these voids.

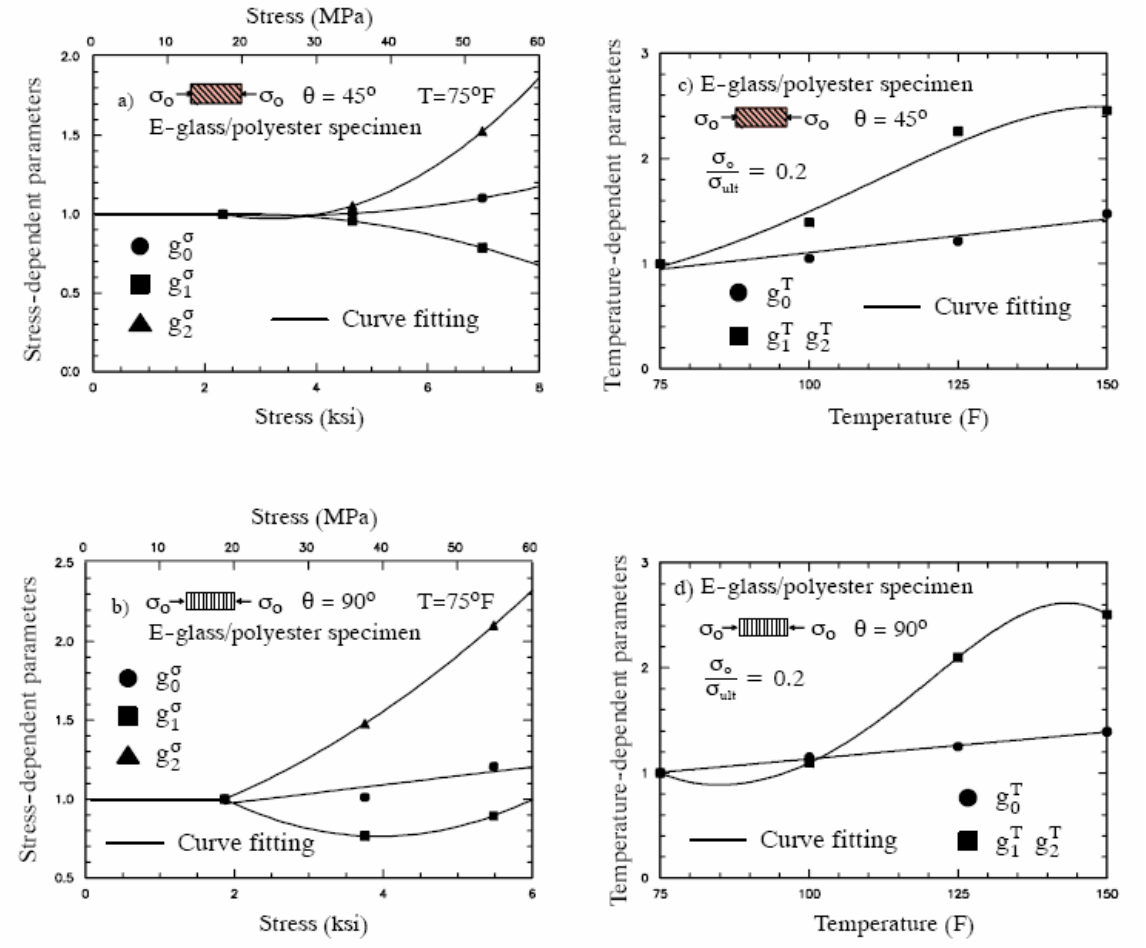


**Figure 2.12 Nonlinear parameters for E-glass/polyester specimens under tensile loads. (a-b) Stress-dependent; (c-d) Temperature-dependent.**

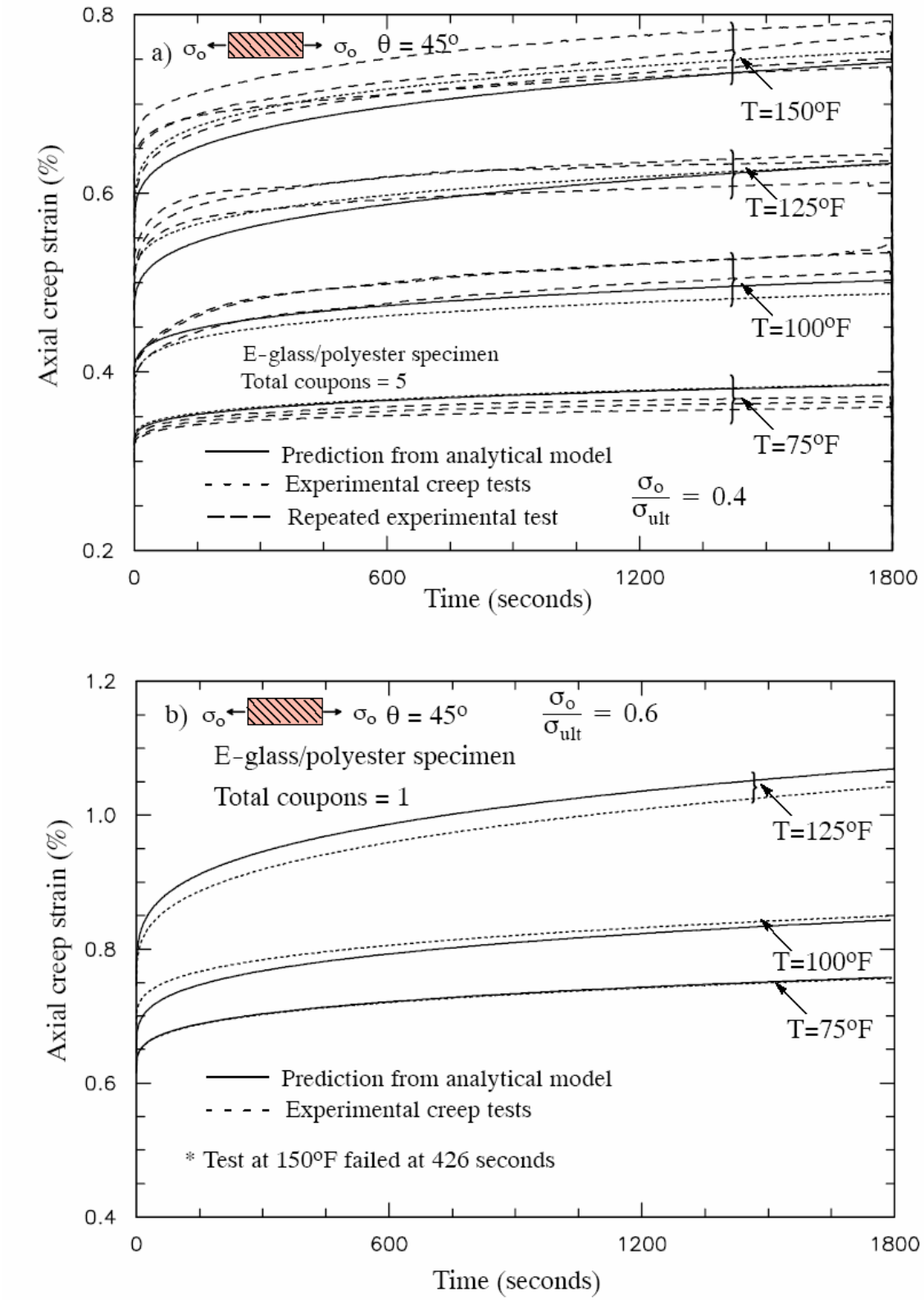


**Figure 2.13 Creep compression responses for 45° off-axis specimens at load ratio a) 0.4 and b) 0.6**

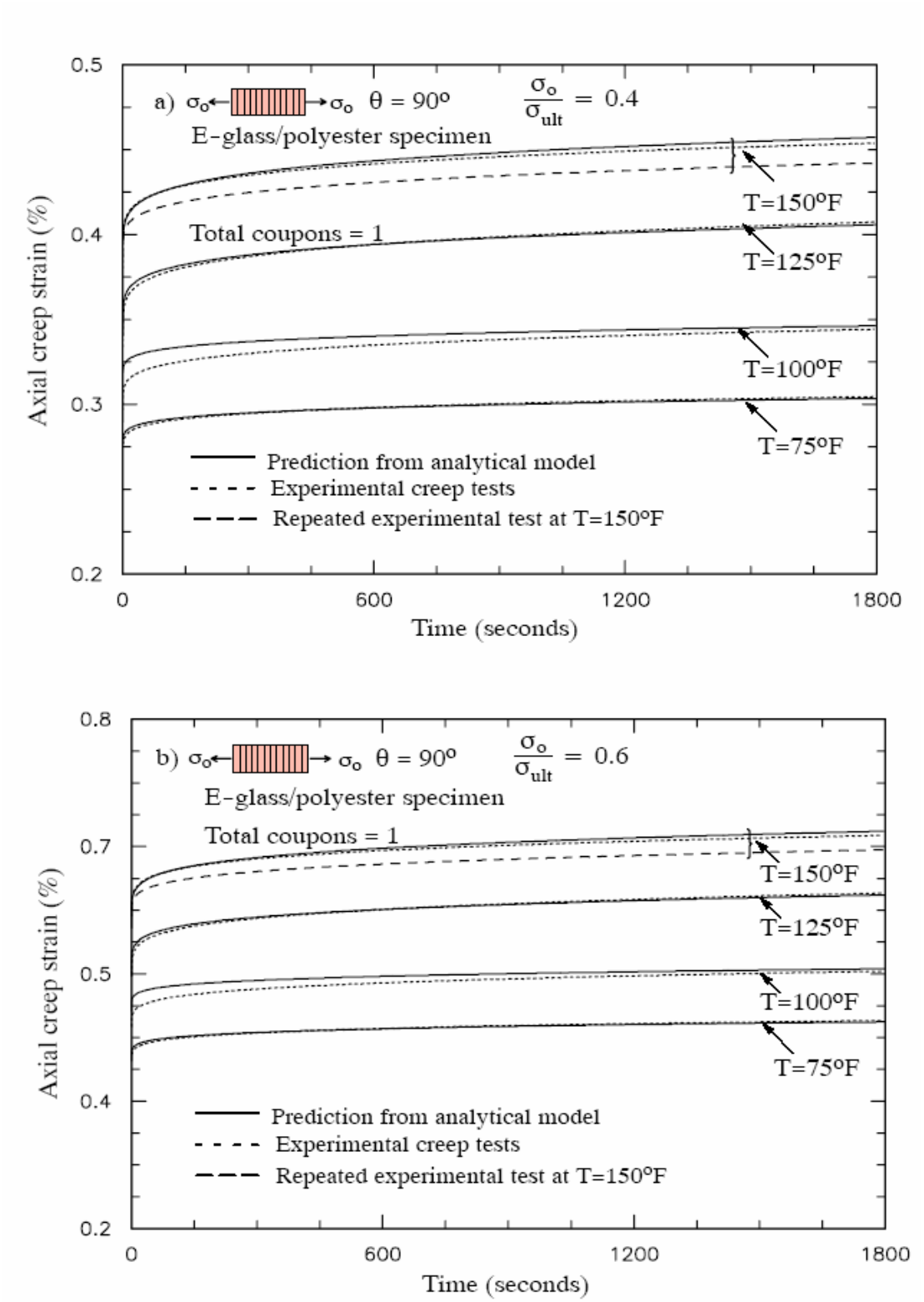


**Figure 2.14 Creep compression responses for 90° off-axis specimens at load ratio a) 0.4 and b) 0.6**

## 2.4 POISSON'S EFFECT AND MATERIAL SYMMETRY IN ANISOTROPIC VISCOELASTIC RESPONSES OF THE MULTI-LAYERED FRP SYSTEMS

The deformations in the normal direction to the uniaxial loading axis are related to the Poisson's ratio of materials. In general, the Poisson's ratio can be dependent on time, temperature, stress and loading rate. Yi et al. [7] indicated that Poisson's ratio is independent of time if the time dependent moduli/compliances are characterized from a creep test, which gives an identical time domain in all directions. Moreover most elastic materials exhibit material symmetry, which show invariant responses under changes of reference configuration with arbitrary rotation. This study examines the material symmetry and Poisson's effect on short-term creep tests for the E-glass/vinylester systems.

Creep-compression test data from the axial and transverse specimens shown in table 2.3 are used to calculate compliances $S_{21}$ and $S_{12,}$ respectively. The transverse compliances are obtained from the uniaxial loading on axial and transverse specimens as: $S_{21} = \varepsilon_2(t)/\sigma_1$ and $S_{12} = \varepsilon_1(t)/\sigma_2$ respectively. Figure 2.15 illustrates the compliances $S_{12}$ and $S_{21}$ for E-glass/vinylester specimens under creep tests at several stresses and temperatures. The compliance $S_{21}$ under load ratio 0.6 and temperatures 100°F to 150°F is not shown due to non availability of strain data at those temperature and stress level. The slight variability in transverse compliances shows that both the compliances ($S_{12}$ and $S_{21}$) are less sensitive to time, stresses and temperatures. Figure 2.15 also indicates that the average value of $S_{12}$ compliance is slightly lower than the averaged $S_{21}$ (15% difference). However, instead of postulating material asymmetric behaviors, it is more reasonable to claim material symmetric responses. The difference in $S_{12}$ and $S_{21}$ values are probably due to material and experimental test variability. It is noted that only one coupon is used for each creep test on the uniaxial and transverse specimens.

Poisson's effects are then calculated directly from the axial and transverse strains recorded on the 0 and 90 specimens, which are: $\nu_{12} = \varepsilon_2(t)/\varepsilon_1(t)$ under applied load $\sigma_1$ and $\nu_{21} = \varepsilon_1(t)/\varepsilon_2(t)$ under applied load $\sigma_2$. Figure 2.16 (a and b) presents the Poisson's

effect from the uniaxial and transverse specimens. Since the strain data (from applied load $\sigma_1$) for uniaxial specimens under stress ratio 0.6 and temperatures 100°F to 150°F were not available, the Poisson's ratio ($\nu_{12}$) at these temperatures and load level are not shown. Time dependence is only shown during early creep time (less than 300 seconds). This is due to the effect of ramp loading on creep deformation. Thus these results justify the time-independence of Poisson's ratio characterized from creep tests (constant load), as mentioned by Yi and Hilton (1990).

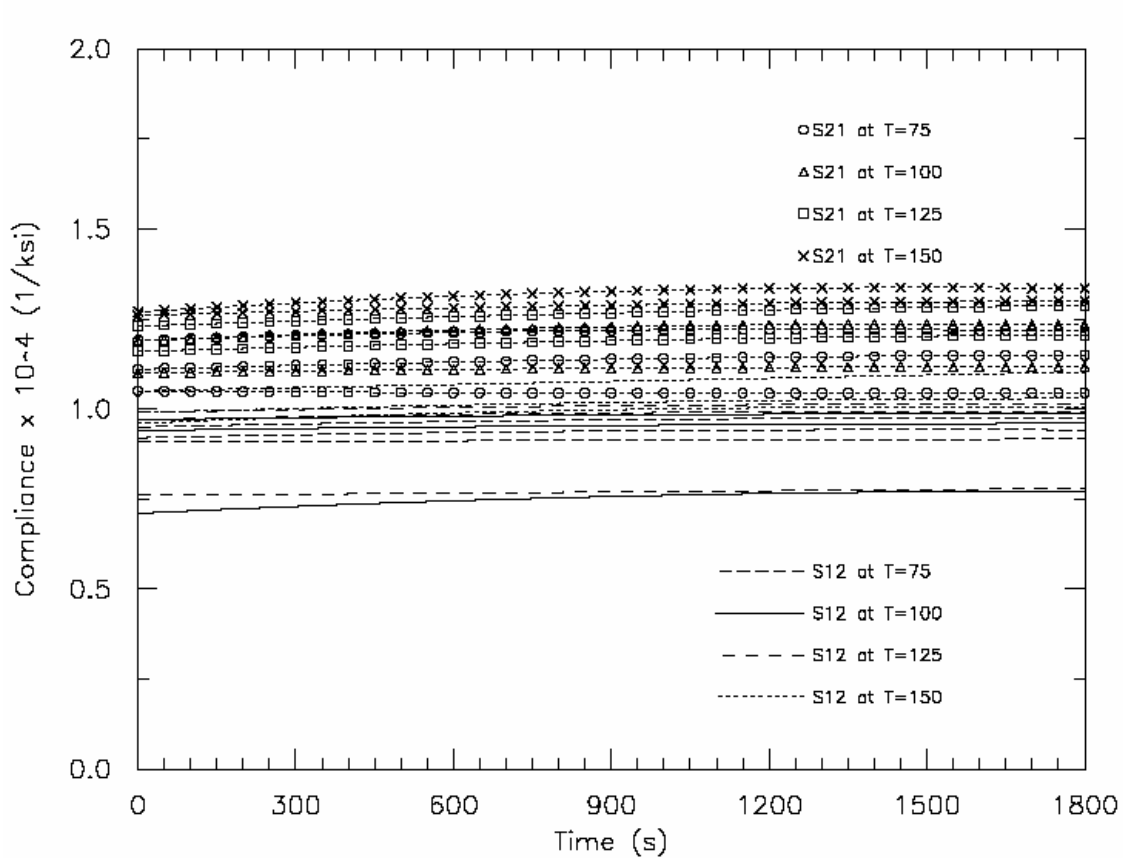


**Figure 2.15 Compliance ($S_{12}$ and $S_{21}$) of E-glass/vinylester specimens at temperatures 75°F-150°F and stress ratios of 0.2, 0.4 and 0.6.**

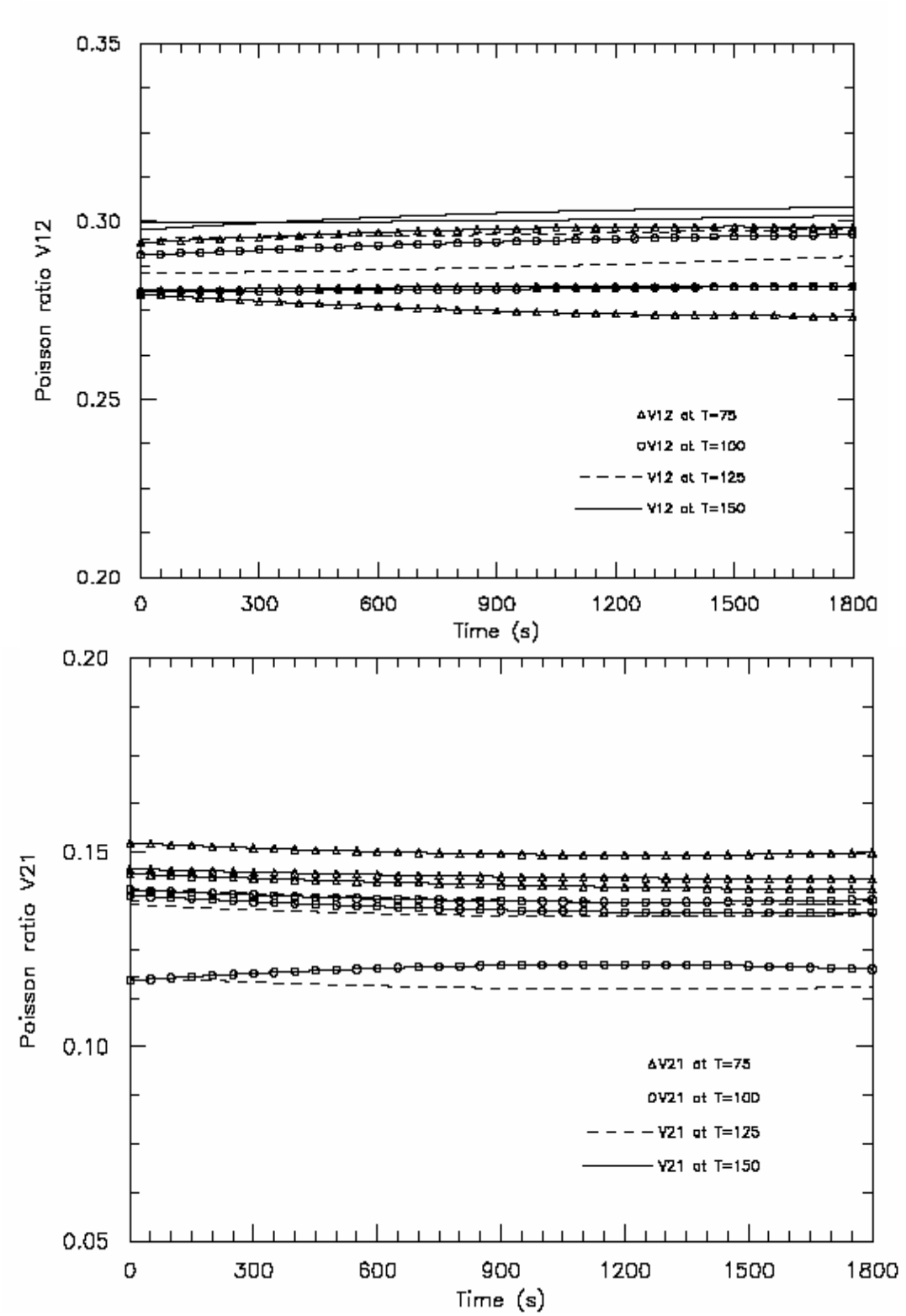


**Figure 2.16 a) Poisson's ratio $v_{12}$ b) Poisson's ratio $v_{21}$ at temperatures T=75°F-150°F and stress ratios 0.2, 0.4 and 0.6.**

# CHAPTER III

# TIME SCALING TECHNIQUES FOR PREDICTING LONG-TERM MATERIAL RESPONSES

Creep responses of materials tested at higher load levels or elevated temperatures show stronger time-dependent effects. Thus, creep testing at higher load levels or elevated temperatures can be used to create accelerated long-term material responses. Several accelerated characterization methods have been proposed to predict the long term material behaviors from short-term creep tests, using time shifting procedures. The time temperature superposition principle (TTSP) involves creating a master curve by shifting relaxation moduli or creep compliances from short-term tests at different temperatures to the ones at the reference temperature. The master curve represents long term material behaviors at the reference temperature. Another method of importance is the time stress superposition principle (TSSP). This method involves creating a master curve from short-term creep compliances or relaxation moduli at various stress levels. Short-term creep tests under combined stresses and temperatures have also been used to create a master curve for predicting long-term material responses. This method is known as the time temperature stress superposition principle (TTSSP). The above time scaling methods have been extensively applied by several researchers (Yeow et al., [20], Dillard et al., [49], Yen and Williamson, [17]) to predict the long term behavior of laminated composite materials. The frequency time transformation method (FTT) is another method that has been used to predict the long term behaviors. This method is applicable only within limited times, at which tertiary creep and/or micro-structural changes have not yet occurred.

The present chapter examines different time scaling techniques for predicting long-term material behaviors of the multi-layered composite systems, which belong to a class of thermo-rheologically complex materials (TCM). The TTSP and TSSP are first used to create master curves signifying long-term behavior at the chosen reference conditions.

Master curves are also created using the TTSSP with the lowest temperature and stress level chosen as the reference state. The long-term behaviors created from these methods are then compared. A sensitivity analysis is also performed on the calibrated material parameters used in the Schapery nonlinear viscoelastic equation to examine the effect of experimental data scatter on the material long term predictions.

## 3.1 TIME TEMPERATURE SUPERPOSITION PRINCIPLE

The time-temperature superposition principle (TTSP), proposed by Leaderman [50], has been extensively and successfully applied to characterize long-term behaviors of various viscoelastic materials. The method involves creating a master curve by shifting relaxation moduli or creep compliances from a short-term test duration at different temperatures to the ones at the reference temperature. The master curve is associated with a long-term material behavior at the chosen reference temperature. For a class of thermorheologically simple material (TSM), a master curve can be formed by horizontal shifting alone in a logarithmic time scale. The horizontal distance required to shift the short-term creep/relaxation responses to the master curve is equal to the log of *the inverse of the time-temperature shift factor* $a^T$ in Eq. (2.1). It should be emphasized here that the parameter $a_T$ is a time shift factor used to produce a creep/relaxation response at a non-reference temperature by performing time shifting of the response at the reference condition. For a class of thermorheologically complex material (TCM), vertical shifting of the short-term data prior to the horizontal shifting is required (Griffith et al., [15]; Tuttle, [16]; Yen and Williamson, [17]). This study includes both vertical and horizontal shifting in the TTSP to create master curves for predicting long-term material behaviors from a series of short-term creep tests at elevated temperatures. Vertical shifting is associated with instantaneous nonlinear stress and temperature dependent behaviors. The amount of vertical shifting is defined by a vertical shift factor:

$$a_v = \left(g_0^T - 1\right)D_0 \tag{3.1}$$

Figure 3.1 illustrates compression creep compliances of the E-glass/vinylester uniaxial specimens at load level 0.2 and several temperatures. A master curve at the reference temperature of 75°F (linear viscoelastic response) is created. The master curve represents creep behaviors up to 500 hours (1000 times longer than the conducted creep tests). The vertical shift factors are computed using the previously calibrated $D_o$ and $g_0^T$ parameters, reported in Table 2.6 and Figure 2.8f. The horizontal time shift factors for the uniaxial specimens are shown in Fig. 3.2a. The 500 hour creep strain data from the TTSP are comparable to the long-term creep tests of E-glass/vinylester specimens under load level 0.2 conducted by Scott and Zureick [32], as illustrated in Fig. 3.3a.

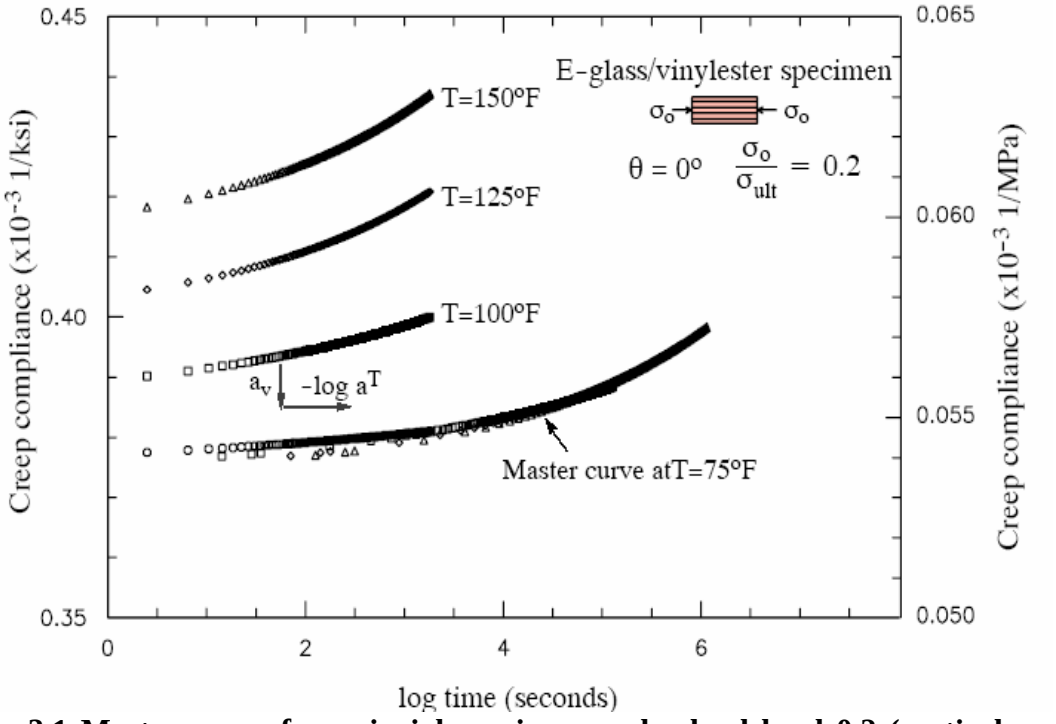


**Figure 3.1 Master curve for uniaxial specimen under load level 0.2 (vertical and horizontal shifting by TTSP)**

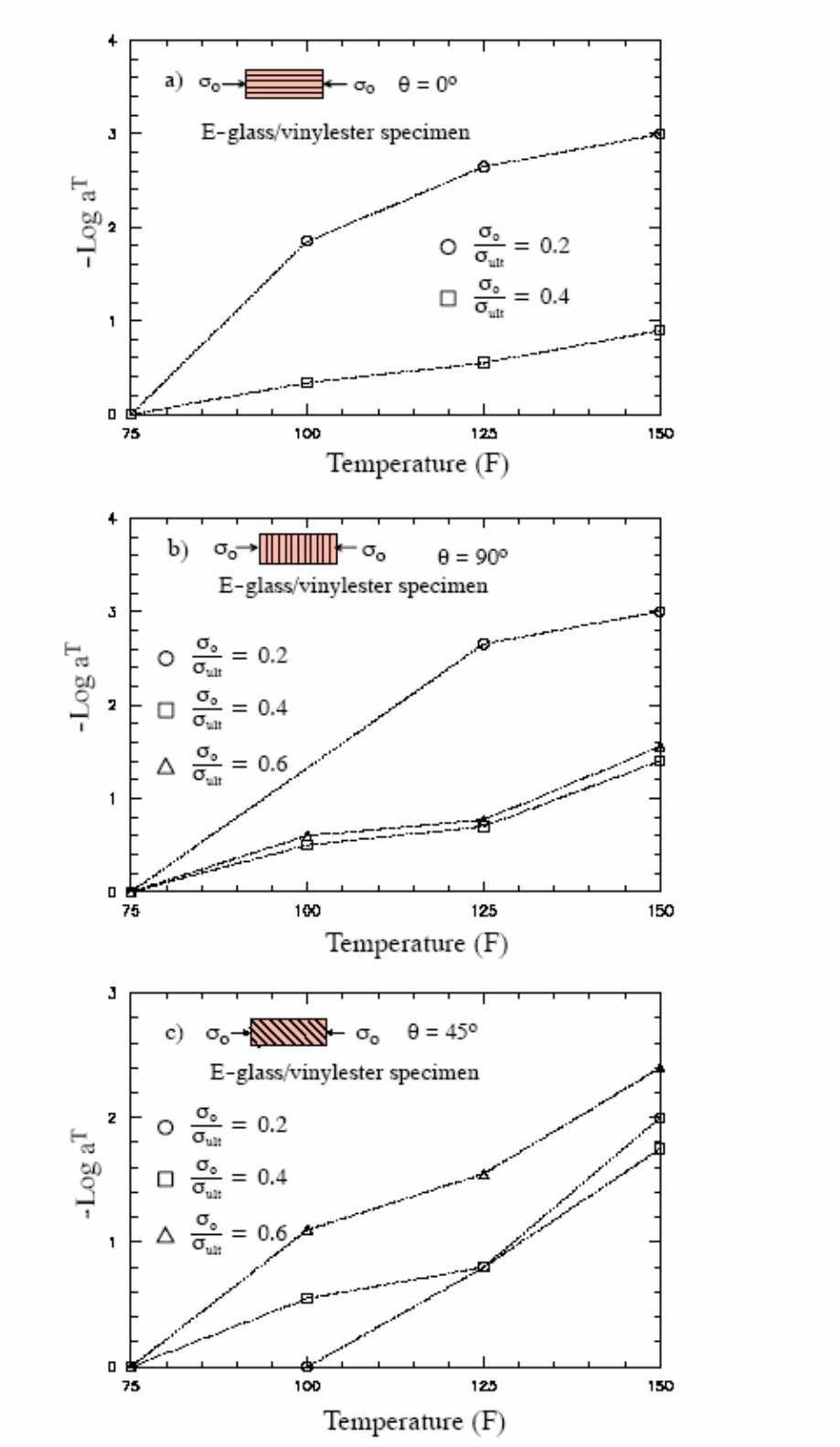


**Figure 3.2 Temperature shift factors for E-glass/vinylester composites.**

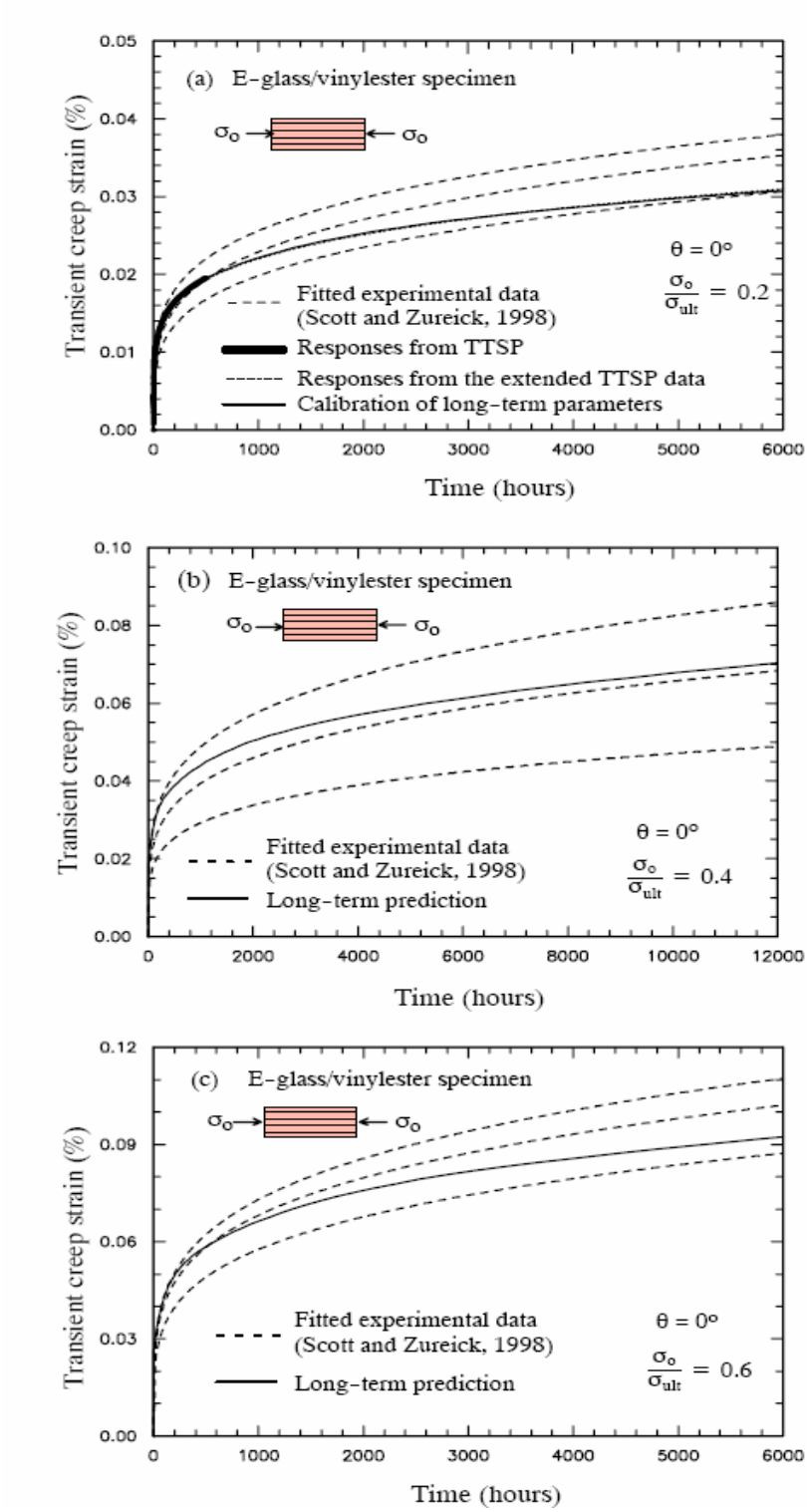


**Figure 3.3 Long term transient creep strains for uniaxial E-glass/vinylester coupons at T=75°F and load ratios a) 0.2 b) 0,4 and c) 0.6.**

In order to create longer time responses in the TTSP, short-term creep tests with longer time periods at several elevated temperature are required. Another way to extend long-term material behaviors is using extrapolation of the available creep data. The extrapolation technique was first used to predict long-term behaviors of metallic materials. Since it is usually easier to extend a curve if it is linear, an attempt is made to plot the data in such a way that it is linear or nearly linear. Equation (2.14) shows that the transient creep compliance is a linear function of time in double logarithmic scales. Thus, the master curve from the TTSP is plotted in double logarithmic scales, Figure 3.4, and expressed in terms of Eq. (2.14).

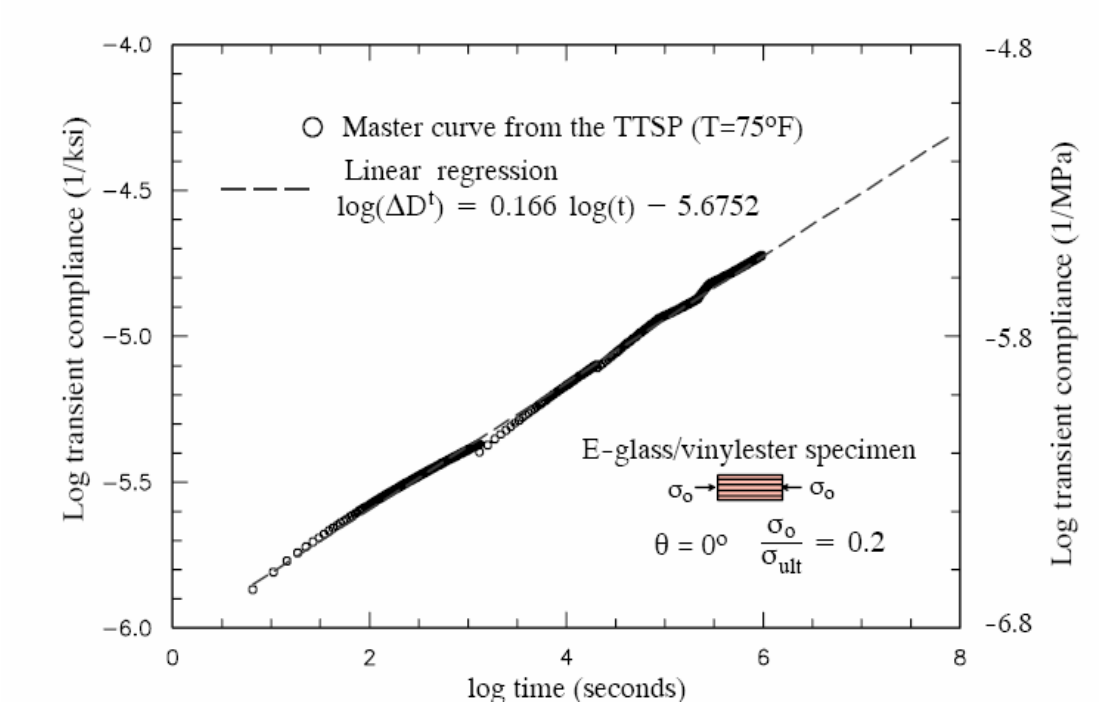


**Figure 3.4 Linear extrapolated master curve for uniaxial specimens under load level 0.2.**

This allows extending the material long-term prediction using a linear extrapolation function. Figure 3.3a presents a long-term response created from the TTSP and the linearly extended TTSP response, which predict 6000 hour compression creep tests of the E-glass/vinylester specimens of Scott and Zureick [32]. It should be noted that the linear extrapolation creep strains will only be valid for limited times, at which the tertiary creep stage has not been occurred yet or the materials have not exhibited microstructural changes. The time-dependent material parameters in Eq. (2.3) are recalibrated to match the long-term responses. The slope of log transient compliance in Figure 3.4 is a long-term exponent of the power law model (n=0.166), which is higher than the power law exponent from the short-term calibration (n=0.16), reported in Table 2.6. The long-term Prony coefficients with an hour unit time are then calibrated by matching the extended long-term responses, also shown in Figure 3.3a. The long-term Prony parameters are presented in Table 3.1. Using the calibrated long-term Prony series and stress-dependent parameters, the long-term creep strains for the E-glass/vinyleseter axial specimens under stress levels 0.4 and 0.6 are predicted, as illustrated in Figs. 3.3(b and c), respectively. The predicted creep strains are compared with the long-term data performed by Scott and Zureick [32].

**Table 3.1 Prony series coefficients for E-glass/vinylester from extended long term responses.**

| n | $\lambda_n$ (1/hr) | $D_n \times 10^{-6}$ (1/ksi) | | |
|---|---|---|---|---|
| | | 45° | 90° | 0° |
| 1 | 1 | 84.70 (12.29) | 69.50 (10.09) | 11.10 (1.61) |
| 2 | $10^{-1}$ | 11.20 (1.63) | 3.50 (0.51) | 0.19 (0.03) |
| 3 | $10^{-2}$ | 75.00 (10.89) | 45.00 (6.53) | 8.35 (1.21) |
| 4 | $10^{-3}$ | 103.00 (14.95) | 51.00 (7.40) | 9.60 (1.39) |
| 5 | $10^{-4}$ | 195.00 (28.30) | 81.50 (11.83) | 16.60 (2.41) |
| 6 | $10^{-5}$ | 274.00 (39.77) | 164.00 (23.80) | 23.60 (3.43) |
| 7 | $10^{-6}$ | - | - | 47.40 (6.88) |

The TTSP is also used to create master curves for the 45° off-axis and transverse E-glass/vinylester specimens at load ratio 0.2, 0.4, and 0.6 and reference temperature (75°F). The calibrated horizontal time shift factors are given in Figure 3.2. Due to the missing creep data for the transverse specimen under load ratio 0.2 and temperature 100°F, the master curve is created only by shifting the responses at temperatures 125°F and 150°F. The linear extrapolation is used to extend the master curve responses up to 25000 hours (nearly 3 years). The long-term Prony parameters, in Table 3.1, and the calibrated nonlinear parameters, in Figure 3.3, are then used to predict the long-term compliances for the axial, transverse, and 45° off-axis specimens. Figure 3.5 shows predictions of long-term creep compliances at load level 0.4. Very good predictions are shown for the axial and transverse specimens, while some deviation is apparent for the shear (45°) specimens and is amplified with longer time. This may be due to highly nonlinear behavior exhibited in 45° off axis specimens; thus, long-term responses created using linear extrapolation may lead to significant errors.

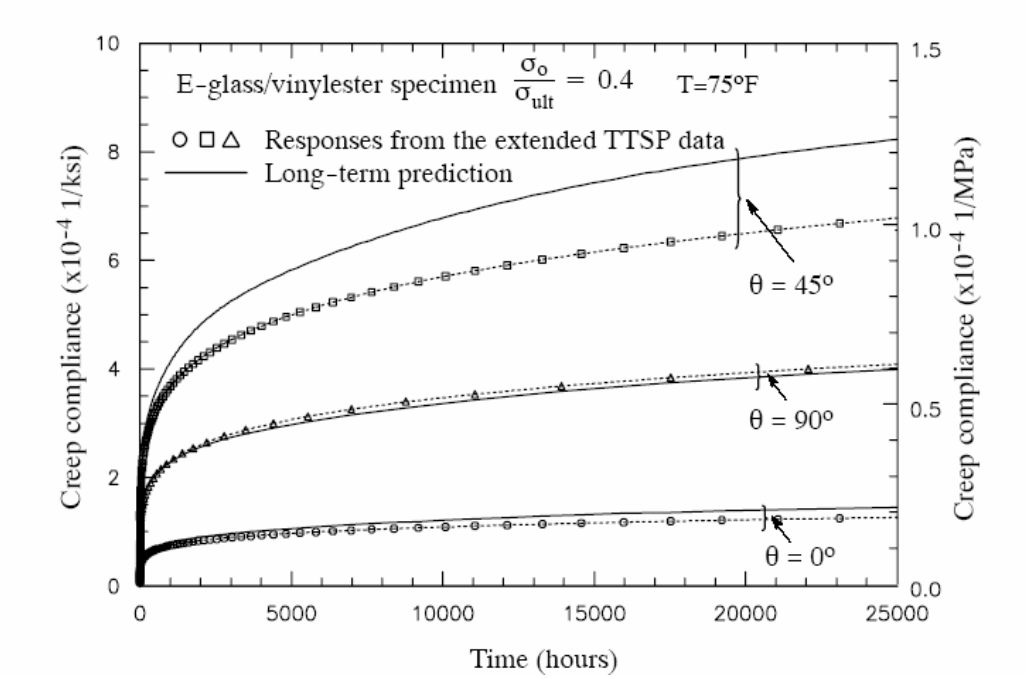


**Figure 3.5 Long term responses for off axis E-glass/vinylester specimens at T=75°F and load level 0.4.**

The TTSP is also applied to create master curve for 45$^{o}$ off-axis and transverse E-glass/polyester specimens under various stress levels. The 45$^{o}$ off-axis specimens failed at 0.6 stress levels under high temperatures, thus the master curve is not created for the 0.6 load ratio. The master curve under load ratio 0.2 for 45$^{o}$ off-axis specimen is shown in figure 3.6 in double logarithmic scales. The master curve for the 45$^{o}$ off-axis specimen under load ratio 0.4 and transverse degree specimens under load ratios 0.2 to 0.6 are given in appendix-B. The calculated horizontal shift factors are shown in figure 3.7.

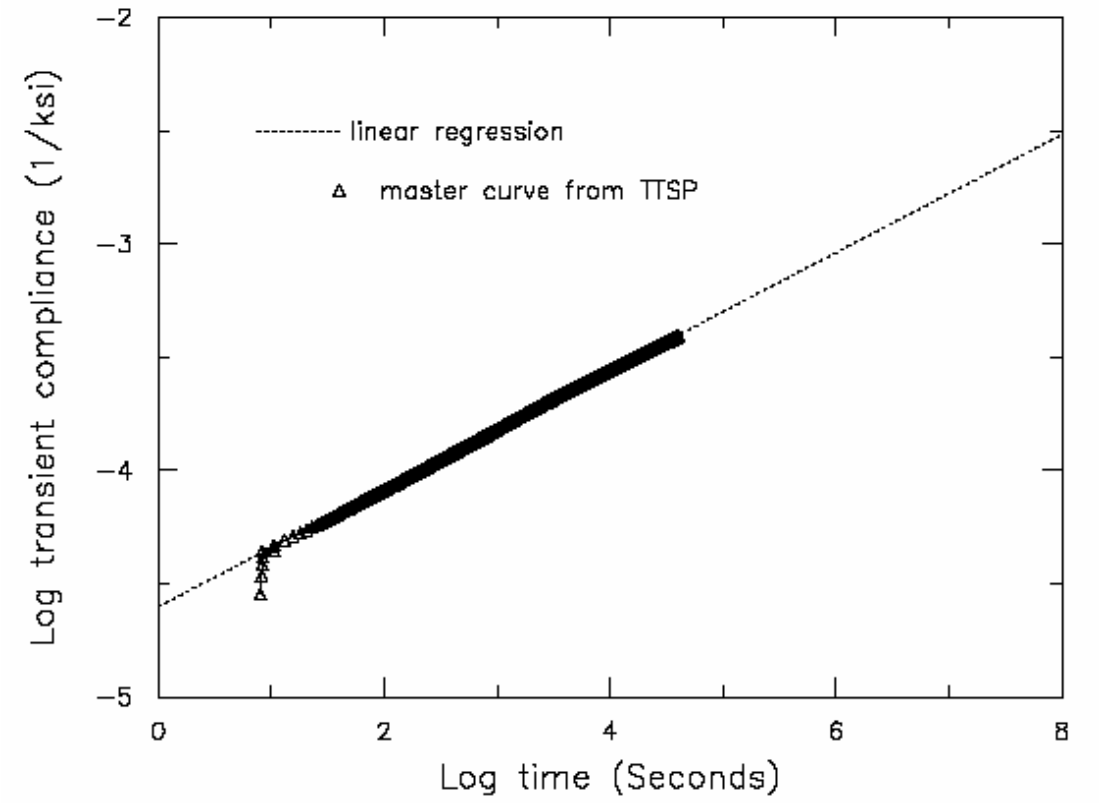


**Figure 3.6 Master curve for the 45° off-axis E-glass/polyester specimens under load level 0.2.**

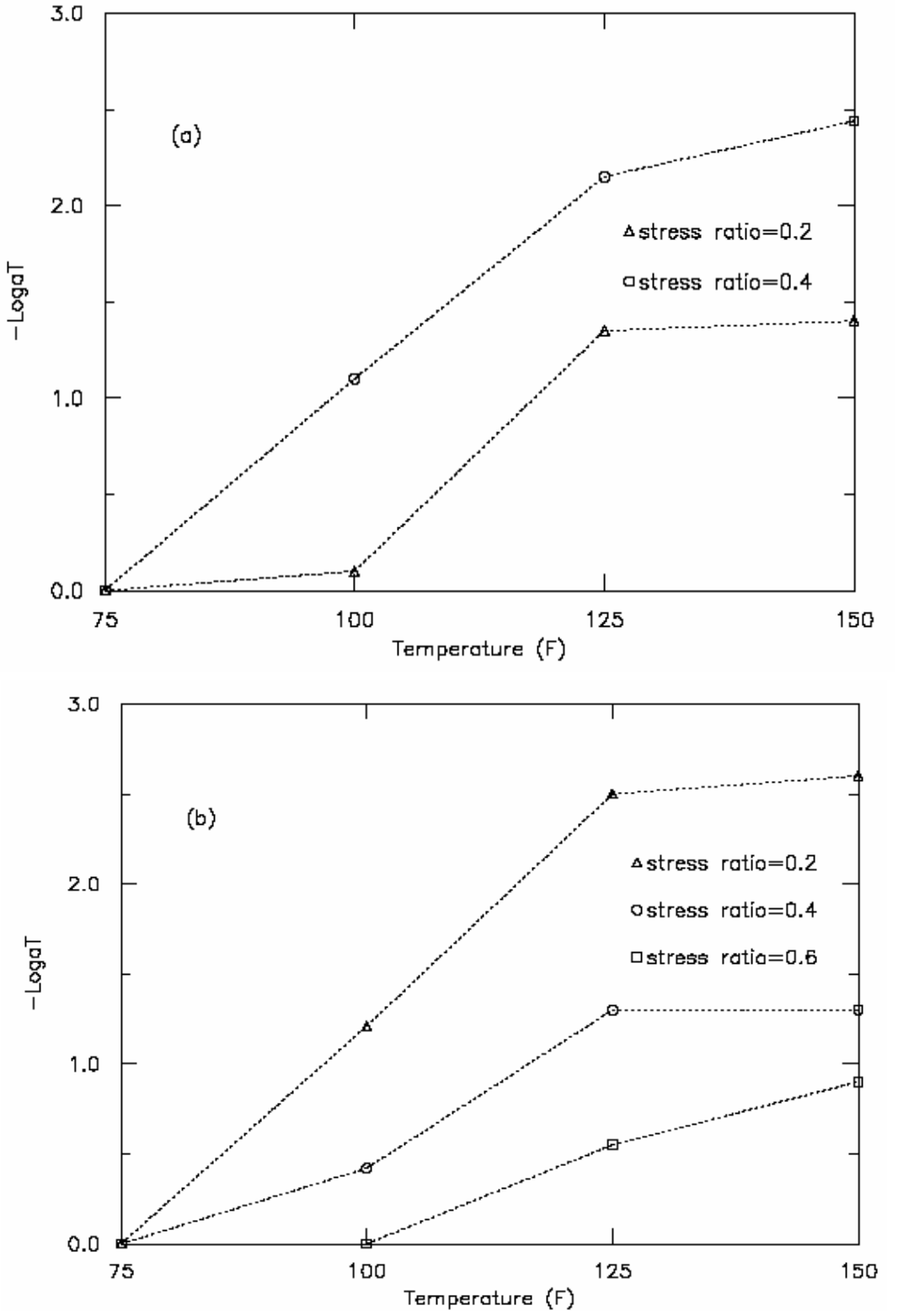


**Figure 3.7 Time-temperature shift factors for the (a) 45° off-axis and (b) transverse E-glass/polyester specimens**

The master curve is extended using linear extrapolation as elucidated for the E-glass/vinylester specimens. The response from the extended master curve for the 45$^{o}$ off-axis and transverse E-glass/polyester specimens are shown in figures 3.8 and 3.9, respectively.

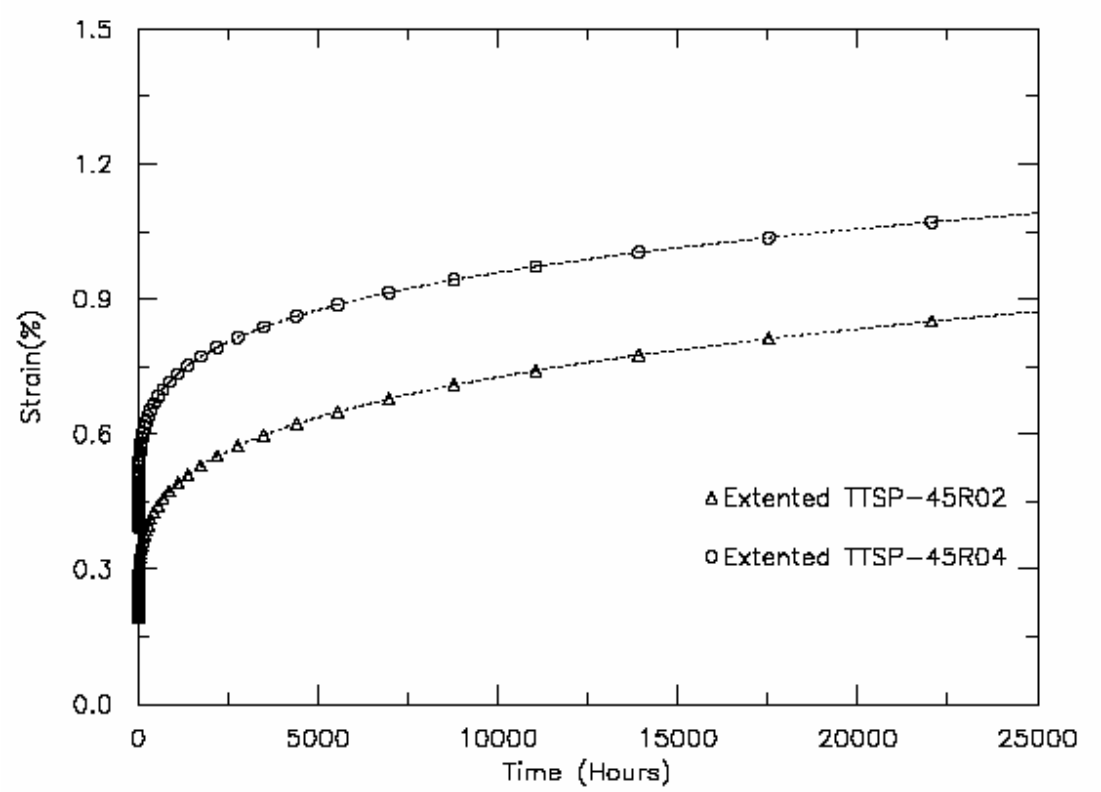


**Figure 3.8 Long-term strain responses for the 45° off-axis E-glass/polyester composites under load levels 0.2 and 0.4 at T=75°F.**

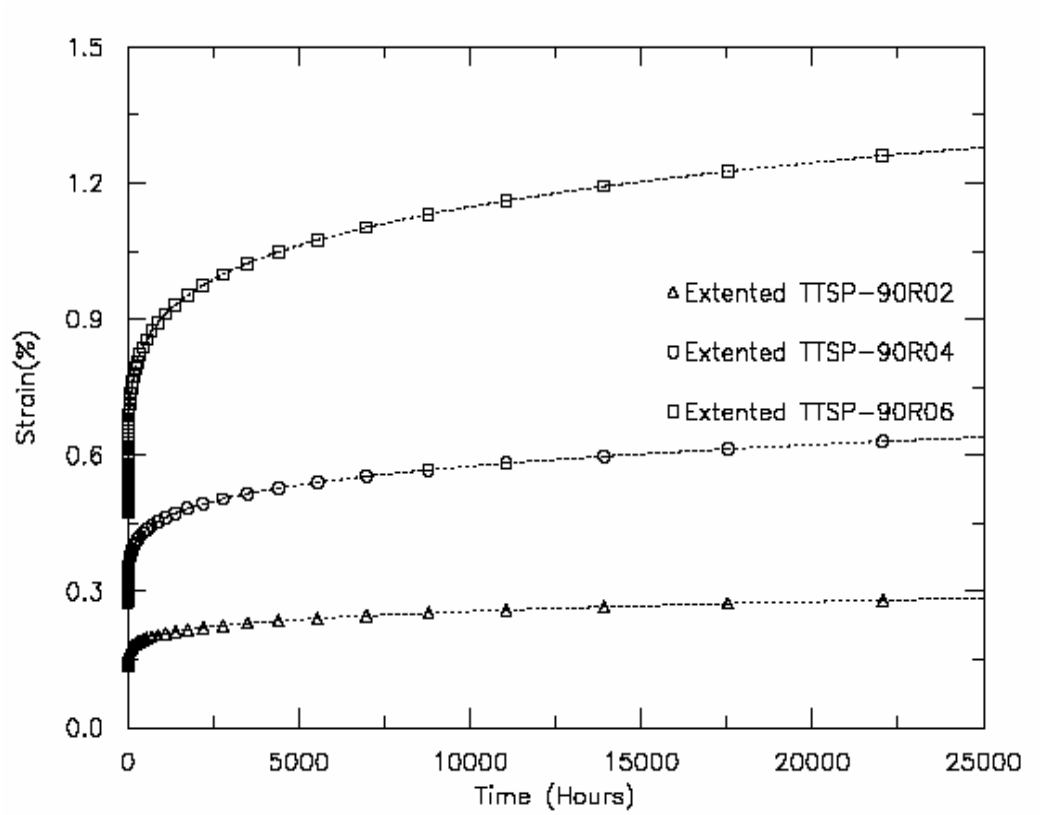


**Figure 3.9 Long term strain responses for the transverse E-glass/polyester composites under load levels 0.2, 0.4 and 0.6 at T=75°F.**

## 3.2 TIME STRESS SUPERPOSITION PRINCIPLE

The time stress superposition principle (TSSP) is another method for creating a master curve from a series of short term creep or relaxation tests at different stresses. The master curve is associated with a long-term material behavior at the chosen reference stress level and fixed environmental conditions. The horizontal distance required to shift the short-term creep/relaxation responses to the master curve is equal to the log of *the inverse of the time-stress shift factor* $a^{\sigma}$ in eq. (2.2). For E-glass/vinylester and E-glass/polyester specimens, both vertical and horizontal shifting in the TSSP are performed due to the stress-dependent material responses. Vertical shifting associated with instantaneous nonlinear stress dependent behaviors for TSSP is given by:

$$a_v = (g_0^{\sigma}-1)D_0 \qquad (3.2)$$

Four master curves are created with the reference stress level of 20% of the ultimate failure stress at temperatures from 75°F to 150°F for each off-axis E-glass/vinylester and E-glass/polyester specimens. The master curve obtained by shifting the transient creep compliances from the higher stress levels at fixed temperatures (75°F) for the E-glass/vinylester and E-glass/polyester specimens are shown in figure 3.10 (a and b) and 3.11. The master curve represents creep behaviors up to 300 hours (600 times longer than the conducted creep tests) for the E-glass/vinylester specimens. The vertical shift factors are determined using the previously calibrated $D_o$ and $g_0^{\sigma}$ parameters. The horizontal shift factors used for creating the long term compliances are shown in figure 3.13 (a and b) for the E-glass/vinylester specimens and 3.14 for the E-glass/polyester specimens. Linear extrapolation of the master curve is performed by the procedure explained in section 3.1. The extrapolated master curves are also shown in the figures 3.10 and 3.11 by the dotted lines. The rest of the master curves at different temperatures for the E-glass/vinylester and E-glass/polyester specimens are given in Appendix-B. While the stress-dependent material parameters were calibrated from various stress levels at T=75°F, the actual stresses during the testing of the transverse E-glass/polyester specimens at 125°F and 150°F varied up to 6% from the applied stress ratio. In this study, instead of determining exact values of the nonlinear stress-dependent parameters based on the applied stresses at 125°F and 150°F, the nonlinear parameters are calculated based on the stress magnitudes at T=75°F. For the $45^o$ off-axis E-glass/polyester systems, fluctuation of stresses during testing was very significant, even at the room temperature. As a result, the transient compliances at higher load levels after vertical shifting are lower than the one at the reference stress. Figure 3.12 shows the transient compliances (in logarithmic scale) for the 45° off-axis E-glass/polyester specimens, which indicates lower compliances for higher stress ratios. In order to

properly construct the master curves by TSSP, the stress dependent parameters should be determined exactly for the applied loads instead of using the stresses at 75°F and constant load should be maintained through the tests. However, in this study the testing system that was used has lower sensitivity. Therefore, under relatively low applied loads, as in the case of the polyester systems, significant load variations were exhibited.

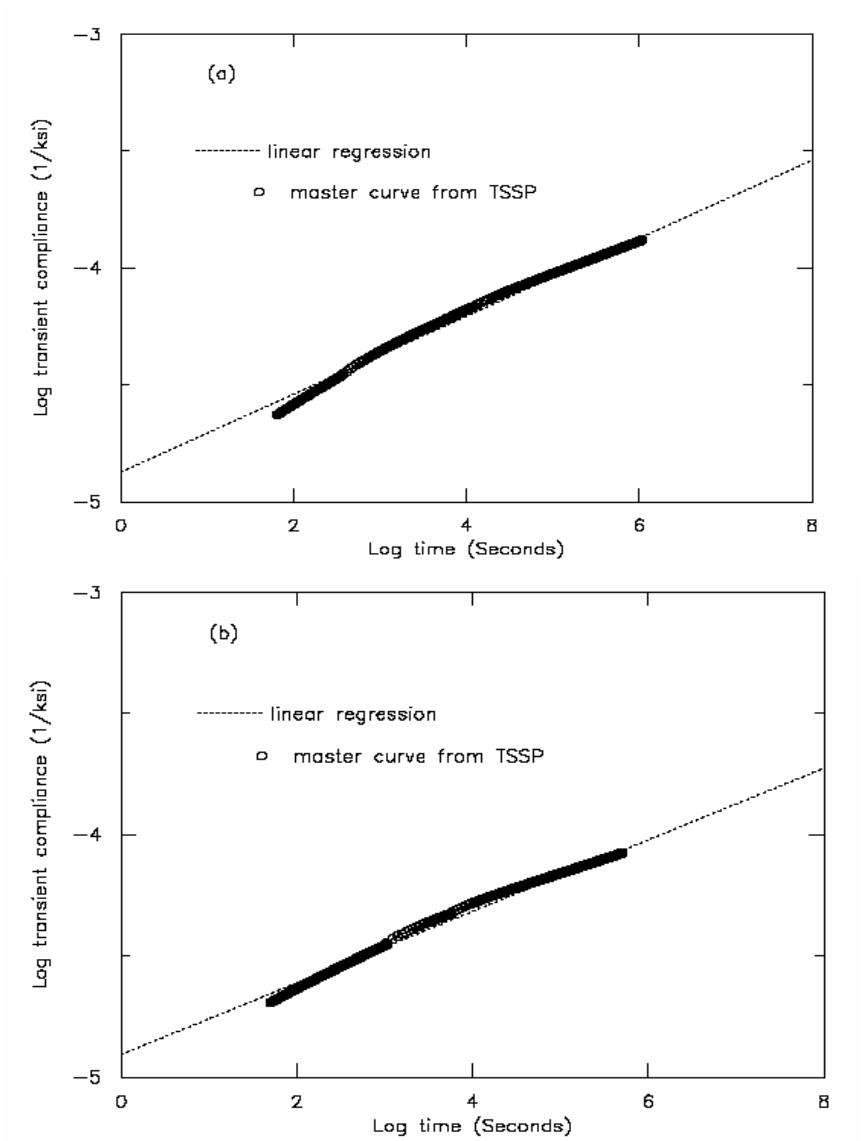


**Figure 3.10 Master curve for the (a) 45° off-axis and (b) transverse E-glass/vinylester specimens at T=75°F.**

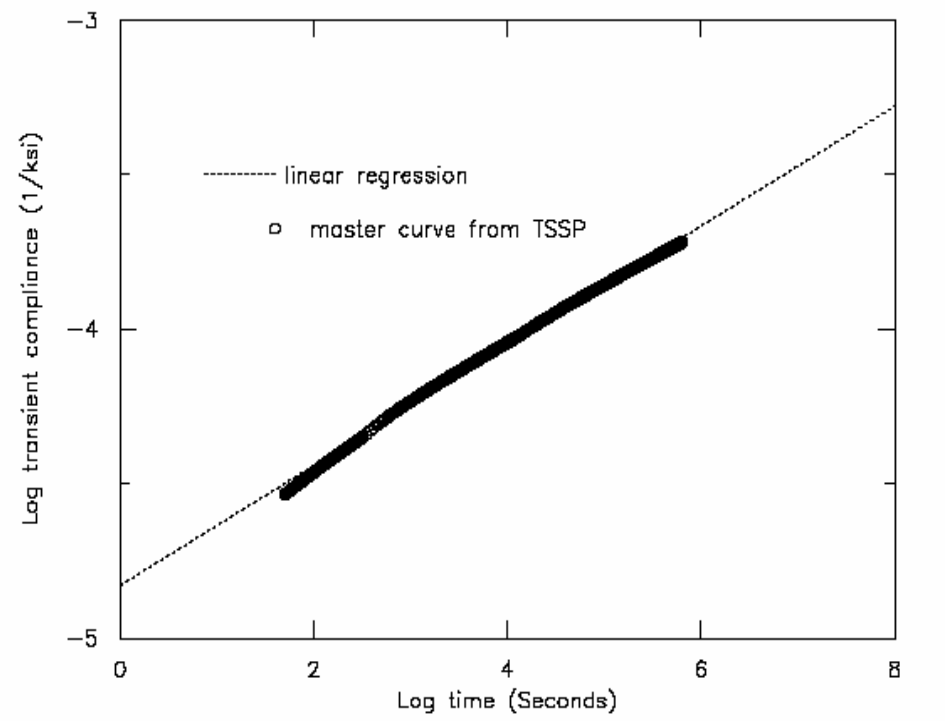


**Figure 3.11 Master curve for the transverse E-glass/polyester specimens at T=75°F.**

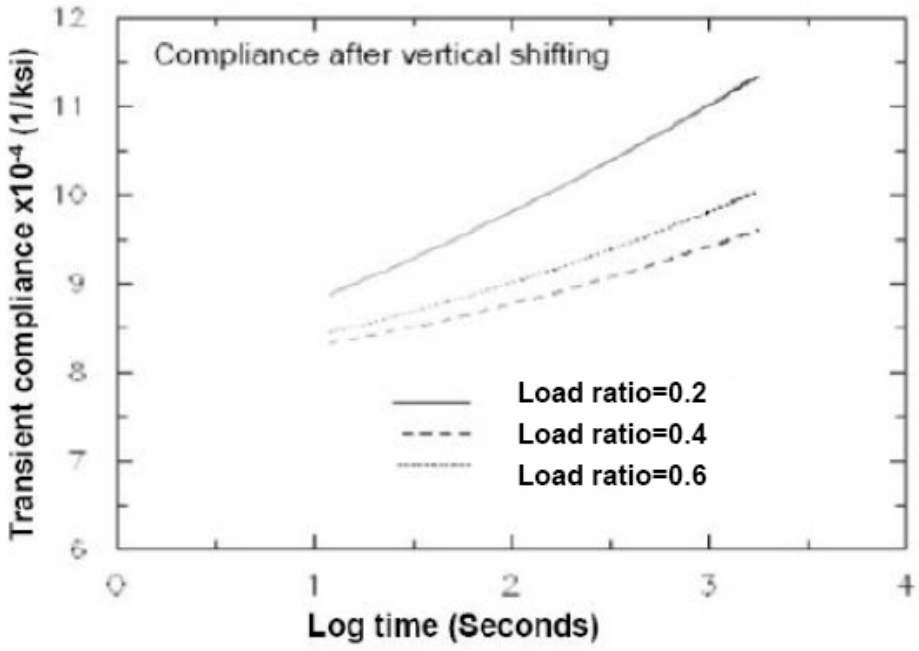


**Figure 3.12 Compliance after vertical shifting for the 45° off-axis E-glass/polyester specimens at T=75°F.**

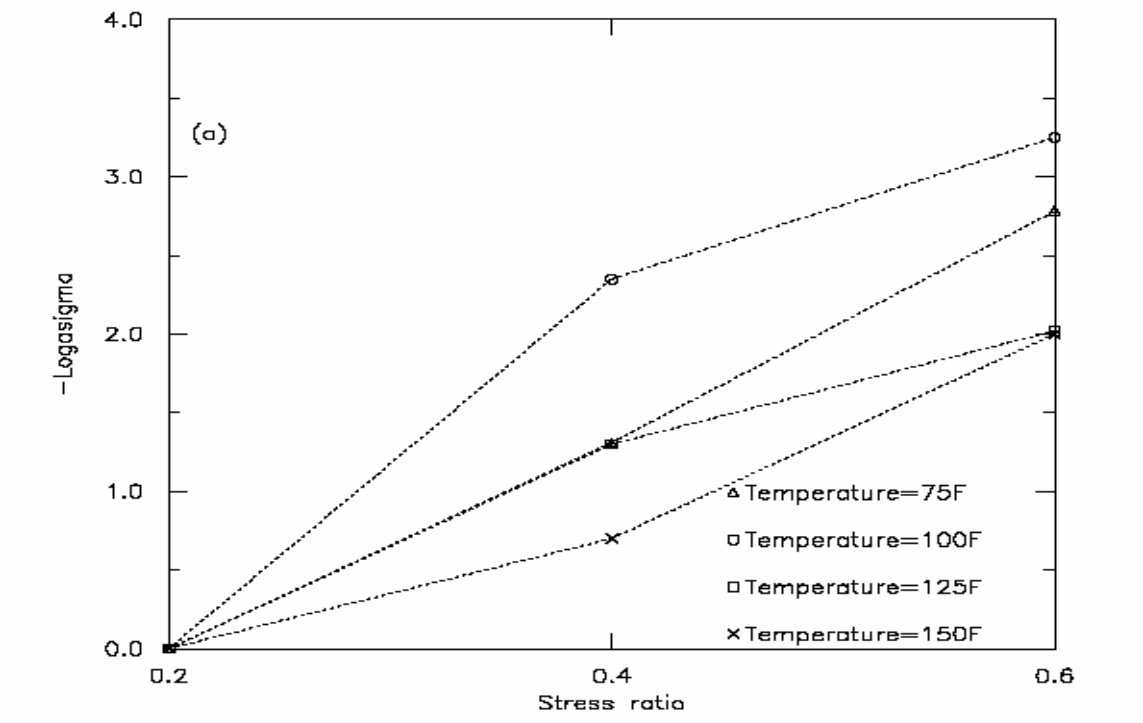


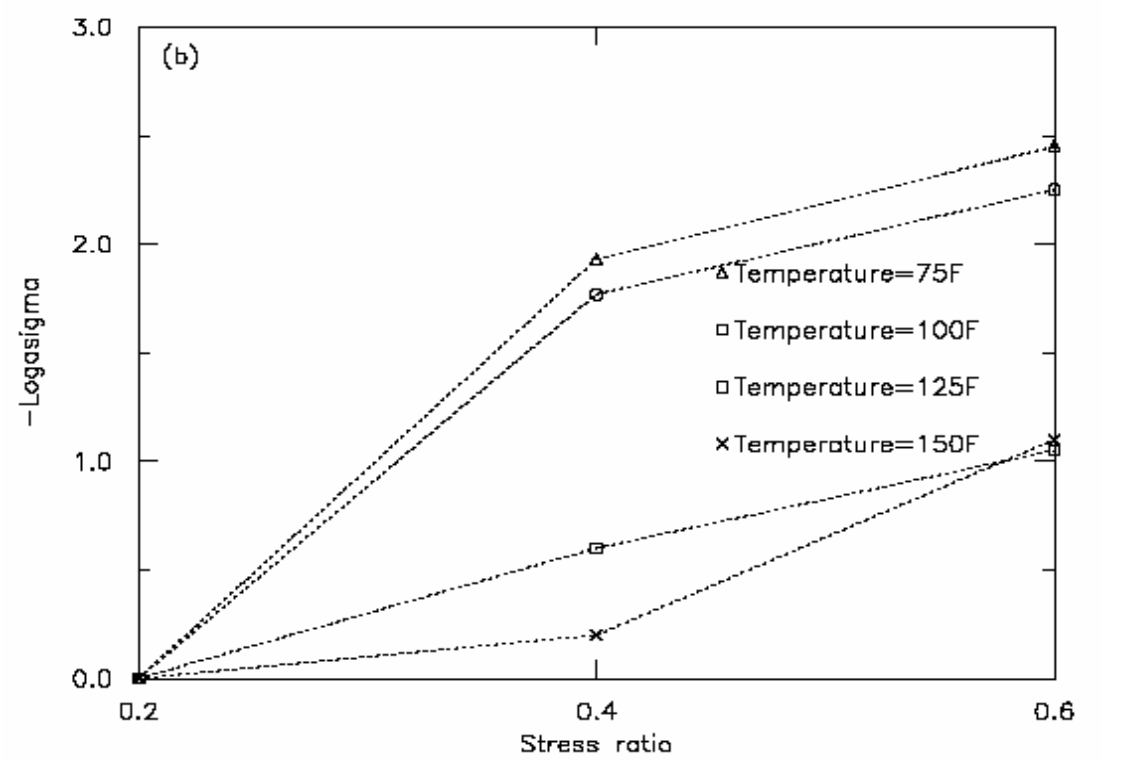


**Figure 3.13 Time-stress shift factors for the a) 45° off-axis and b) transverse E-glass/vinylester specimens.**

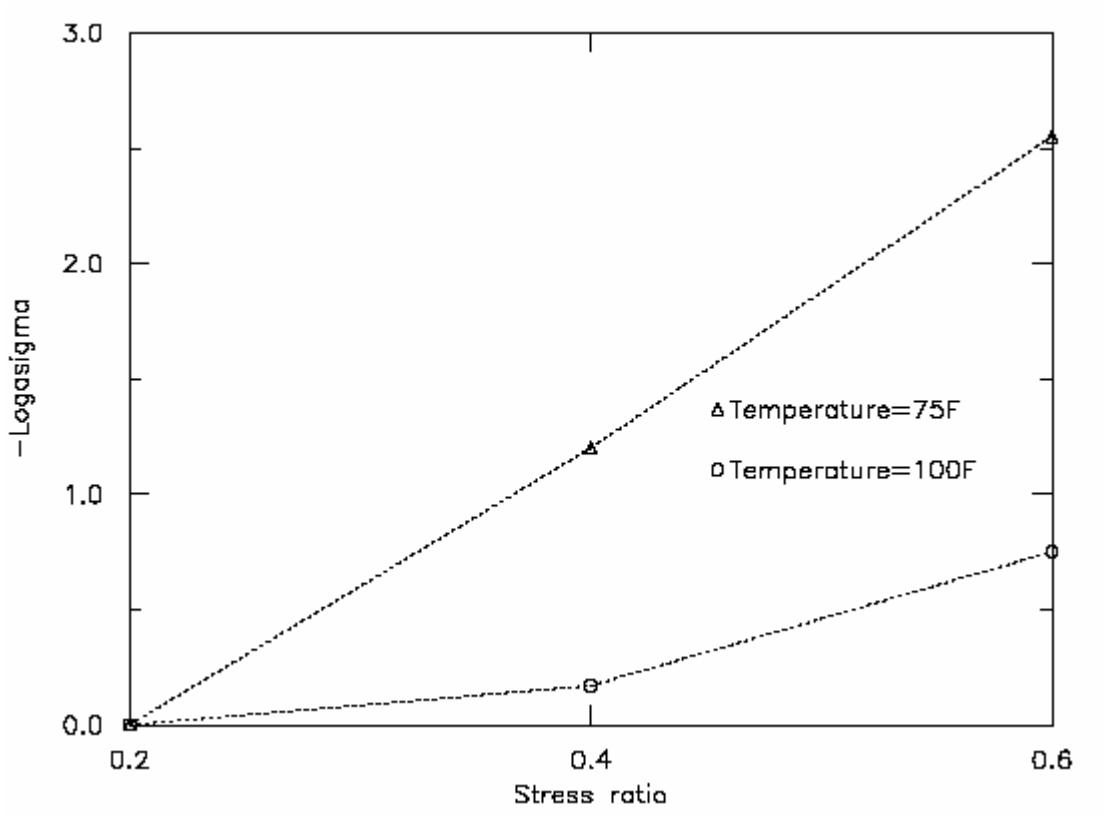


**Figure 3.14 Time-stress shift factors for the transverse E-glass/polyester specimens.**

Figure 3.15 shows the long term responses from the extended master curves for the transverse and 45° off-axis E-glass/vinylester specimens at various temperatures. Figure 3.16 shows the response from the extended master curves for the E-glass/polyester transverse specimens at 75 and 100°F.

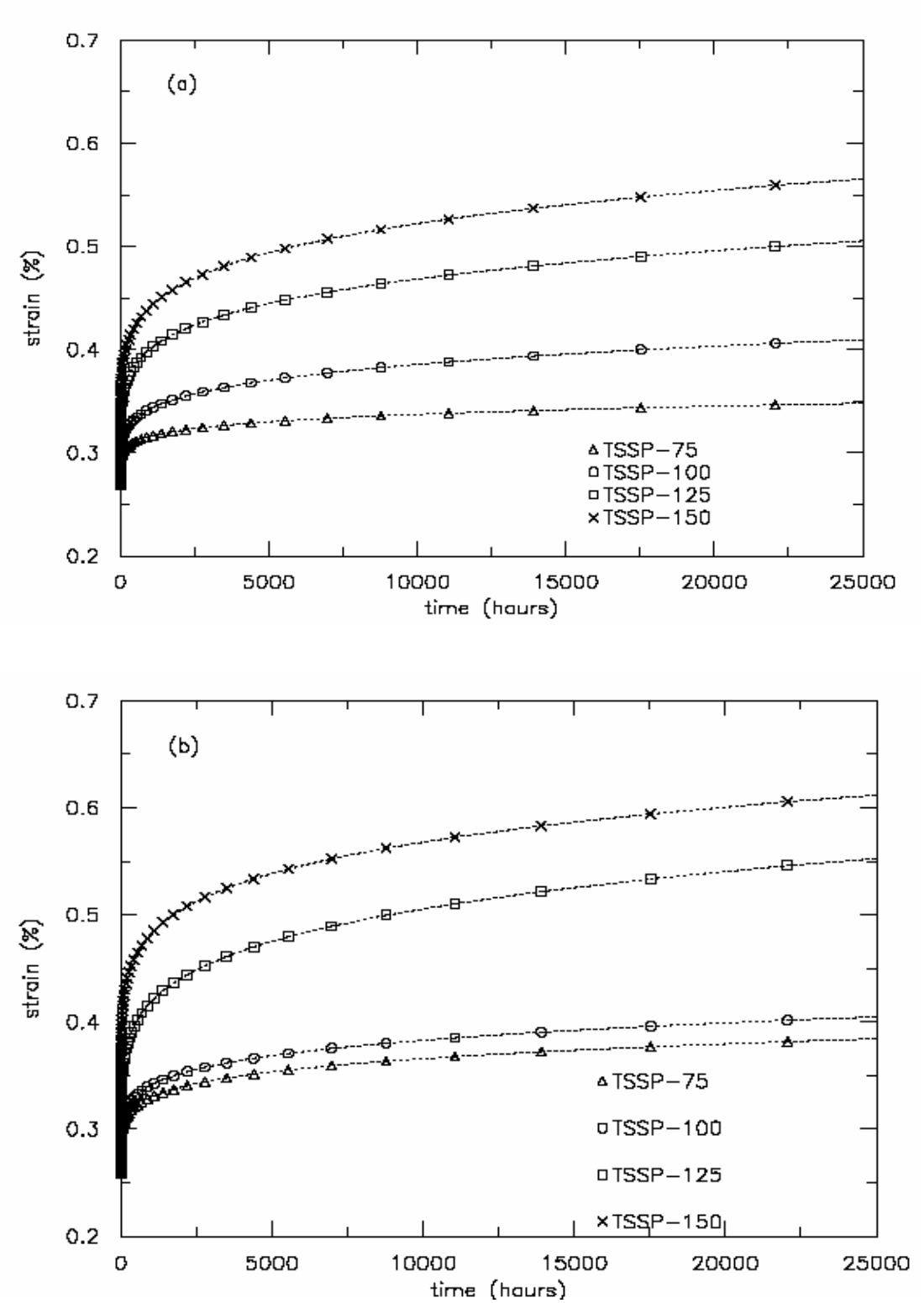


**Figure 3.15 Long term strain responses under load level 0.2 for the a) transverse and b) 45° off-axis E-glass/vinylester specimens.**

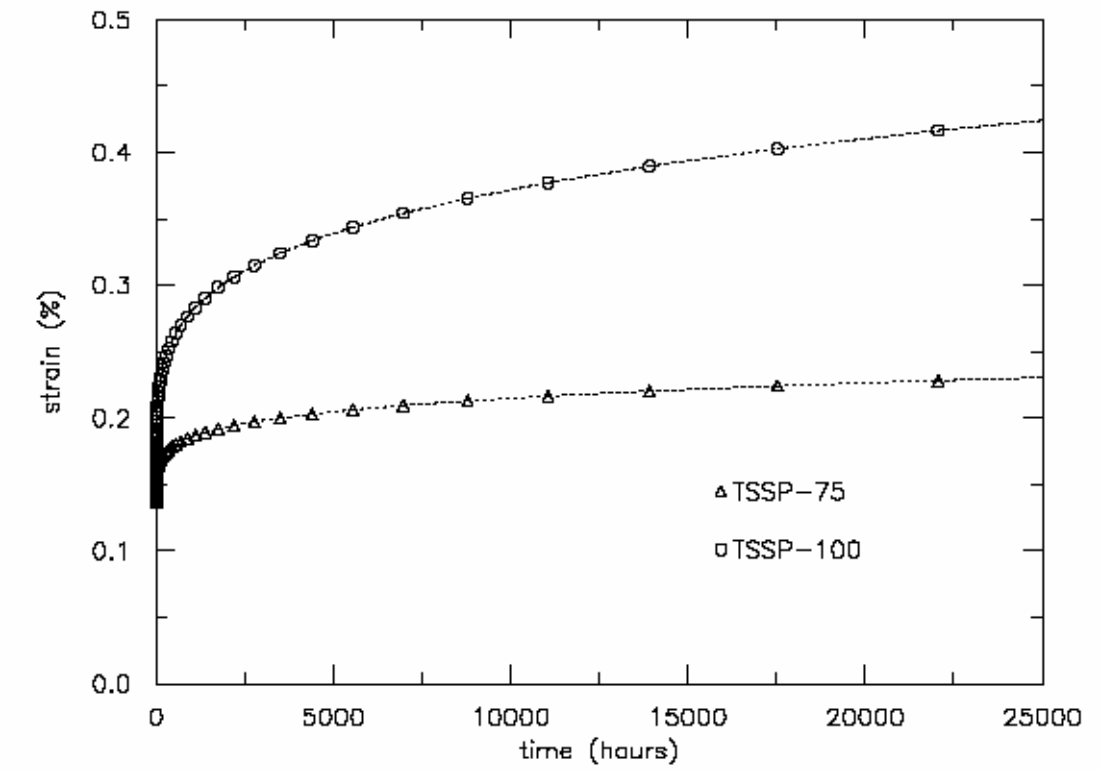


**Figure 3.16 Long term strain responses under load level 0.2 for the transverse E-glass/polyester specimens.**

## 3.3 TIME TEMPERATURE STRESS SUPERPOSITION PRINCIPLE

The time temperature stress superposition principle (TTSSP) is another time-scaling technique used for obtaining long term responses from short term creep tests. Unlike TTSP or TSSP which take into consideration either elevated temperature or stress levels to obtain long term response, TTSSP utilizes both the temperature and stress variation to obtain long term responses. The method of shifting compliances in the time scale is similar to the TTSP and TSSP. The vertical shifting include the effect of stress and temperature, which is defined by:

$$a_v = (g_0^{\sigma}-1)\,(g_0^{T}-1)D_0 \qquad (3.3)$$

For performing the TTSSP, a master curve is created either by first performing a time-temperature shifting (as described in section 3.1 for TTSP) and then a time-stress shifting (described in section 3.2) on the master curves obtained. Similar master curves are shown by first performing a time-stress shifting and then a time-temperature shifting on the master curves generated. Figure 3.17 shows the master curve obtained using the TTSSP on the 45° off-axis E-glass/vinylester specimen at reference temperature 75°F and load ratio 0.2. Master curves created for other off-axis angles for the E-glass/vinylester and E-glass/polyester specimens are provided in appendix-B.

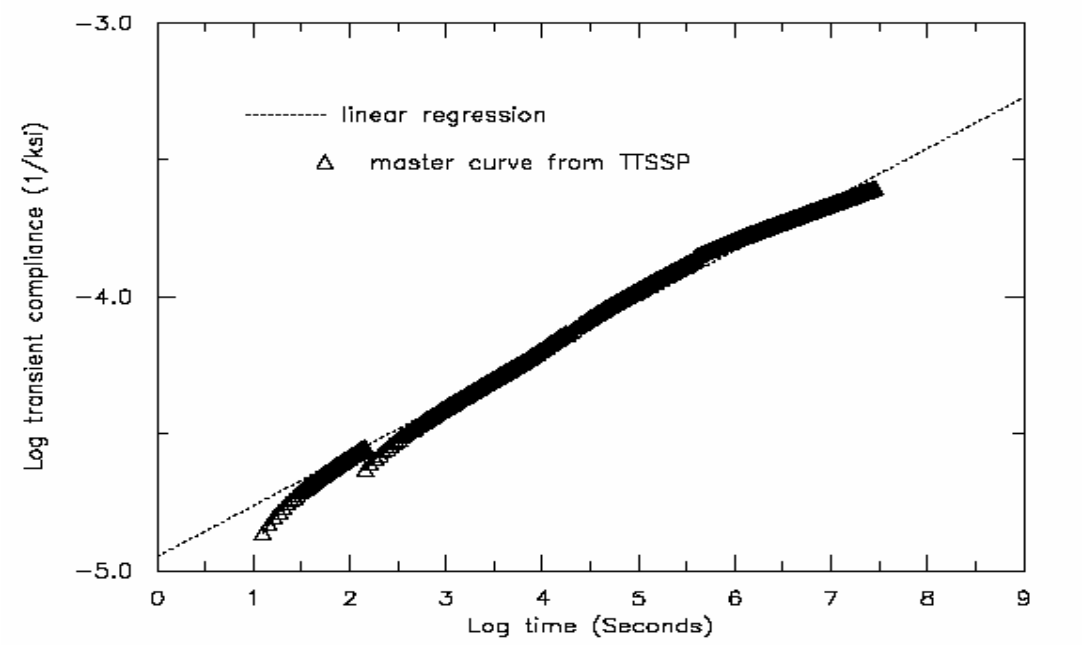


**Figure 3.17 Linear extrapolated master curve for 45° off-axis E-glass/vinylester specimens under reference state of T=75°F and stress level 0.2.**

The master curve created using the TTSSP predicts creep response up to 8000 hours. A comparison is made between the long term creep strain obtained by TTSP, TSSP and TTSSP. Such a comparison can be made only when the reference condition of temperature and stress is the same for the three types of time scaling techniques used. Thus to validate the types of time scaling techniques used, the strain response from the reference stress state of 20% of the ultimate failure strength and room temperature, is chosen for comparison. The response under the reference condition from the TTSP, TSSP and TTSSP are shown in figures 3.18 and 3.19 for E-glass/vinylester and E-glass/polyester specimens.

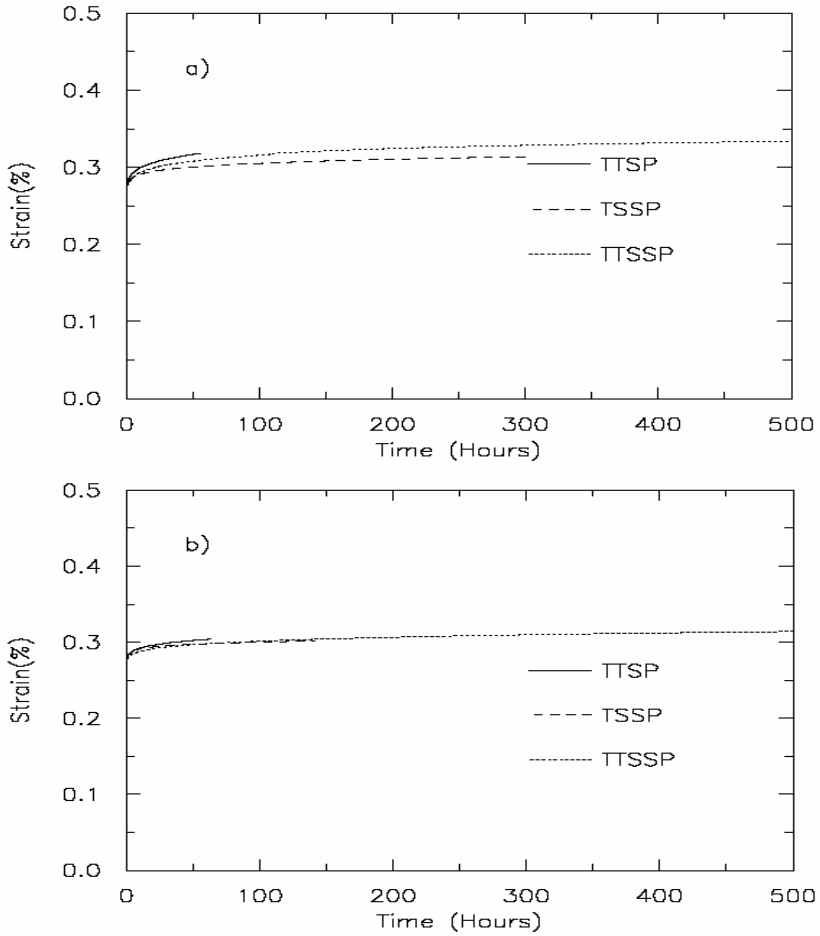


**Figure 3.18 Long term strain responses from TTSP, TSSP and TTSSP under reference load level 0.2 and reference temperature 75°F for a) the 45° off-axis E-glass/vinylester specimens b) transverse specimens.**

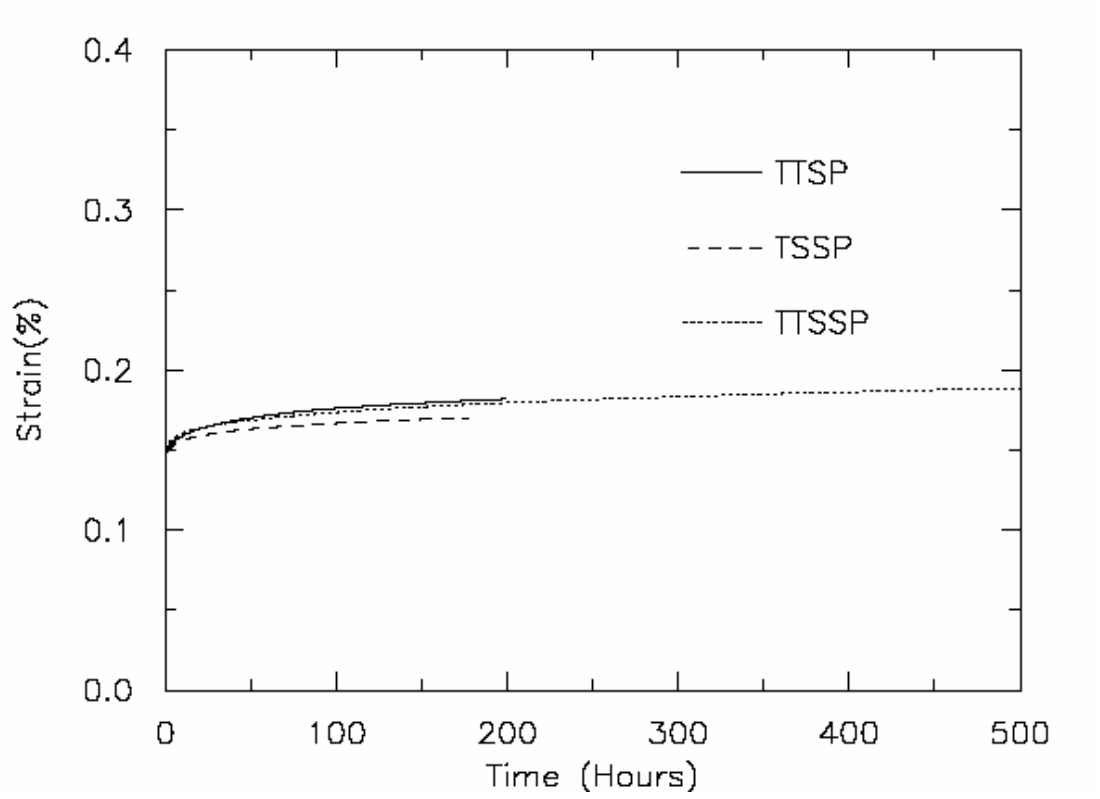


**Figure 3.19 Long term strain responses from TTSP, TSSP and TTSSP under reference load level 0.2 and reference temperature 75°F for the transverse E-glass/polyester composite from extrapolated master curves.**

It is seen from figures 3.18 and 3.19 that the TTSSP can be used to obtain creep responses with longer time duration than the ones obtained by TTSP or TSSP. In the above figures, the master curves from the TTSSP is plotted for only 500 hours even though the actual responses reach up to 8000 hours. The long-term strains from the TTSSP for the transverse E-glass/vinylester specimens provided more than 700 hours of creep response, while the ones for the 45° off-axis E-glass/vinylester specimens provided 8000 hours of creep response.

Long-term strain responses obtained from the linear extrapolation of the master curves from TTSP, TSSP and TTSSP are presented in figures 3.20 and 3.21. Long term responses from the extended TTSP and TSSP are also shown for comparison in figure (3.20 and 3.21). It is seen that the maximum difference in long-term responses obtained by the three methods is only 0.1% over a period of 25,000 hours. It is also seen that the small variation in figure 3.18 and figure 3.19 deviate larger at longer time duration. This shows sensitivity of the exponent parameters in the time dependent compliances.

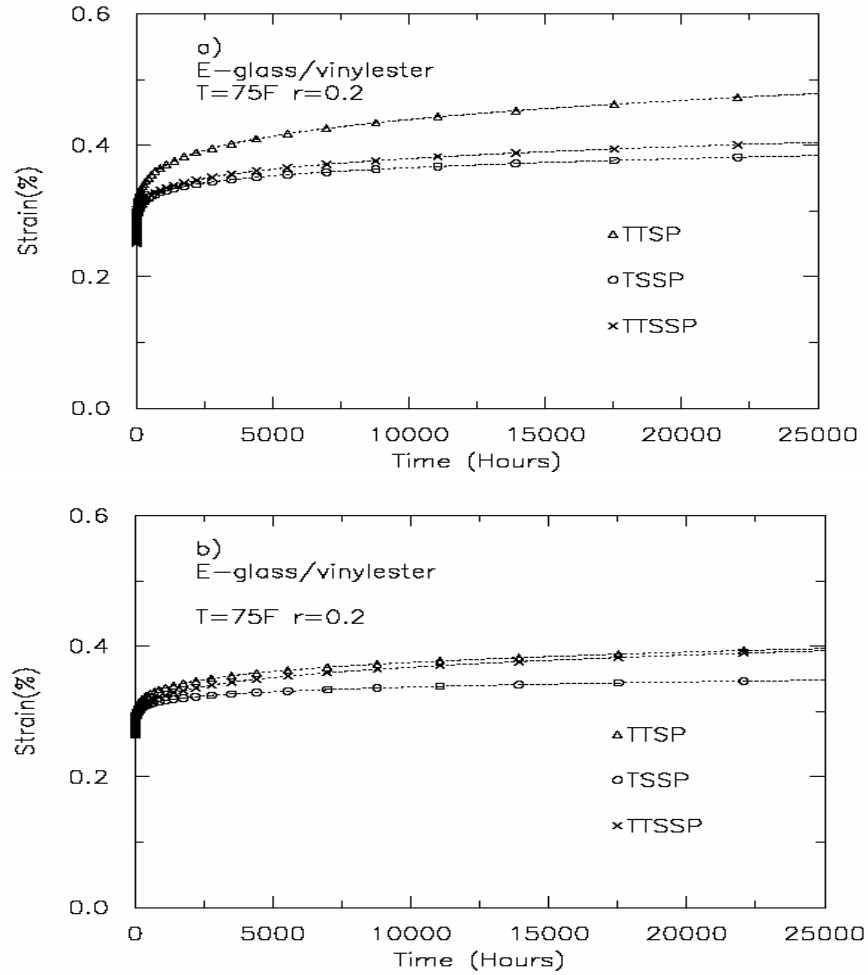


**Figure 3.20 Long term strain response from extrapolated master curves under reference load level 0.2 and reference temperature of 75°F for the a) 45° 0ff-axis E-glass/vinylester specimens b) transverse specimens.**

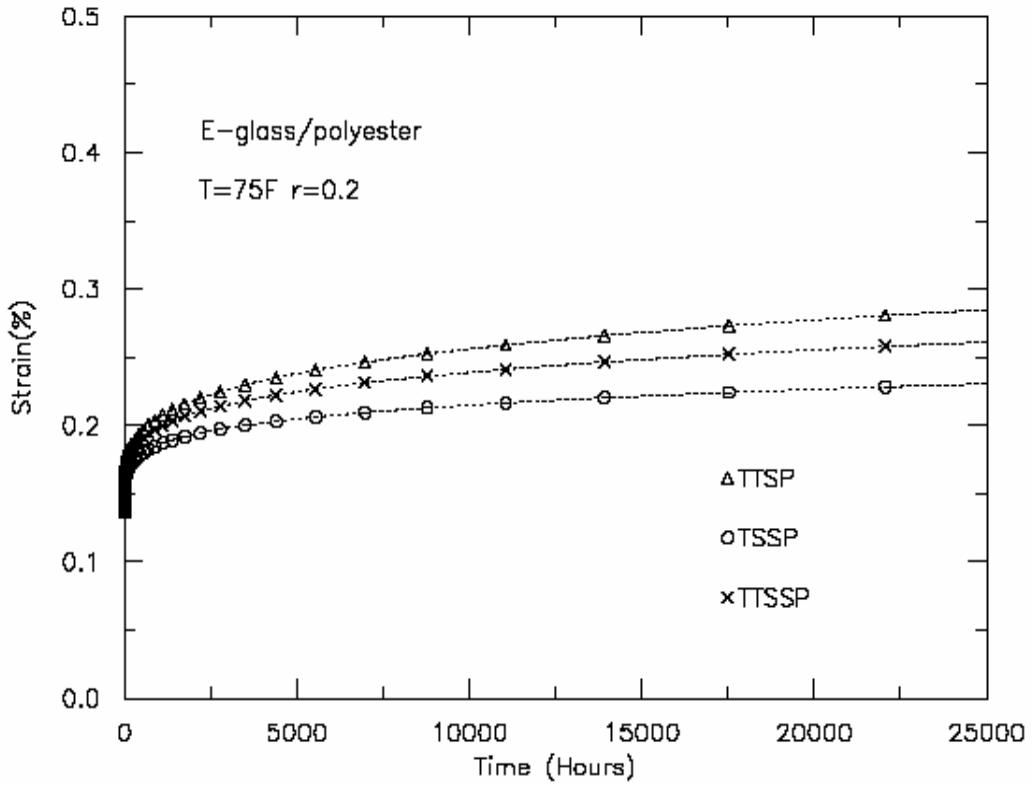


**Figure 3.21 Long term strain response from extrapolated master curves under reference load level 0.2 and reference temperature of 75°F for the transverse E-glass/polyester specimens.**

## 3.4 SENSITIVITY ANALYSES

Slight experimental scatter in strain measurement leads to error in material parameter characterizations and long-term predictions. The data scatter is due to variability in material and geometry from specimen to specimen, fluctuated testing conditions, and possible damage accumulation during creep tests. Dillard et al. [49] and Tuttle [16] have reported the need of performing sensitivity analyses to measure effects on error in material characterization on the long-term responses. Dillard et al. [49] showed that determining exponent (n) parameter in the power law time dependent model from a short-term creep tests caused significant error in the long-term material predictions.

Tuttle [16] investigated the predictions of long-term behavior of laminated composites due to errors in short-term (480 minutes) material's characterization. The Schapery's nonlinear viscoelastic model was used to predict the creep responses. It was shown that the effect of error in exponent parameter was negligible at short-term creep but became very significant over long-term ($10^5$ minutes) periods. While error in power law coefficient showed low effects in long-term behaviors.

Sensitivity analyses of the Schapery material parameters are performed to examine the impact of slight error in material parameter characterization of the long-term predictions. As mentioned earlier in the experimental part of this study, the maximum deviation in the recorded strains of the repeated tests is 3%. This data scatter will lead to different values in the calibrated material parameters. A deviation of ±5% error of the calibrated material parameters is used to simulate the experimental data scatter. From Eq. (2.4), it is seen that parameters $D_0$ and $g_0$ have similar effects on the overall creep responses and parameters $g_1$, $g_2$, and C influence creep behavior in a similar way. Therefore, sensitivity analyses are performed due to error in parameters $g_0$, n, C, and $a^T$. Figure 3.22 presents percentage of error in long-term compliances due to ±5% error in calibrated $g_0$, n, and C parameters. The responses, predicted using TTSP, are shown for the E-glass/vinylester transverse specimen under load ratio 0.4. Error in $g_0$ parameter affects the instantaneous creep only. Therefore, ±5% compliance error occurs at the t=0 and decreases with time. Error in parameter C influences the transient part only, which is shown by the nearly constant error in the creep compliances. While error in parameter n has insignificant effects at short-term creep, but becomes significantly large over long-term period.

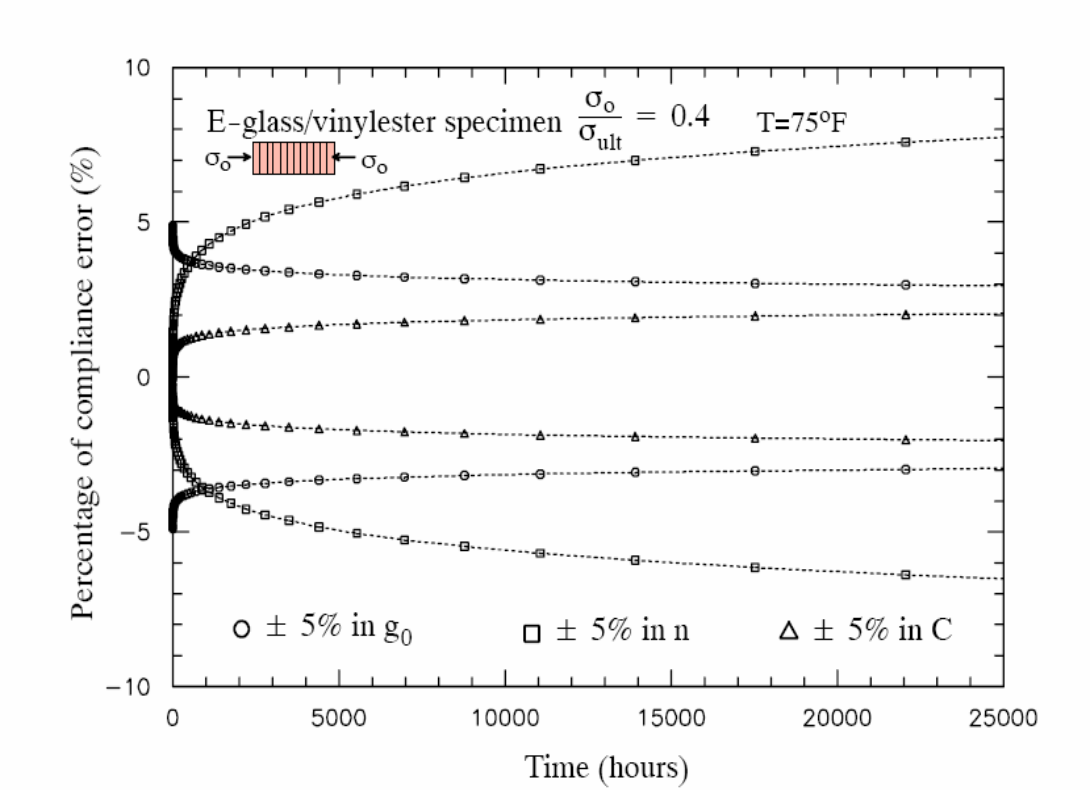


**Figure 3.22 Percent error in predicted creep compliance due to error in parameters $g_0$, n, and C calibrations.**

Next, data scatter in long-term compliances due to error in time-shift factor characterization is illustrated in Fig. 3.23. The deviation in calibrated time shift-factor affects the transient compliances, which increases compliance error rapidly at the short-term and the error becomes stable over long periods.

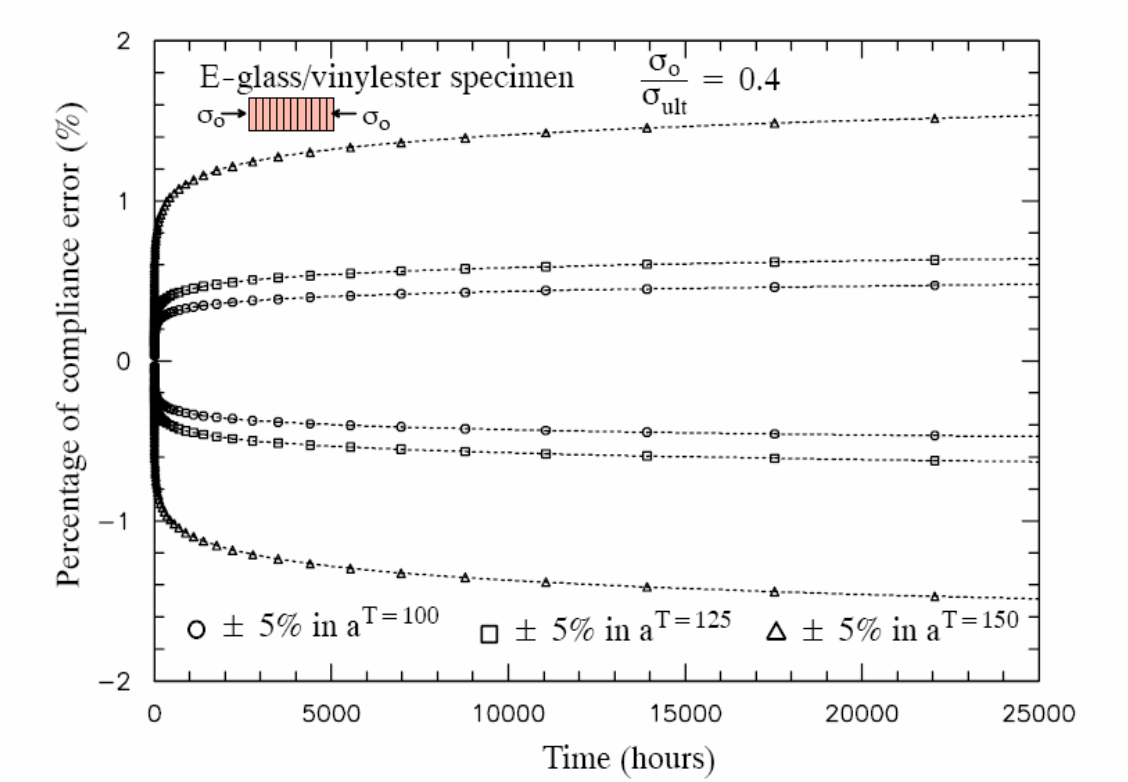


**Figure 3.23 Percent error in predicted creep compliance due to error in time-shift factor calibrations.**

# CHAPTER IV
# INTEGRATED MICROMECHANICAL MODELS AND FINITE-ELEMENT ANALYSIS FOR PREDICTING LONG-TERM BEHAVIORS OF MULTI-LAYERED COMPOSITE STRUCTURES

This chapter presents an integrated material-structural modeling approach for analyzing long-term behaviors of multi-layered composite structures. Previously developed viscoelastic micromodels of multi-layered composites (Haj-Ali and Muliana, [35,36]) are used to generate the effective nonlinear viscoelastic responses of the studied composite systems. These micromodels are implemented as a material subroutine in ABAQUS [51] finite element (FE) code to perform structural analysis. Analysis of time-dependent buckling in I-shaped composite slender columns and flat panels; long-term responses an assembled composite beam under three point bending, and a composite transmission tower under lateral loads are performed. The long-term behavior from the integrated micromechanical-FE analysis of the assembled beam structures is verified with the long-term creep data by Mottram [30]. FE models with 1D, shell and 3D structural elements are employed in this study. A comparison of the results for creep and buckling from the three element models are also provided.

## 4.1 INTEGRATED MICROMECHANICAL MODEL AND FINITE ELEMENT STRUCTURAL ANALYSIS

An integrated micromechanical and FE models for the multi-layered composite materials and structures is shown in Figure 4.1. The upper level depicts a FE structural model using 1D (beam, truss), 2D (continuum plane, shell), and 3D continuum (brick) type elements. The effective nonlinear viscoelastic response is sampled at different material points (Gaussian integration points). This study applies the micromechanical-structural framework, proposed by Muliana and Haj-Ali [43], for analyzing nonlinear and long-term responses of the studied multi-layered FRP composite structures. A sublaminate model is used to homogenize the responses from the roving and CFM layers. This results in 3D effective nonlinear orthotropic viscoelastic behaviors. Two 3D nonlinear time-dependent micromodels of roving and CFM layers are used for the alternating layer in the multi-layered composite systems. The Schapery [22] integral equation is used for the isotropic matrix. The fiber is modeled as a linear elastic material. In the case of shell typed FE, a constraint of a plane stress condition is added to the 3D formulation, while in the case of 1D element, a uniaxial stress-strain constraint is incorporated to the sublaminate model. The complete nonlinear time-dependent micromechanical formulations were formulated by Haj-Ali and Muliana [35] and Muliana and Haj-Ali [36].

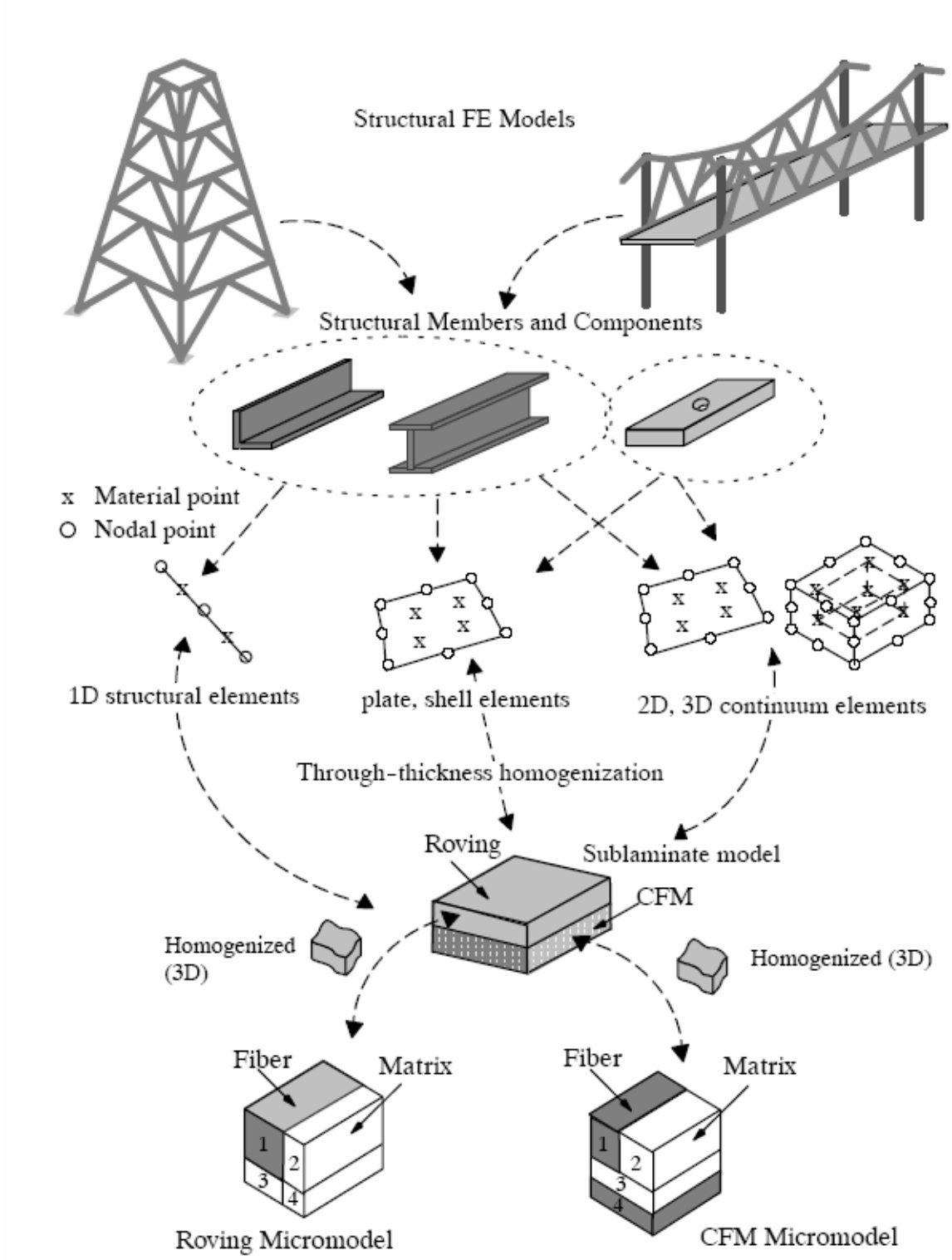


**Figure 4.1 Integrated structural and micromechanical framework for analyses of multi-layered composite materials and structures. [Haj-Ali and Muliana, [43]]**

In this study, the extended master curve from linear extrapolation up to period of 25000 hours (nearly 3 years) for the E-glass/vinylester and E-glass/polyester composites is used to calibrate the long-term time-dependent material parameters for the polymeric matrix. The fiber medium is assumed as linear elastic and transversely isotropic behaviors. The Prony parameters of the isotropic matrix are calibrated from the long-term compression response of the $45^o$ off-axis E-glass/vinylester specimen at load level 0.2, as shown in Figure 4.2. The Prony parameters for the polyester matrix are obtained from the tensile creep response of the $45^o$ off-axis E-glass/polyester composite specimens under load level 0.2. The long-term Prony series in hour unit time are given in Table 4.1 for E-glass/vinylester system and in Table 4.2 for E-glass/polyester system.

**Table 4.1 Long-term Prony series coefficients for the vinylester matrix (from 25,000 hour extended creep data)**

| n | $\lambda_n$ (hour$^{-1}$) | $D_n$ x $10^{-6}$(ksi$^{-1}$) |
|---|---|---|
| 1 | 1 | 481 |
| 2 | $10^{-1}$ | 311 |
| 3 | $10^{-2}$ | 330 |
| 4 | $10^{-3}$ | 351 |
| 5 | $10^{-4}$ | 390 |
| 6 | $10^{-5}$ | 3850 |
| 7 | $10^{-6}$ | 4500 |

**Table 4.2 Long-term Prony series coefficients for the polylester matrix (from 25,000 hour extended creep data)**

| n | $\lambda n$ | $Dn \times 10^{-6}$ ($ksi^{-1}$) |
|---|---|---|
| 1 | 1 | 151 |
| 2 | $10^{-1}$ | 66 |
| 3 | $10^{-2}$ | 55 |
| 4 | $10^{-3}$ | 71 |
| 5 | $10^{-4}$ | 70 |
| 6 | $10^{-5}$ | 450 |
| 7 | $10^{-6}$ | 500 |
| 8 | $10^{-7}$ | 980 |
| 9 | $10^{-8}$ | 2050 |
| 10 | $10^{-9}$ | 2000 |

The nonlinear stress-dependent parameter for the vinylester matrix, which follows the Ramberg-Osgood (R-O) stress-strain relation, is taken from Haj-Ali et al. [45,35]. Long-term predictions of the micromechanical model with the calibrated nonlinear and long-term material parameters are presented for higher stress level, illustrated in Figure 4.2. Mismatch in the long-term prediction at high load level (0.6 ratio) is due to the high value of $g_0\sigma$, represented by R-O stress-strain relation (Figure 4.3).

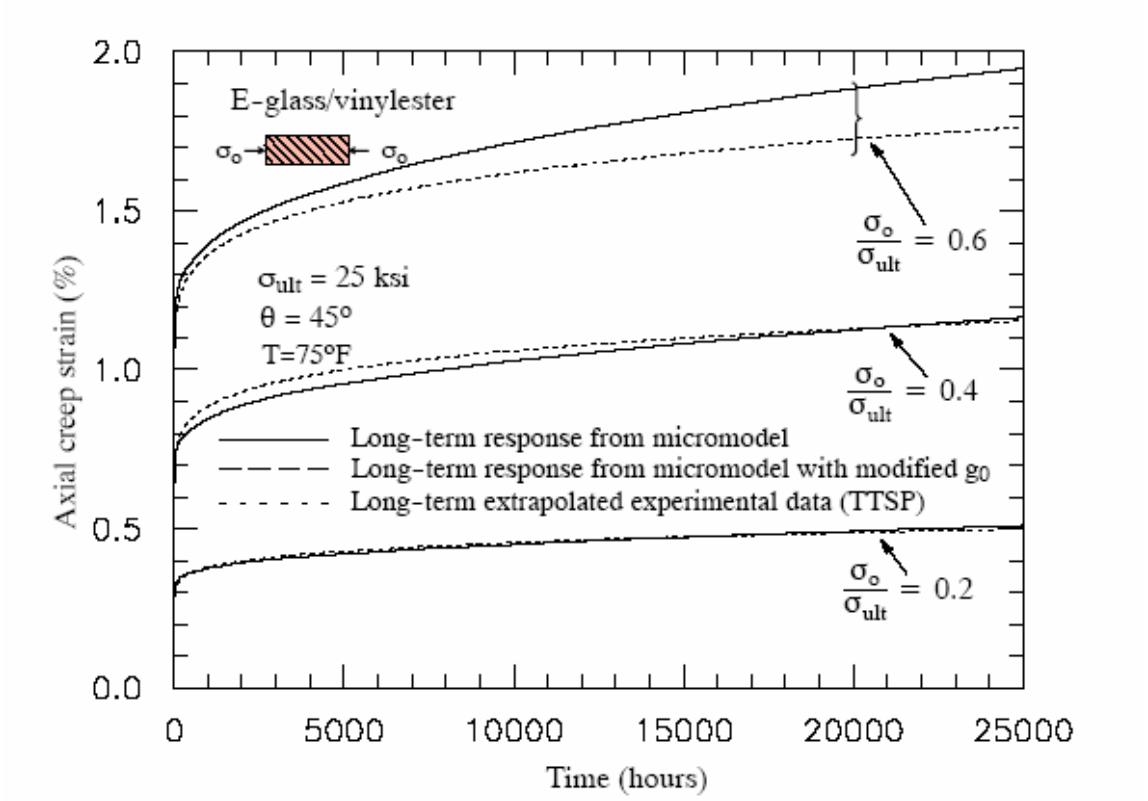


**Figure 4.2 Long-term creep strains for E-glass/vinylester 45° off-axis specimens.**

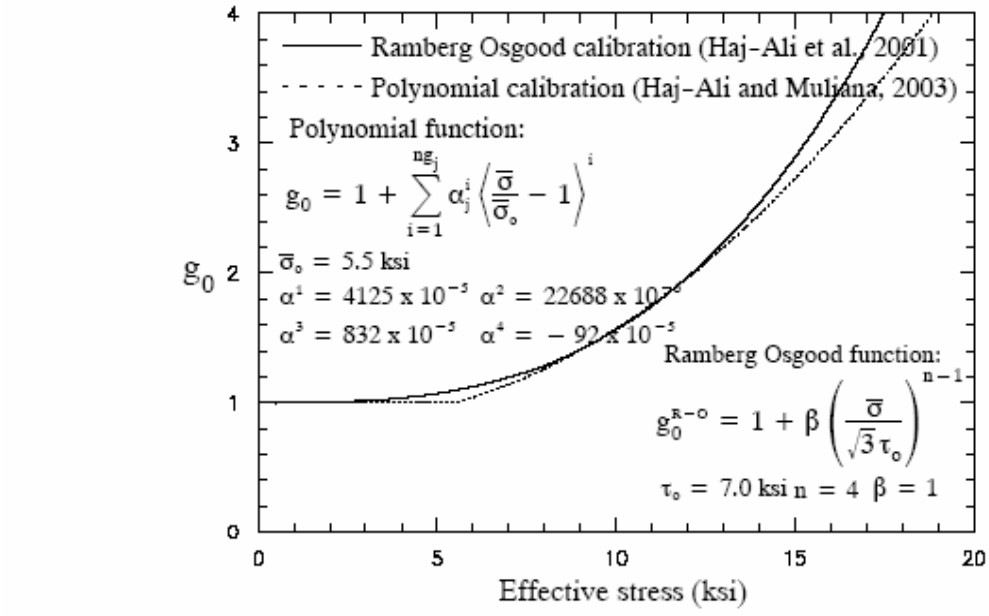


**Figure 4.3 Nonlinear stress dependent parameter for vinylester matrix.**

In their previous paper (Haj-Ali and Muliana, 35), the authors have mentioned the out of range $g_0^{\sigma}$ calibration at stress level 0.6. In addition, there is no guarantee that one function (in terms of effective stress) will match all levels of applied stress. Therefore, segmental functions for the different ranges of applied stress may be a better alternative.

## 4.2 LONG-TERM BEHAVIORS OF MULTI-LAYERED COMPOSITE STRUCTURES

The viscoelastic constitutive micromechanical model is implemented in the user material subroutine (UMAT) in ABAQUS-FE code. Several thick section composite structural components are generated using 1D, 2D and 3D typed elements. The integrated micromechanical-FE analyses are performed for time-dependent buckling of an I-shaped composite column and a composite panel and long-term performances of an assembled multi-layered composite beam under point loading, and a composite transmission tower due to lateral loads. Convergence studies are first performed for the above structural analyses. Results using 1D, 2D and 3D typed elements are also compared with the analytical model or available experimental data.

### 4.2.1 Time-dependent buckling on an I-shaped slender composite column

FE models of an I-shaped composite column with a constant cross section of 4 x 2 x 0.25 $in^3$, shown in figure 4.4, are generated using quadratic beams (B32) elements, quadratic shell (S4R) with reduced integration, and eight nodded brick element using reduced integration (C3D8R). The cross-sectional dimensions of the members are taken from available dimensions of the manufactured structural members (Creative Pultrusion). The column with a slenderness ratio of 100, which is comparable to 150 in. length, is considered. The column consists of the E-glass/vinylester composite system. A fiber volume fraction (FVF) of 33% is used for analysis. The roving fiber direction is placed along the longitudinal axis of the I-shaped column.

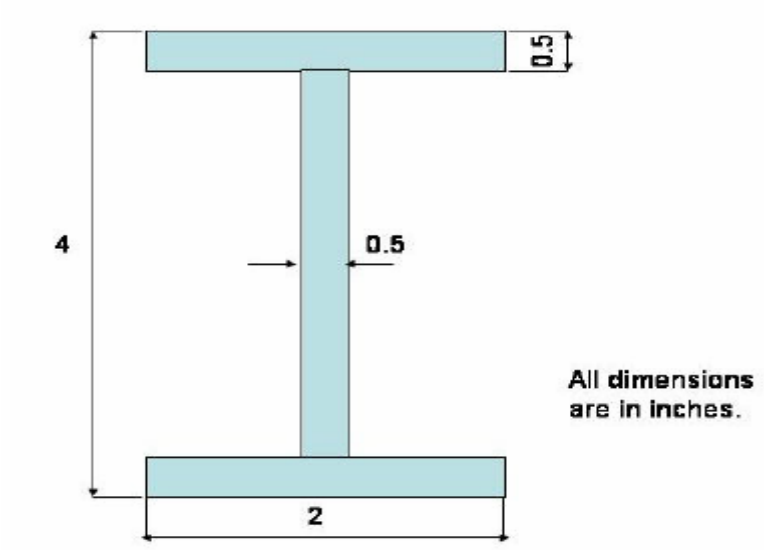


**Figure 4.4 Cross-sectional geometry for the I-shaped column.**

Creep bending analyses of the I-shaped column with fixed end support are first performed by applying lateral force at the mid-span of the column. The applied load is taken as 75% of the ultimate failure load. Figure 4.5 shows the mid-span creep deflection of the I-shaped column using beam, shell and brick elements. The purpose of this analysis is to verify the capability of the 3D micromechanical model in integrating with different typed finite elements.

The allowable mid-span displacement for design purposes is often calculated based on

$$\Delta \text{ (allowable)} = \Delta 1 + \Delta 2 - \Delta 3$$

Where, $\Delta 1$ is the deflection due to live loads, $\Delta 2$ is the deflection due to dead loads which is usually taken as L/300 to L/350 to account for creep (L is the length of the beam), and $\Delta 3$ is the displacement due to gravity or self-weight of the beam, which is assumed to be zero. In this study, the allowable deflection for the studied composite column application is given as

$\Delta$ (Allowable) = 4.30 +0.40 +0.0 = 4.70 in.

It is seen from figure 4.5 that the time at which the allowable displacement (4.70 in.) is exceeded is around 4,600 hours, which indicates a critical time.

It is noted that the analysis using shell elements require longer CPU time. This is due to the higher number of elements and the UMAT (homogenized micromechanical-FE) subroutine which required increased iterations for imposing plane stress conditions of the 3D micromechanical model. Some deviation is shown in the analysis using beam element. This is due to the existence of flange deformation of the I-shaped member, which cannot be captured using 1D (beam) element. Therefore, the analyses using 1D element is valid only when the columns are slender enough, in which the effect of flange deformations are small.

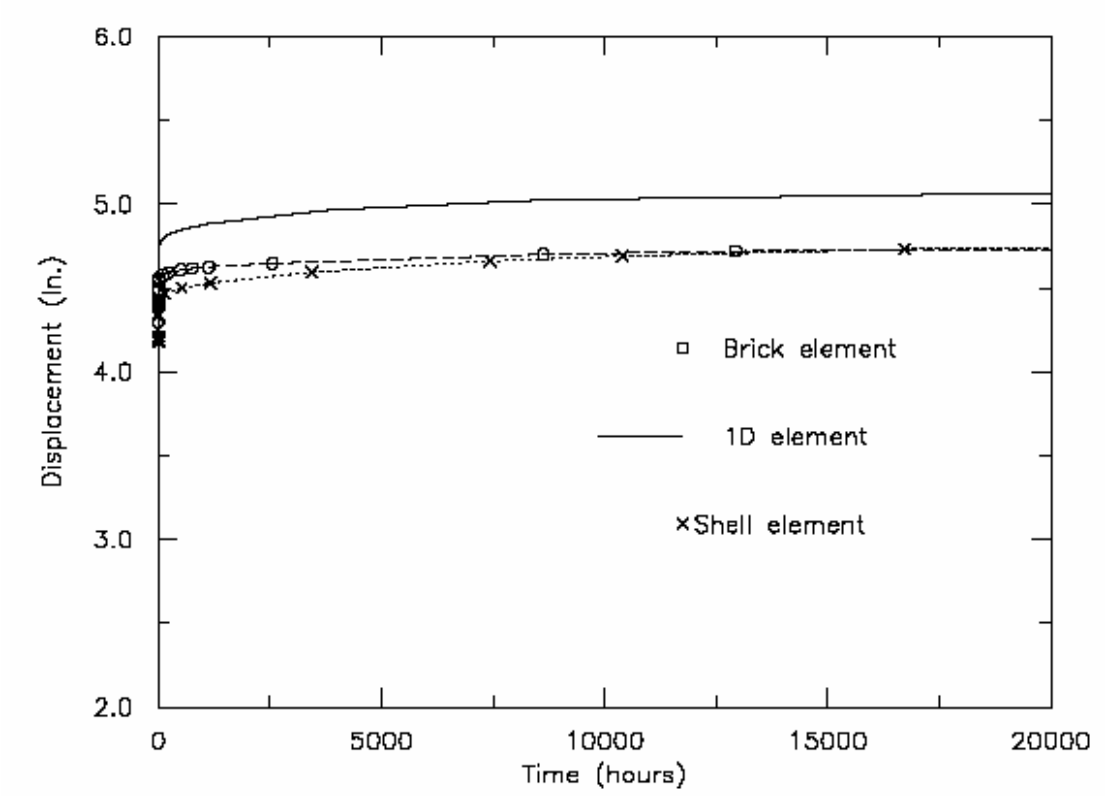


**Figure 4.5 Mid-span lateral creep deflection of the I-shaped E-glass/vinylester composite column using different element models.**

Next, post buckling and creep buckling analyses are performed for the I-shaped E-glass/vinylester composite column, with fixed end support under axial compression loads. The FE model with 1D, shell, and brick elements are used. Elastic critical buckling loads are calculated from the FE analyses are compared with the Euler buckling load, given in table 4.3. The first five eigen modes using 3D elements are represented in figure 4.6.

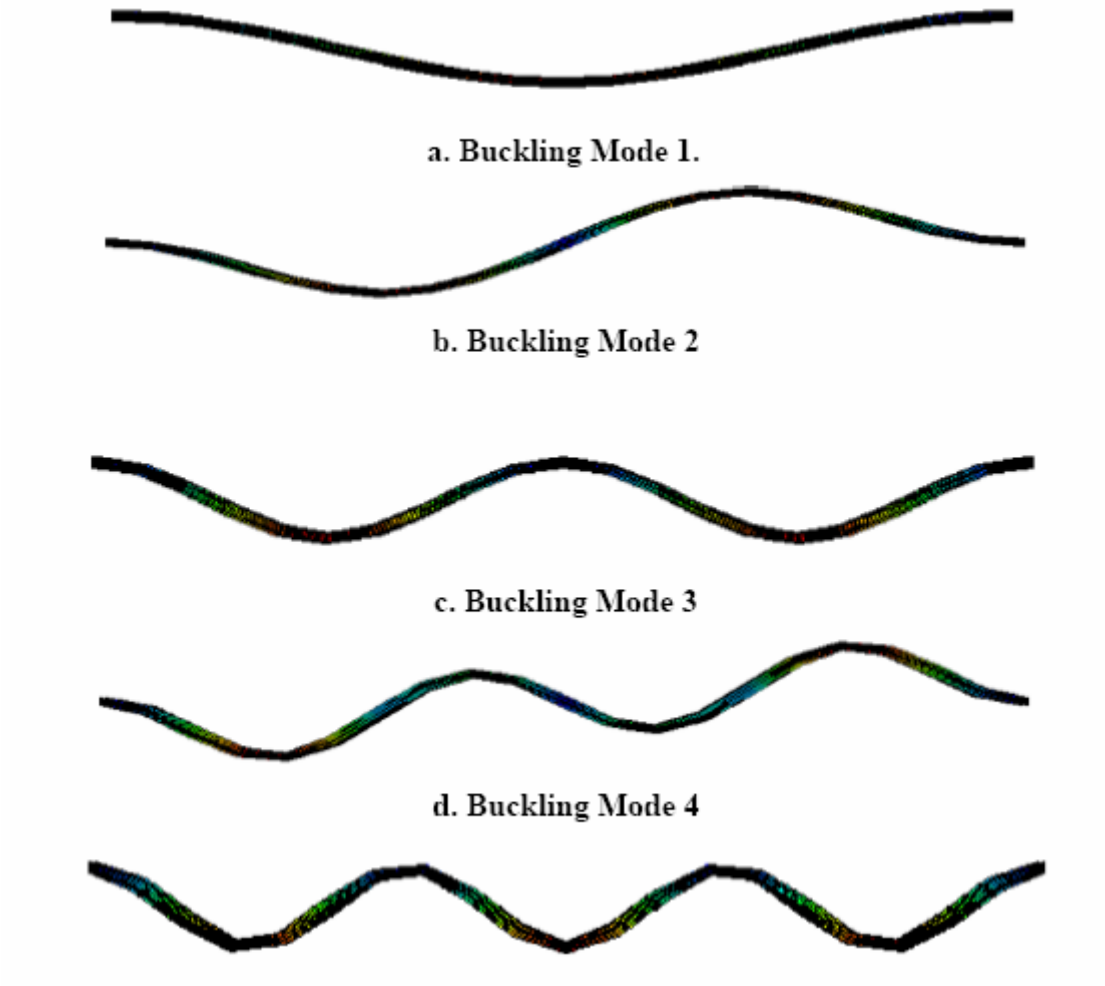


**Figure 4.6 Buckling modes 1 to 5 (a-e).**

**Table 4.3 Buckling load under mode 1.**

| Element type | Critical buckling load (kips) |
|---|---|
| Analytical euler buckling load | 1.6093 |
| 1D (beam element) | 1.5810 |
| 2D (Shell Element) | 1.6024 |
| 3D (Brick element) | 1.6093 |

Geometric imperfections are modeled by perturbing the perfect structure with several buckling modes. Different imperfection factors ranging from L/100 (for a highly imperfect structure) to that of L/5000 (for a nearly perfect structure) are employed for each chosen buckling mode. Parametric studies are conducted to examine the effect of geometric imperfection on the overall composite structural responses under axial compression load. FE models with 1D and 3D elements are used. The shell element is used only for one particular case having an imperfection factor of L/1000 for the first eigen mode. Figure 4.7 (a-e) shows the postbuckling analysis using only the first buckling mode with different imperfection ratios. Comparable postbuckling responses are shown for the analysis with different types of elements. Figure 4.8 represents the buckling with combinations of the first five modes and two imperfection factors (L/1000 and L/5000).

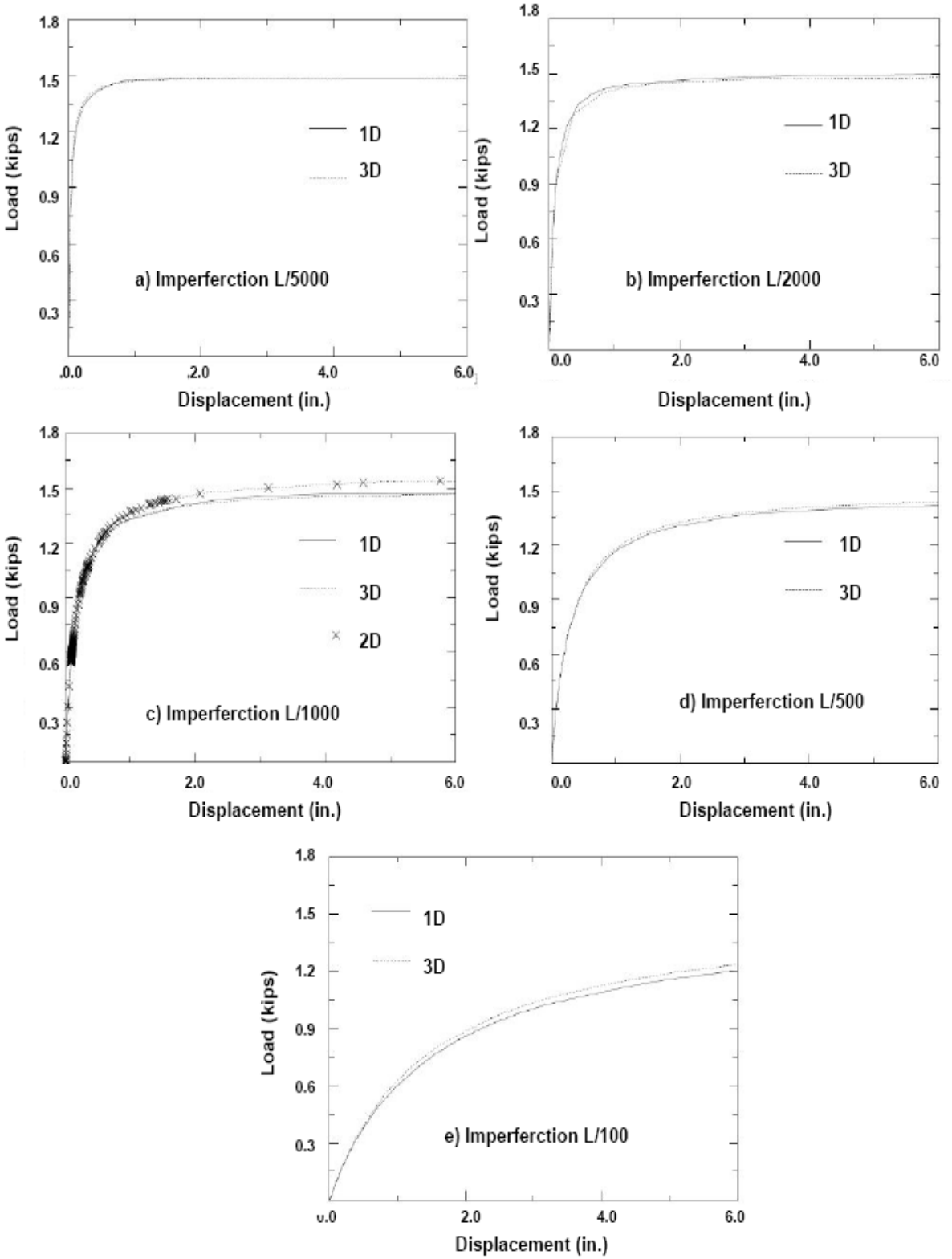


**Figure 4.7 Post buckling analyses of column with different imperfection factors of mode 1.**

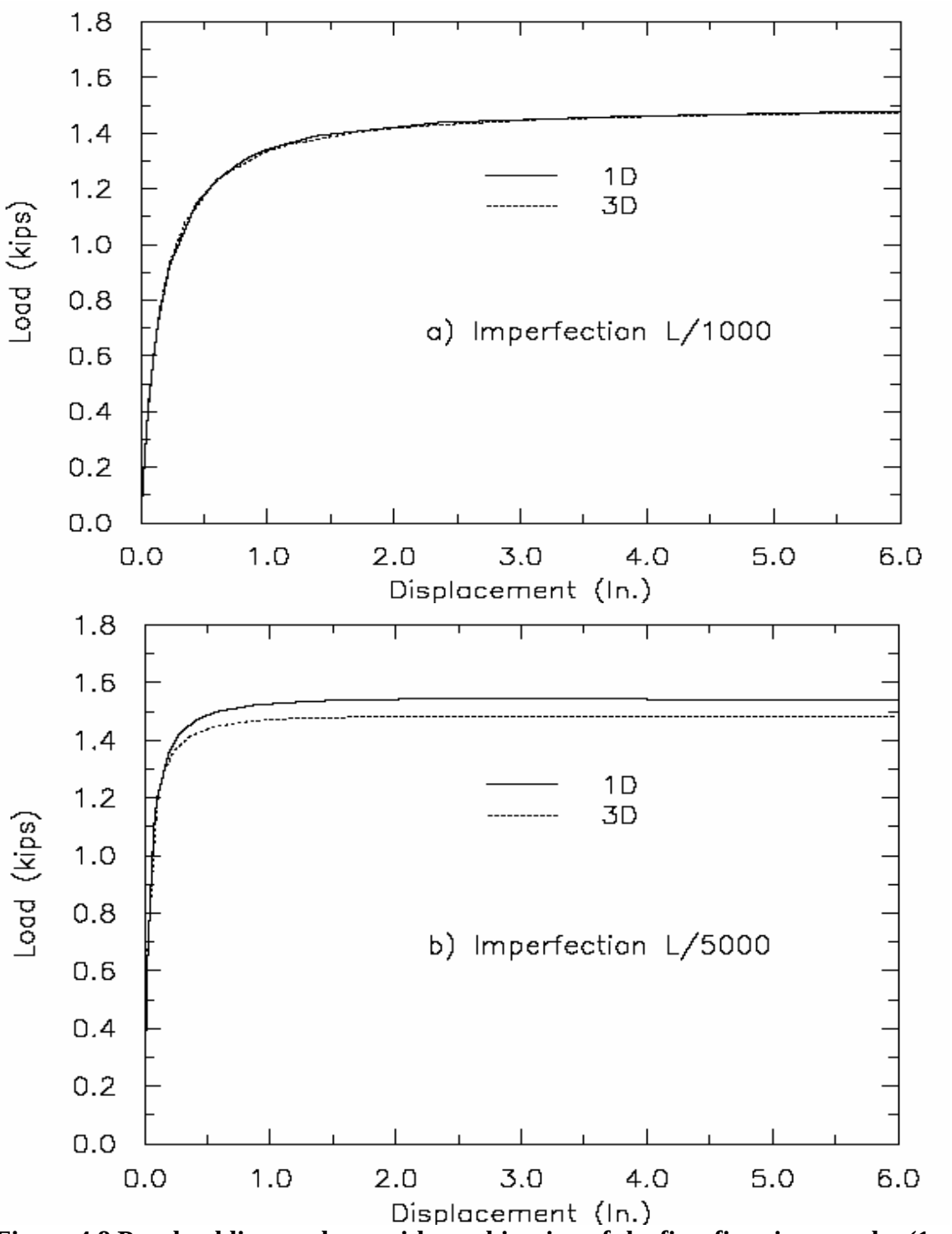


**Figure 4.8 Post buckling analyses with combination of the first five eigen modes (1 to 5).**

Creep buckling analyses are then performed on the I-shaped composite column under 90% of the critical buckling load. The 90% load is chosen to accelerate the buckling response. Since the results from the post buckling analyses using 1D and 3D elements were within 0.05% difference (even at the most imperfect structure analyzed), only the FE model with 3D type elements were used for creep buckling analyses. The time to buckle is noted under various imperfection factors and Eigen modes. Thus a comprehensive study is undertaken to study the relationship between load- imperfection-mode and time characteristics of the I-shaped structures. The results are shown in figure 4.9 (a and b) for imperfections L/1000 and L/5000 under the $1^{st}$ eigen mode.

It is seen from the figure 4.9 that under imperfection factor of L/1000, the critical displacement, displacement at which buckling occurs, is reached at 8600 hours, while for a more perfect structure with imperfection factor L/5000 the buckling critical displacement is reached in approximately 100,000 hours (infinite time) or more than 10 times the duration seen in a structure with 5 times its imperfection. Creep buckling under 80% of the critical buckling load, even at imperfection factor L/1000 takes infinite time to buckle as shown in figure 4.10. From the creep buckling analysis under various imperfection factors of buckling modes (1-5), it is noted that higher imperfections of the first buckling mode results in an accelerated buckling of the structure. However, at low load levels, even for a highly imperfect structure, it requires a long time (infinite) to buckle.

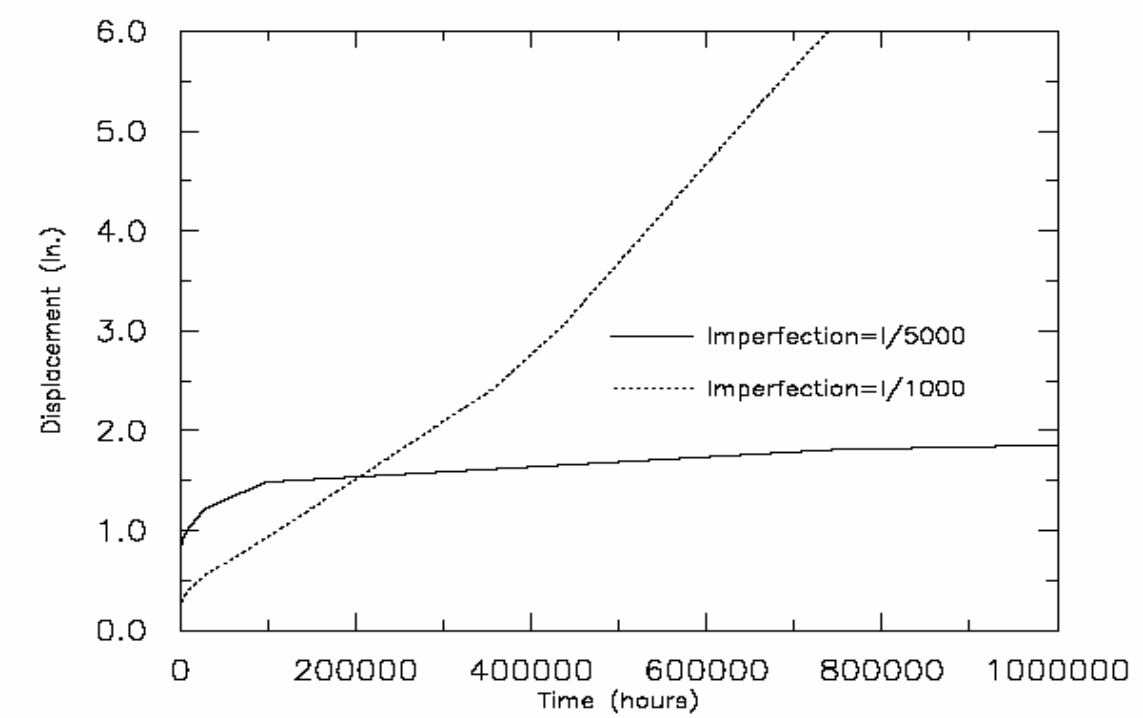


**Figure 4.9 Creep buckling under 90% critical buckling load and imperfections a) L/1000 b) L/5000 of mode 1.**

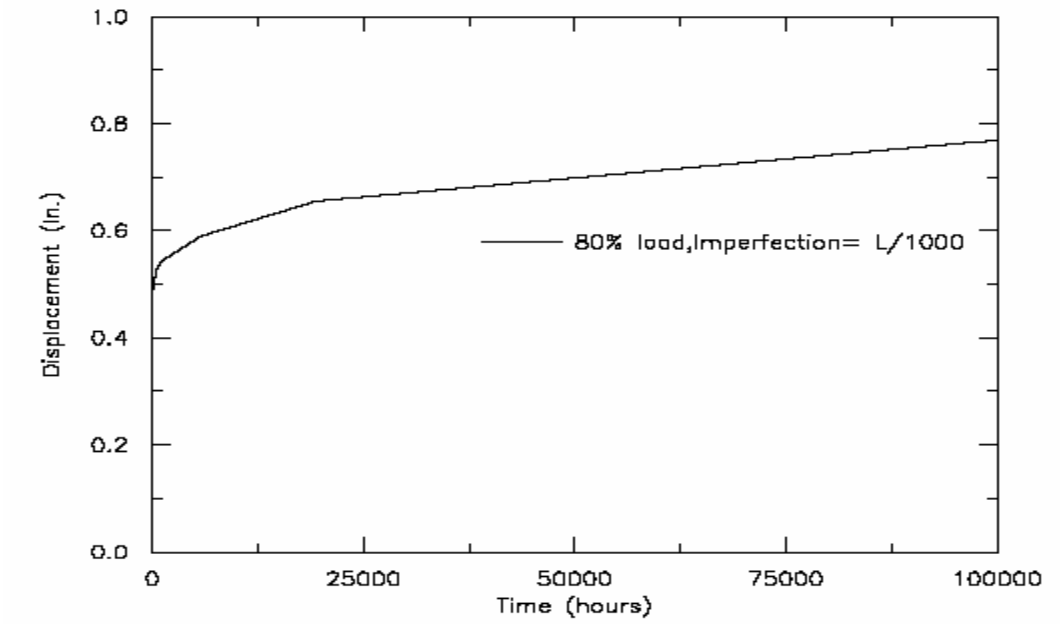


**Figure 4.10 Creep buckling under 80% critical buckling load and imperfection L/1000.**

### 4.2.2 Creep buckling analyses of a composite panel

Flat composite panels used as structural members are studied in this section. The dimensions of the panel (96x 48x 0.5 in.), shown in figure 4.11, are obtained from the composite sheets manufactured by Creative Pultrusions. The panel consists of the studied E-glass/vinylester composite systems with roving fiber direction placed along the length of the plate.

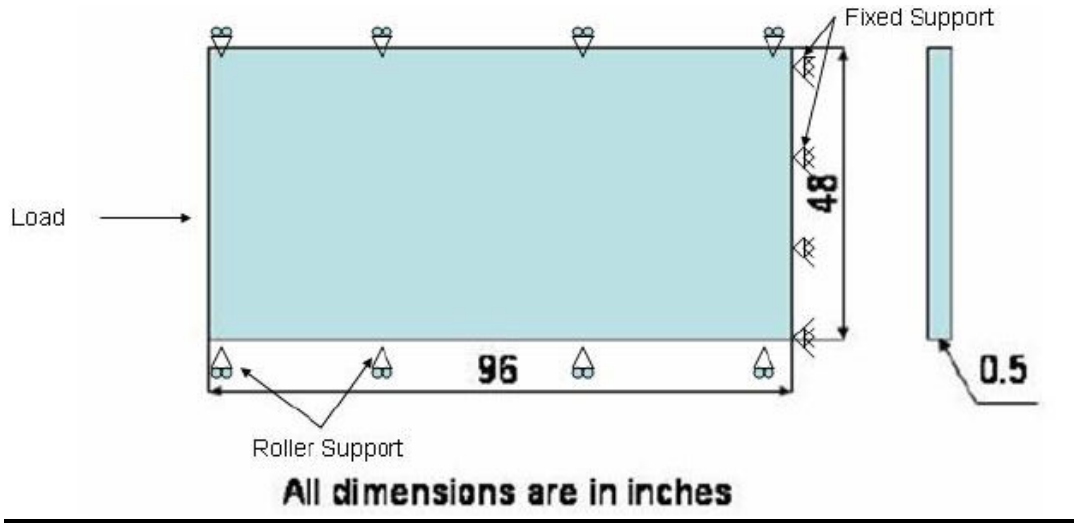


**Figure 4.11 Geometry of the flat panel.**

Buckling analysis is performed on the panel to obtain the critical buckling load. The panel is fixed on one of the sides with roller supports on the adjacent sides, as shown in figure 4.11. Shell elements are chosen for the analysis. A doubly curved quadratic shell element with reduced integration (S8R) is employed for the analysis. Convergence study was performed on the structural member by monitoring the deflection of the central node with mesh refinement. The refined mesh of 40 x20 elements was used for buckling analysis on the panels with fixed end conditions A unit load was applied to the central node of one of the sides (shown in figure 4.11), to obtain the Buckling modes. It is seen

that buckling occurs primarily through two modes. The different eigen modes in buckling are represented in the figures 4.12.

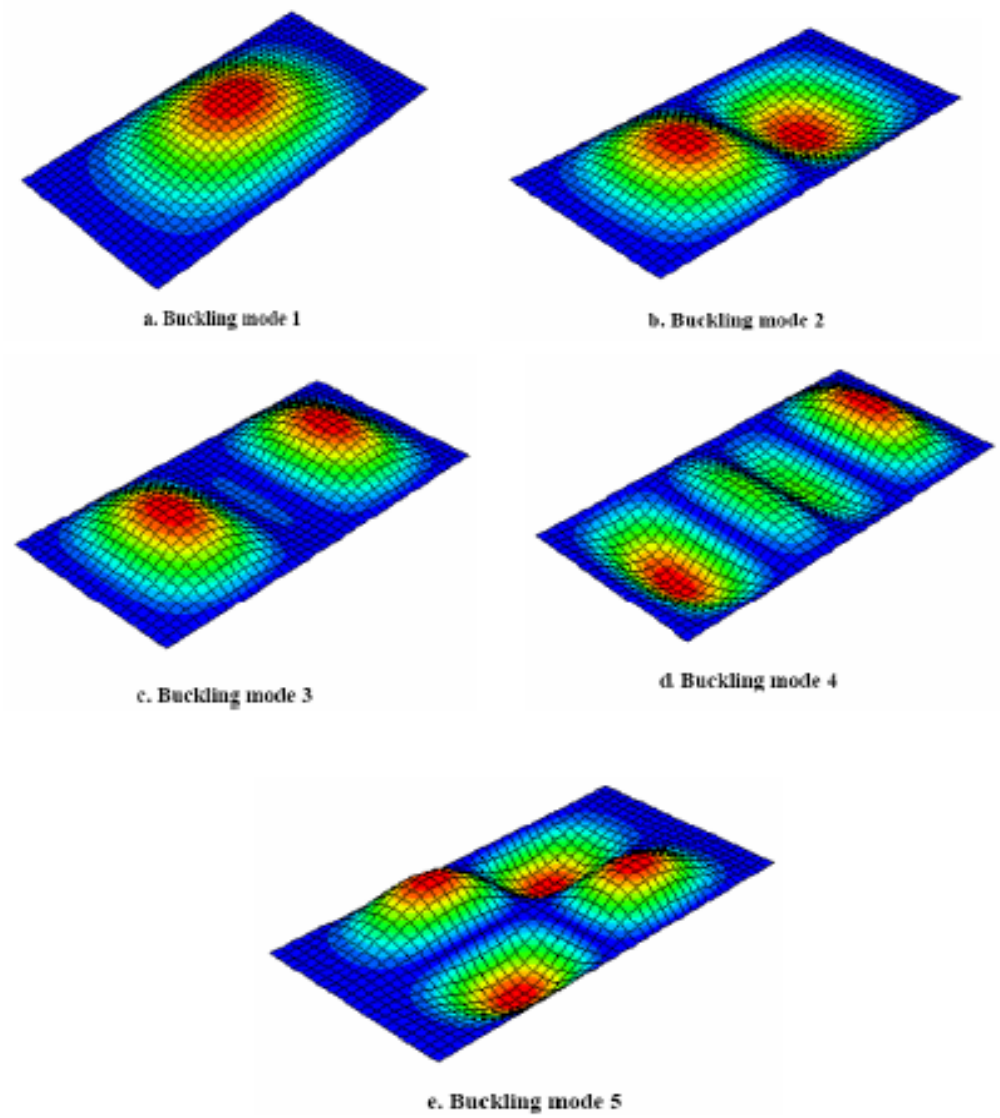


**Figure 4.12 Buckling modes 1-5 (a-e) for the composite panel.**

Once the critical buckling load is obtained, post buckling analysis with geometry imperfections is performed on the structure. Imperfections are modeled by perturbations on the perfect geometry with the buckling modes. Two imperfection factors are considered. The first perturbation factor of 0.003 represents a nearly perfect structure. Second post buckling analyses was performed with an imperfection factor of 0.03. Figure 4.13 shows the post buckling analyses with the two imperfection factors of the first eigen mode.

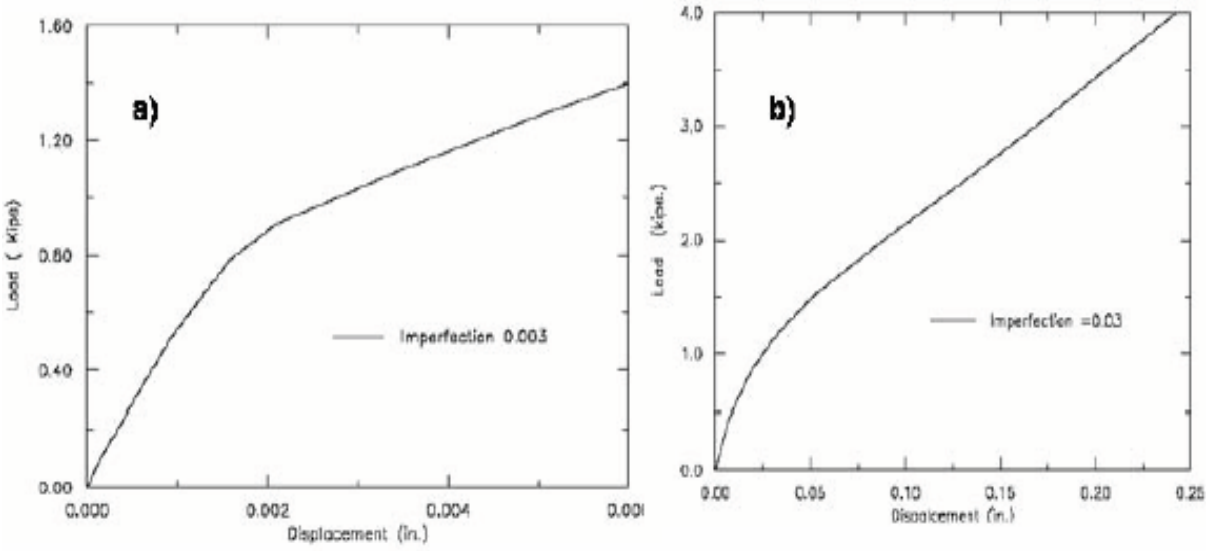


**Figure 4.13 Post buckling analyses of panel with different imperfection factors of mode 1.**

Creep buckling analyses was then performed under loads of 90% of the critical buckling load on an imperfect plate with imperfection factor 3. Once again, the 90% of the critical buckling load was chosen to accelerate plate buckling. It is evident from figure 4.14, that under such high imperfections the plate will buckle within a short time span, where as with relatively lower imperfection a plate could sustain higher loads for longer duration before buckling occurs.

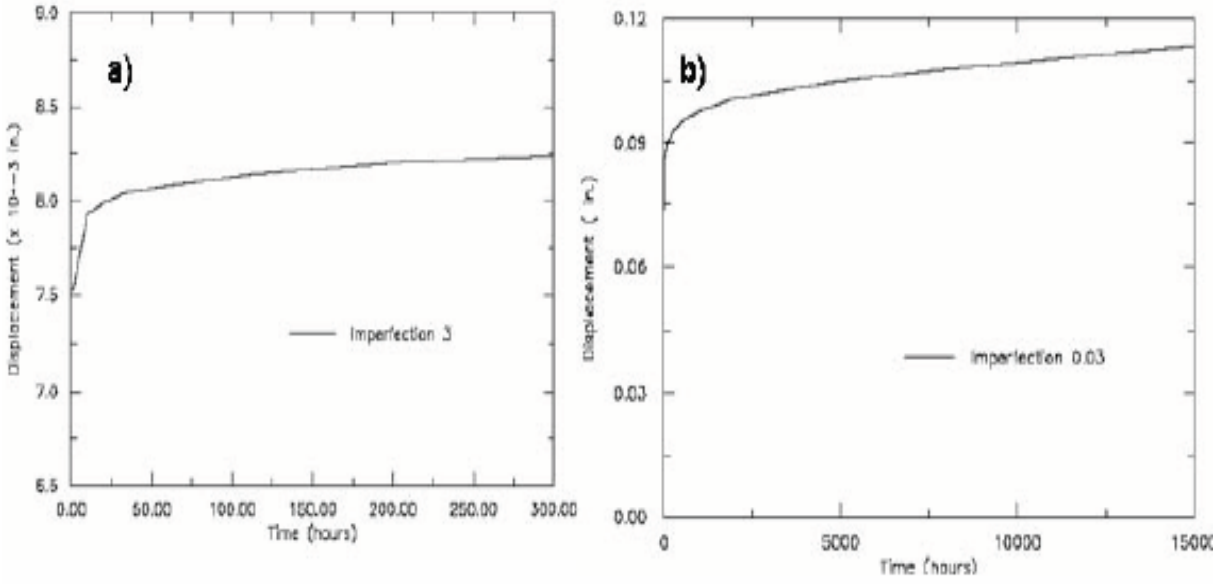


**Figure 4.14 Creep deformation with a) imperfection factor=3 b) imperfection factor=0.03 under 90% of the critical buckling load.**

### 4.2.3 Long-term analyses of an assembled multi-layered composite beam

Motram [30] performed static and long term structural tests on assembled multi-layered composite beam made of E-glass reinforcements in isophthalic polyester matrix under three point bending. The assembled beam consisted of two I-sections sandwiched between flat sheets. The beam assembly had dimensions 735x 76x 90 mm with two 76x 38x 6.25 mm I-sections between 1/4 in. flat sheets. The bonded beam assembly configuration analyzed by Mottram is shown in figure 4.15. It was shown that the central deflections of the assembled beam increase by 25, 60 and 100% of its elastic deformation in periods of week, 1 year and 10 years respectively. The creep testing by Mottram [30] was carried out with simply supported end conditions. The properties of the I-section and Flat panels from Mottram [30] are given in Tables 4.4 and 4.5 respectively. The beam assembly was loaded to 22.8kN at a constant load rate of 0.2kN/s over the mid section. This load corresponds to a factored design load for a proposed

application in light weight floor system. Two creep tests were performed on the assembled beams. On the first test, flat panels were aligned in the longitudinal axis of the I-section of the assembled beam. The second test was performed with the flat panels aligned with the transverse direction of the I-sections.

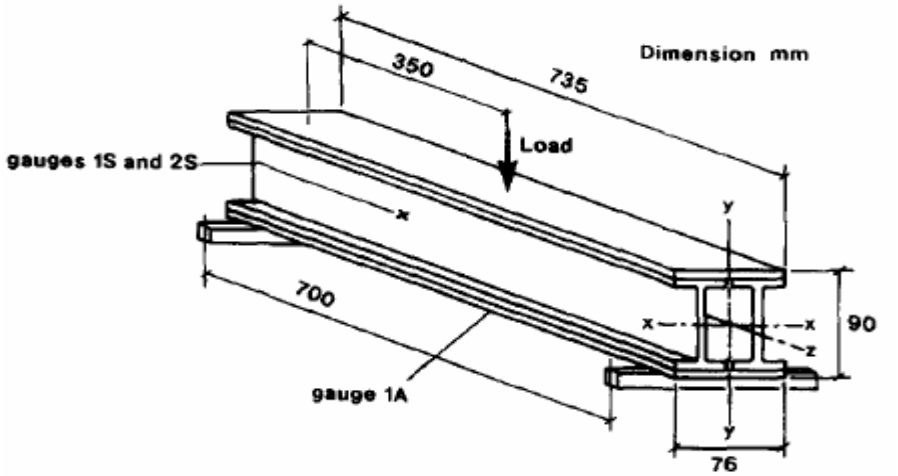


**Figure 4.15 Three-point bend test and bonded assembly configuration from Mottram [30].**

**Table 4.4 Minimum ultimate coupon properties of MMFG series 500/525 structural shapes from Mottram [30].**

| Property | ASTM test | Units | Longi-tudinal | Trans-verse |
|---|---|---|---|---|
| Tensile strength | D638 | N mm$^{-2}$ | 210 | 50 |
| Tensile modulus | D638 | kN mm$^{-2}$ | 17 | 5·5 |
| Compressive strength | D695 | N mm$^{-2}$ | 210 | 103 |
| Compressive modulus | D695 | kN mm$^{-2}$ | 17 | 7 |
| Shear strength | D2344 | N mm$^{-2}$ | 31 | 31 |
| Flexural strength | D790 | N mm$^{-2}$ | 210 | 70 |
| Flexural modulus | D790 | kN mm$^{-2}$ | 14 | 5·5 |
| Poisson's ratio | D3039 | | 0·33 | |

**Table 4.5 Minimum ultimate coupon properties of MMFG series 500/525 flat sheet from Mottram [30].**

| Property | ASTM test | Units | Longi-tudinal | Trans-verse |
|---|---|---|---|---|
| Tensile strength | D638 | N mm$^{-2}$ | 138 | 70 |
| Tensile modulus | D638 | kN mm$^{-2}$ | 12·4 | 6·2 |
| Compressive strength | D695 | N mm$^{-2}$ | 165 | 114 |
| Compressive modulus | D695 | kN mm$^{-2}$ | 12·4 | 7 |
| Shear strength | D2344 | N mm$^{-2}$ | 41 | 41 |
| Flexural strength | D790 | N mm$^{-2}$ | 241 | 103 |
| Flexural modulus | D790 | kN mm$^{-2}$ | 13·8 | 7·6 |
| Poisson's ratio | D3039 | | 0·31 | 0·29 |

FE model of beam assembly configuration shown in figure 4.16 is generated using 3D elements (shown in figure 4.15).

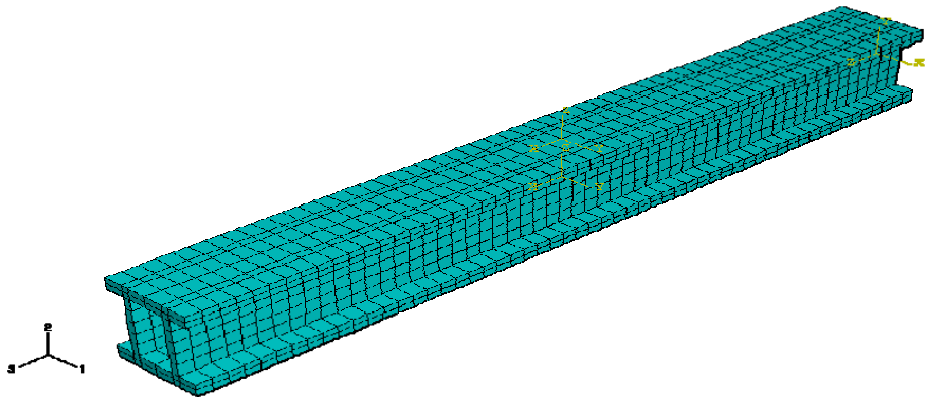

**Figure 4.16 FE model of bonded beam assembly configuration.**

The elastic properties of the I-section and flat sheets given by Mottram, were slightly different than the ones used in this study. This could possibly be due to the differences in

the fiber volume fraction and differences in in-situ material properties between the two members. The effective property used in this analysis is given in table 4.6. Since the details of the fiber volume and in-situ properties were not provided, this analysis used E-glass/polyester system with a FVF of 33% for both I-shaped and panel composite members.

Another deviation during the modeling of beam assembly from Mottram is due to the transverse shear property of the beam. From the uniaxial tension tests performed on the specimens (given in section 2 of the chapter II), only in-plane material properties were calibrated. Hence, the exact transverse shear stiffness could only be approximated.

**Table 4.6 Effective material property (Pultruded E-glass/polylester composite system)**

| $E_{12}$ (kN $mm^{-2}$) | $E_{22}$ (kN $mm^{-2}$) | $E_{33}$ (kN $mm^{-2}$) | $\nu_{12}$ | $\nu_{23}$ | $\nu_{13}$ | $G_{12}$ (kN $mm^{-2}$) | $G_{23}$ (kN $mm^{-2}$) | $G_{13}$ (kN $mm^{-2}$) |
|---|---|---|---|---|---|---|---|---|
| 17.995 | 10.011 | 12.424 | .273 | .295 | .32 | 3.71 | 2.48 | 2.34 |

The result from the FE analysis for the creep deflection at the central section of the beam assembly is provided in figure 4.17 and 4.18 for flat sheets aligned to the longitudinal and transverse directions to the I-sections respectively. Since continuous deflection was not provided by Mottram, the available data was fitted by an exponential curve, shown (by dotted lines) in the figure. The result provided by Mottram at sampling points is represented in symbols.

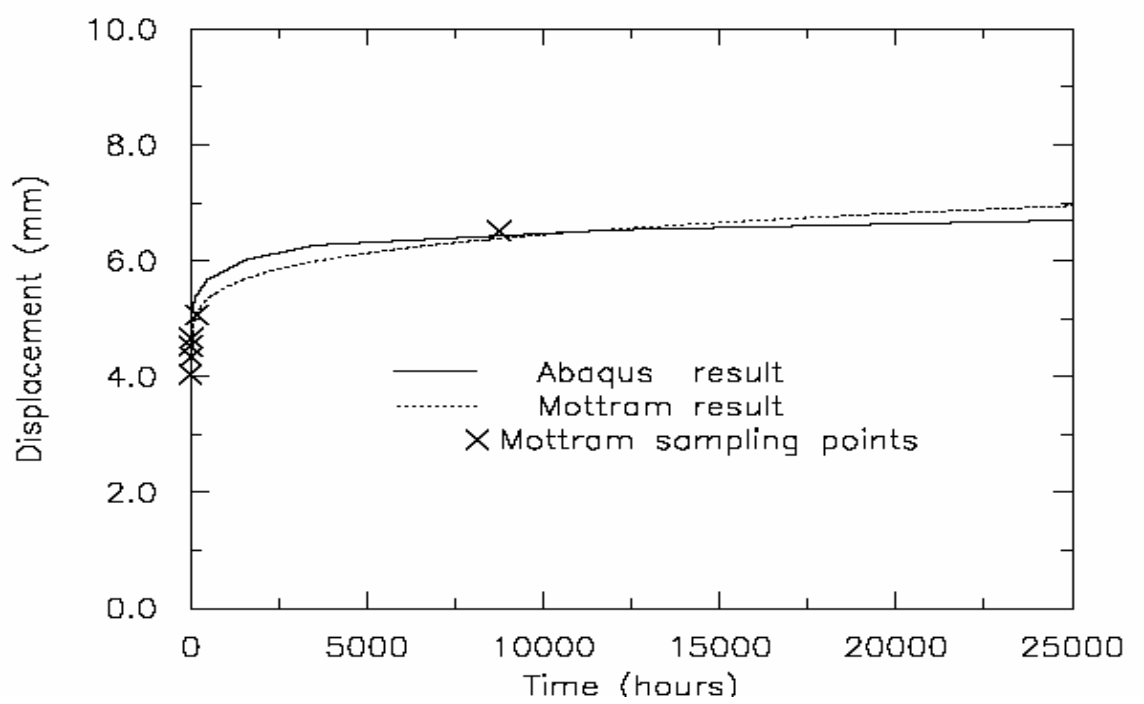


**Figure 4.17 Deflection at the central section of the beam assembly with flat sheets aligned longitudinal to the I-sections.**

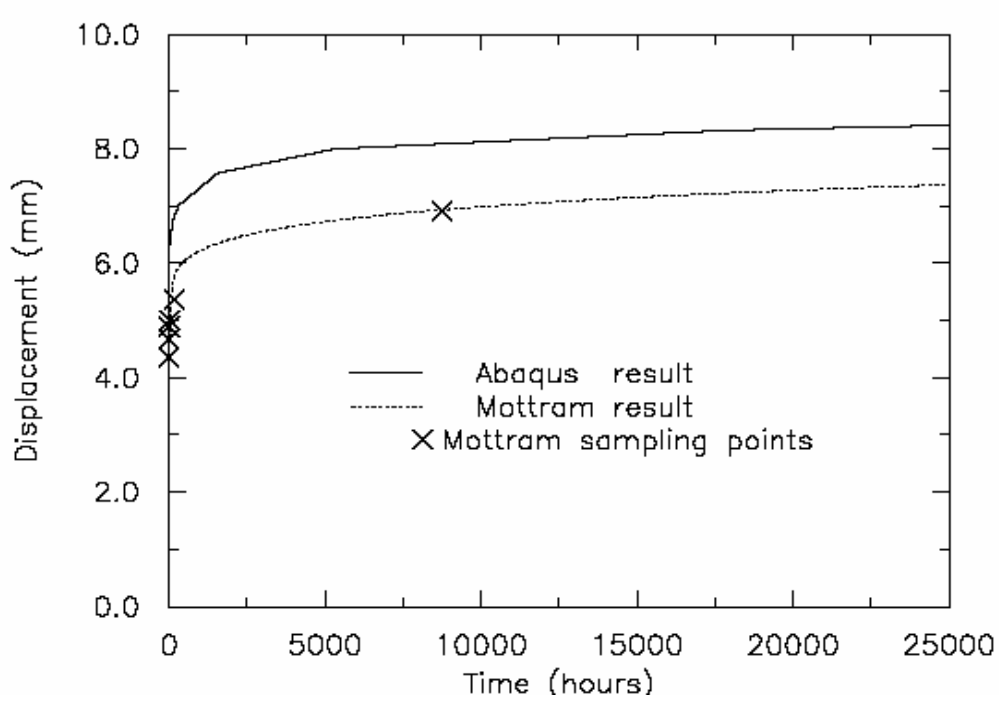


**Figure 4.18 Deflection at the central section of the beam assembly with flat sheets aligned transversely to the I-sections.**

It is noted from the figures (4.17 and 4.18), that the results from the integrated micromechanical-FE analysis of the beam are comparable to the ones provided by Mottram. The slight variation could be due to the differences in the properties of the I-section and flat panels, which could not be properly calibrated due to the unavailability of the experimental data.

### 4.2.4 Long-term Lateral deformation of transmission tower

This section examines the deformation of an over-head electric transmission tower made of the studied thick section multilayered FRP composite system (E-glass fibers (roving and CFM) in vinylester matrix) by prolonged wind loads. Various factors considered in the design of transmission towers are the applied loads, wind loads on supports, load combinations, and the deformation of the structure. The geometric configuration of tower also depends on the type of transmission line (e.g. voltage), and the electric clearance required. The basic geometry of self-supporting transmission tower structure, obtained from ABB inc. [52], is shown in figure 4.19a.

For the purpose of analysis, transmission tower is usually represented by a model composed of primary and secondary members. Primary members form the outer triangulated system that carries the load from their application points down to the tower foundation (figure 4.19a, b). The secondary members form intermediate bracing points to primary members, reducing the unsupported length.

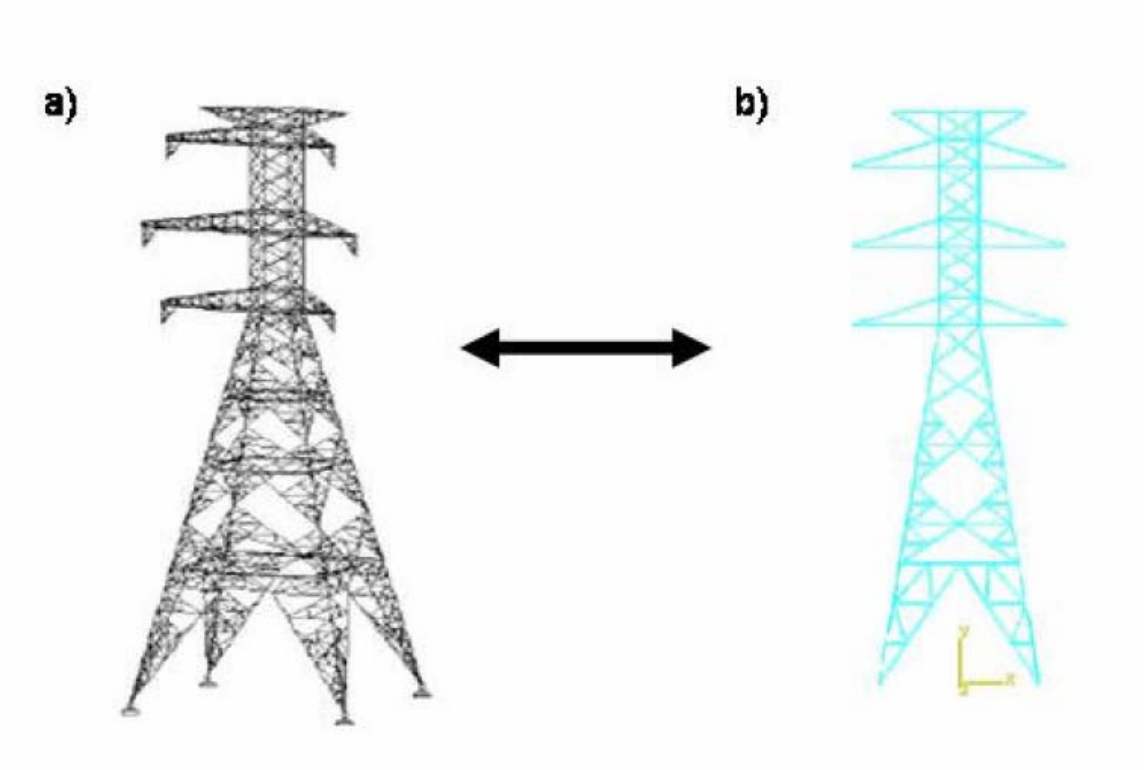


**Figure 4.19 Structure of a) self-supporting over-head transmission tower (ABB inc.) b) simplified FE model used for over-head transmission tower.**

Two types of towers are commonly used for over head electric power transmission; they are the self-supporting towers and the guyed towers. The difference between the two types of towers is on the stability of the structure. Guyed towers require pre-tensioned wire supports with the foundation for stability. The present analysis on transmission tower is performed on a double circuit 500kV self-supporting tower structure, similar to figure 4.19a. The dimensions of the latticed tower structure are chosen to conform to the present industrial specifications. A typical latticed self-supporting transmission tower of 50-65m height has a base width of 10-13m. The total tower width is usually in the range of 20 to 25m.

The FE model of transmission tower has the dimensions shown in Table 4.7. Primary members in towers are usually modeled using beam elements while the secondary

members using truss elements (www.powline.com [53]), however even beam elements can be used for the purpose (www.nenastran.com [54]). In the present analyses, the primary and secondary structural members in the tower are modeled using two nodded linear beam elements (B31). The B31 beam elements follow the Timoshenko beam theory which can be used to formulate members with large axial strains and rotations. In addition they also allow for transverse shear deformation. Since the analysis of the latticed tower structure is time consuming, a two dimensional model of the tower, formed by planar projection of one of the sides of the tower was used for analysis. The actual latticed transmission tower structure and the two dimensional structure used for analysis is shown in figure 4.19b. The uniaxial stress-strain relation is imposed to the 3D micromodel in order to communicate with the 1D type element.

**Table 4.7 Dimensions of the transmission tower**

| **Base width (m)** | **Total height (m)** | **Tower width (m)** | **Tower head height(m)** |
|---|---|---|---|
| **12** | **43** | **16** | **16** |

Figure 4.20 shows the deformation of the tower under load acting at different points on one of the lateral sides of the tower due to wind at very high velocity. The velocity of wind was taken such that it represents the maximum wind load that can act on such a tower. For the present analyses, load acting on the Eiffel tower was used for the calculations. Five points were chosen 1 m. apart from the top of the tower, with the maximum wind load acting on the top.

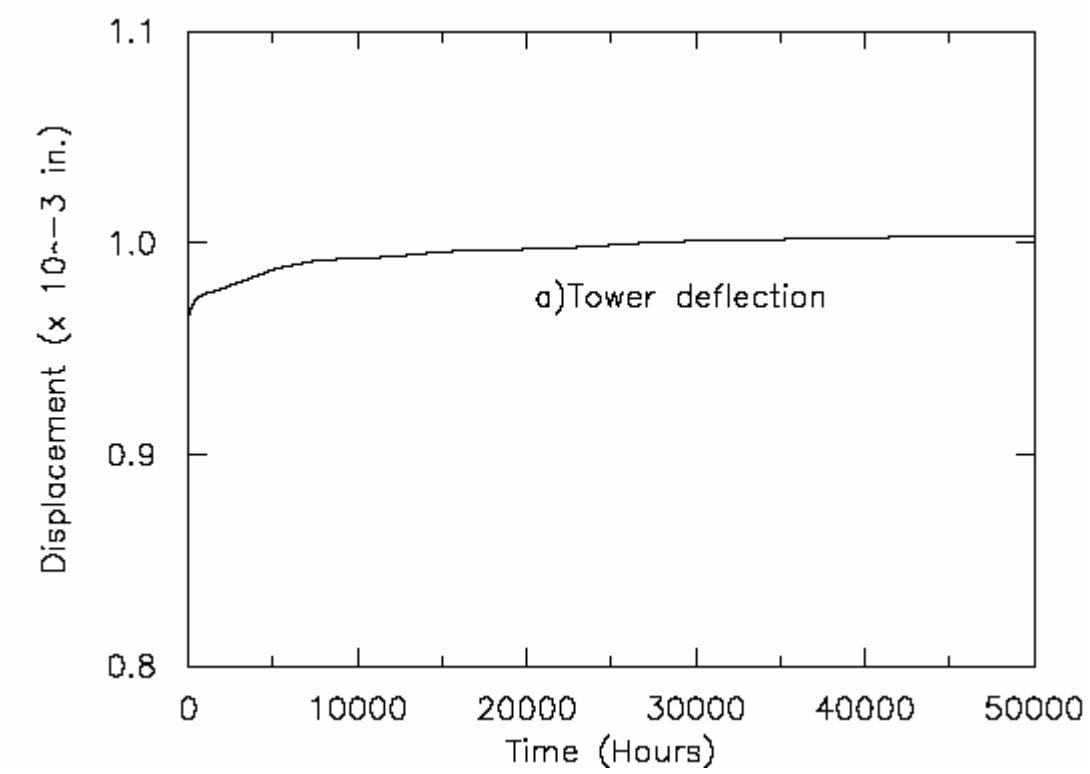


**Figure 4.20 deformation of the transmission tower under lateral load equal to the maximum wind load at the Eiffel tower.**

It should be noted that power transmission towers are not subjected to a constant wind load over long periods of time. The wind speed and hence the wind pressure on the tower varies from season to season. It should also be noted however that the loading pattern analyzed does not reflect the actual condition in any tower. Moreover the analysis performed with high wind velocity does not guarantee the wind pressure on any particular location for the tower. These factors, mentioned above, should be taken into consideration for calculating wind loads or combination of loads for a better prediction of the deformation in transmission towers.

# CHAPTER V
# CONCLUSIONS AND FURTHER RESEARCH

## 5.1 CONCLUSIONS

This study introduces characterization of thermo-mechanical and long-term behaviors of multi-layered composite systems that follow thermo-rheologically complex materials (TCM). The Schapery single integral model is modified for the nonlinear time-dependent behaviors of the TCM. It is shown that the stress and temperature effects on the overall nonlinear multi-axial responses can be coupled in product forms, provided that the materials still retain their elastic behaviors. The time, temperature and stress dependent material parameters in the nonlinear time integral model are calibrated from short-term creep-recovery tests on off-axis specimens performed under several stresses and isothermal temperatures. Good predictions are shown for the overall time-stress-temperature responses of the off-axis coupons that were not used in the calibration process.

It is seen that the nonlinear time-dependent behaviors are more pronounced on off-axis specimens. High temperatures and stresses accelerate the nonlinear deformations. It is also shown that tensile loads intensify microstructural deformations and lead to early failure time in the multi-layered composites due to void opening. It is established that the same specimen can be used for repeated creep tests at higher stresses and temperatures without developing damages provided that sufficient recovery time is given prior to each consecutive test. Finally the Poisson's effect on the thermo-mechanical viscoelasic behaviors are investigated from the off-axis creep strains obtained from the short-term creep tests. The results justify the time-independence of Poisson's ratio characterized from creep tests (constant load), as mentioned by Yi and Hilton (1990).

Several accelerated characterization methods, which are the time-temperature shifting, time-stress shifting and the combined time-temperature-stress shifting

techniques are examined to create long-term behaviors from the available short-term creep tests. In this study, both vertical and horizontal shifting is used to create master curves for predicting long-term material responses. The linear extrapolation is proposed to extend the long-term predictions. The long-term creep strain responses from all the three shifting procedure are comparable. It is seen that the maximum difference between the three shifting procedures is only 0.1% over a period of 25,000 hours. Limited experimental data available in this study may lead to error in material characterization and long-term predictions. Thus, sensitivity analyses have also been performed to examine the impact of slight error in material parameter characterization to the overall time-dependent material behaviors. It is shown that long-term responses are most sensitive to error in the time-dependent parameters and less sensitive to error in the stress and temperature dependent parameters.

Finally, an integrated material-structural modeling approach for analyzing long-term behaviors of E-glass/vinylester and E-glass/polyester multi-layered composite structures is also presented. Previously developed viscoelastic micromodels of multi-layered composites (Haj-Ali and Muliana, 2003, 2004) are used to generate the effective nonlinear viscoelastic responses of the studied composite systems. These micromodels are calibrated for long-term material responses. Analysis of time-dependent buckling in I-shaped composite slender columns and composite flat panels; long-term responses an assembled composite beam under three point bending, and a transmission tower under lateral loads are performed. The long-term behavior from the integrated micromechanical-FE analysis for the assembled composite beam is verified with the long-term experimental data available in the literature. The advantages of using an integrated micromechanical modeling approaches are:

1. It reduces the number of material parameters needed for calibration,
2. It allows for performing multi-axial nonlinear structural responses,
3. It is easy to incorporate different material parameters.

## 5.2 FURTHER RESEARCH

The current study for thermo-mechanical and the long-term behavior of the multi-layered composite systems are limited to conditions without damage and failure. The time-shifting methods are applicable only within limited times at which tertiary creep and/or micro-structural changes have not yet occurred. In order to better understand complete long-term responses, failure criterion should also be included to study the effect of micro-structural changes or damage accumulation in the composites.

The Schapery single integral equation has been modified to include the stress and temperature dependence of the material with time. However, other environmental factors such as moisture can significantly affect the creep deformation of the material. Moisture dependence on the deformation with time should also be studied. The integrated micromechanical-finite element (FE) model used for predicting the long-term behaviors of composite structures can be modified to include viscoplastic behavior in the matrix and include moisture dependent parameters.

# REFERENCES

[1] Schapery, R. A., Stress Analysis of Viscoelastic Composite Materials, J. Composite Materials, 1967;1(3), 228.

[2] Tuttle, M. E., Pasricha, A., and Emery, A. F., The Nonlinear Viscoelastic-Viscoplastic Behavior of IM7/5260 Composites Subjected to Cyclic Loading, Journal of Composite Materials, 1995; 29(15), 2025.

[3] Pasricha, A., Tuttle, M. E., and Emery, A. F., Time-Dependent Response of IM7/5260 Composites Subjected to Cyclic Thermo-Mechanical Loading, Composite Science and Technology,1995; 55, 49.

[4] Taouti, D. and Cederbaum G., Post Buckling of Non-linear Viscoelastic Imperfect Laminated Composite Plates Part-1: Material Considerations, Composite Structures, 1998; 42, 33.

[5] Yi, S., Hilton, H. H, and Ahmad, M. F., Nonlinear Thermo-Viscoelastic Analysis of Interlaminar Stresses in Laminated Composites, J. Applied Mechanics, 1996; 63, 218.

[6] Yi, S., Finite Element Analysis of Free Edge Stresses in Nonlinear Viscoelastic Composites Under Uniaxial Extension, Bending, and Twisting Loadings, International J. for Numerical Methods in Engineering, 1997; 40, 4225.

[7]. Yi, S., Ahmad, M. F., and Hilton, H. H., Nonlinear Viscoelastic Stress Singularities near Free Edges of Unsymmetrically Laminated Composites, International J. Solids Structures, 1998; 35(24), 3221.

[8] Mohan, M. and Adams, D. F., Nonlinear Creep-Recovery Response of Polymer Matrix and its Composites, Experimental Mechanics, 1985; 25, 262.

[9] Sternstein, S. S., Srinivasan, K, Liu, S. H., and Yurgartis, S., Viscoelastic Characterization of Neat Resins and Composites, Polymer Preprints, 1984; 25(2), 201.

[10] Greenwood, J.H, Creep and Fracture of CFRP at 180-200°C, Composites, 1975; 6(5), 203.

[11] Howard and Holloway, Characterization of Nonlinear Viscoelastic Properties of Randomly Oriented Fiber/Matrix Composite, Composite, 1987; 18(4), 317.

[12] Katouzian, M., Bruller, O. S., and Horoschenkoff, A., On the Effect of Temperature on the Creep Behavior of Neat and Carbon Fiber Reinforced PEEK and Epoxy Resin, Journal of Composite Materials, 1995; 29(3), 372.

[13] Violette, M. G. and Schapery, R. A., Time-dependent Compressive Strength of Unidirectional Viscoelastic Composite Materials, Mechanics of Time-dependent Materials, 2002; 6(2), 133.

[14] Jain, R. K., Goswamy, S. K., and Asthana, K. K., A Study of the Effect of Natural Weathering on the Creep Behavior of Glass Fiber Reinforced Polyester Laminates, Composites, 1979; 1, 39.

[15] Griffith, W. I., Morris, D. H., and Brinson, H. F., The Accelerated Characterization of Viscoelastic Composite Materials, Virginia Polytechnic Institute and Virginia State University (VPI& VSU) Report, VPI-E-80-5, 1980.

[16] Tuttle, M. E., Accelerated Viscoelastic Characterization of T300/5208 Graphite-Epoxy Laminates, PhD Dissertation, Blackburg, VA: Virginia Polytechnic Institute and State University, 1984.

[17] Yen, S. C., and Williamson, F. L, Accelerated Characterization of Creep Response of an Off Axis Composite Material, Composite Science and Technology, 1990; 38,103.

[18] Schwarzl and Staverman, Time-temperature Dependence of Linear Viscoelastic Behavior, Journal of Applied Physics, 1952; 23(8), 838.

[19] Brinson, H.F, Morris, D.H., and Yeow, Y.T., A New Experimental Method for the Accelerated Characterization of Composite Materials, Sixth International Conference on Experimental Stress Analysis, Munich, 1978.

[20] Yeow, Y.T., Morris, D. H., and Brinson, H. F., Time-Temperature Behavior of a Unidirectional Graphite/Epoxy Composite, Composite Material: Testing and Design (Fifth Conference), 1979; ASTM STP 674. Tsai Ed., ASTM, 263.

[21] Hiel, C.C., Brinson, H. F., and Cardon A. H., The Nonlinear Viscoelastic Response of Resin Matrix Composites, In: Composite Structures, Marshall. I. H, Editor, Essex, England: App. Science Publishers, 2, 271, 1983.

[22] Schapery, R. A., On the Characterization of Nonlinear Viscoelastic Materials, Polymer Engineering and Science, 1969; 9(4), 295.

[23] Tuttle, M. E. and Brinson, H. F., Prediction of the Long-Term Creep Compliance of General Composite Laminates, Experimental Mechanics, 1986; 26, 89.

[24] Brinson, H. F. and Dillard, D.A., The Prediction of Long Term Viscoelastic Properties of Fiber Reinforced Plastics, in Proc. Fourth International Conference on Composite Materials, T. Hayashi, K. Kawata, and S. Umekawa, Editors, Progress in Science and Engineering of Composites, 1982; 1, 795.

[25] Brinson, H. F., Viscoelastic Behavior and Life Time (Durability) Predictions, in Proc. European Mechanics Colloquium, 1985; 182, 3.

[26] Findley, W. N., Lai, J.S., and Onaran, K, Creep and Relaxation of Nonlinear Viscoelastic Materials, New York: Dover Publication, 1976.

[27] Brinson, H. F., Matrix Dominated Time Dependent Failure Predictions in Polymer Matrix Composites, Composite Structures, 1999; 47, 445.

[28] Spence, B. R., Compressive Viscoelastic Effects (Creep) of A Unidirectional Glass/Epoxy Composite Material, 35$^{th}$ International SAMPE Symposium, Anaheim, California, 1990; 1490.

[29] Bank, L. C. and Mosallam, A. S., Creep and Failure of A Full-Size Fiber Reinforced Plastic Pultruded Frame, Composite Material Technology, 1990; 1, 49.

[30] Mottram, J. T., Short and Long-term Structural Properties of Pultruded Beam Assemblies Fabricated using Adhesive Bonding, Composite Structures, 1993; 25: 387.

[31] McClure, G. and Mohammadi, Y., Compression Creep of Pultruded E-glass Reinforced Plastic Angles, Journal of Materials in Civil Engineering, 1995; 7(4), 269.

[32] Scott, D. W. and Zureick, A. H., Compression Creep of a Pultruded E-glass/Vinylester Composite, Composites Science and Technology, 1998; 58, 1361.

[33] Choi, Y and Yuan, R.L, Time-dependent Deformation of Pultruded Fiber Reinforced Polymer Composite Columns, Journal of Composites for Construction, 2003; 7(4), 356.

[34] Shao, Y and Shanmugam, J, Deflection Creep of Pultruded Composite Sheet Piling, Journal of Composites for Construction, 2004; 8(5), 471.

[35] Haj-Ali, R. and Muliana, A. H., Micromechanical Models for the Nonlinear Viscoelastic Behavior of Pultruded Composite Materials, Int. J. Solids and Structures, 2003; 40, 1037.

[36] Muliana, A. H. and Haj-Ali, R. M., Nested Nonlinear Viscoelastic and Micromechanical Models for the Analysis of Pultruded Composite Structures, Mechanics of Material (MOM) Journal, 2004; 36, 1087.

[37] Hashin, Z., Humphreys, E.A, and Goering, J, Analysis of Thermoviscoelastic Behavior of Unidirectional Fiber Composites, Composites Science and Technology, 1987; 29(2), 103.

[38] Sadkin, Y. and Aboudi, J., Viscoelastic Behavior of Thermo-rheologically Complex Resin Matrix Composites, Composites Science and Technology, 1989; 36, 351.

[39] Yancey, R.N and Pindera, M.J, Micromechanical Analysis of the Creep Response of Unidirectional Composites, Journal of Engineering Materials and Technology, Transactions of the ASME, 1990; 112(2), 157.

[40] Aboudi, J, A Continuum Theory for Fiber-reinforced Elastic-viscoplastic Composites, International Journal of Engineering Science, 1982; 20(5), 605.

[41] Haddad, Y.M and Tanari, S, On the Micromechanical Characterization of the Creep Response of a Class of Composite Systems, Jounal of Pressure Vessel Technology, Transactions of the ASME, 1989; 111(2), 177.

[42] Brinson, L.C and Knauss, W.G, Thermorheologically Complex Behavior of Multiphase Viscoelastic Materials, Journal of the Mechanics and Physics of Solids, 1991; 39(7), 859.

[43] Muliana, A. H. and Haj-Ali, R. M., Multi-scale Modeling for the Long-term Behaviors of Composite Structures, AIAA Journal, 2005; 43(8), 1815.

[44] Harper, B. D. and Weitsman, Y., Characterization Method for a Class of Thermorheologically Complex Materials, Journal of Rheology, 1985; 29, 49.

[45] Haj-Ali, R. M. and Kilic, H., Nonlinear Behavior of Pultruded FRP Composites, Composite Part B, 2002; 33, 173.

[46] ASTM D3410/D3410M-03, Standard Test Method for Compressive Properties of Polymer Matrix Composite Materials with Unsupported Gauge Section by Shear Loading, Philadelphia: American Society of Testing Materials, 2003.

[47] ASTM D3039/D3039M-00, Standard Test Method for Tensile Properties of Polymer Matrix Composite Materials, Philadelphia, American Society of Testing Materials, 2000.

[48] Lou, Y. C., Schapery, R. A., Viscoelastic Characterization of a Nonlinear Fiber-Reinforced Plastic, Journal of Composite Materials, 1971; 5, 208.

[49] Dillard, D. A., Morris, D. H., and Brinson, H. F., Creep and Creep Rupture of Laminated Graphite-Epoxy Composites, Virginia Polytechnic Institute and Virginia State University (VPI& VSU) Report, VPI-E-81-3, 1981.

[50] Leaderman, H., Elastic and Creep Properties of Filamenteous Materials and Other High Polymers, The Textile Foundation, Washington, D.C, 1943.

[51] ABAQUS Version 6.4 Documentation; Providence, RI: ABAQUS, 2003.

[52] Structural Design of Steel Latticed Towers, ABB Mexico. Available at www.abb.com.mx, Accessed: March, 2006.

[53] Watson, George T., Efficient Transmission Tower Modeling, Centre Point Energy, Houston, available at www.powline.com, Accessed: May, 2006.

[54] Rao, Prasada N., Mohan, S.J and Lakshmanan, N, Lessons from Premature Failure of Cross Arms in Transmission Towers During Prototype Testing, Structural Research Centre, CSIR Campus, TTTI, India, available at www.nenastran.com, Accessed: May, 2006.

# APPENDIX A

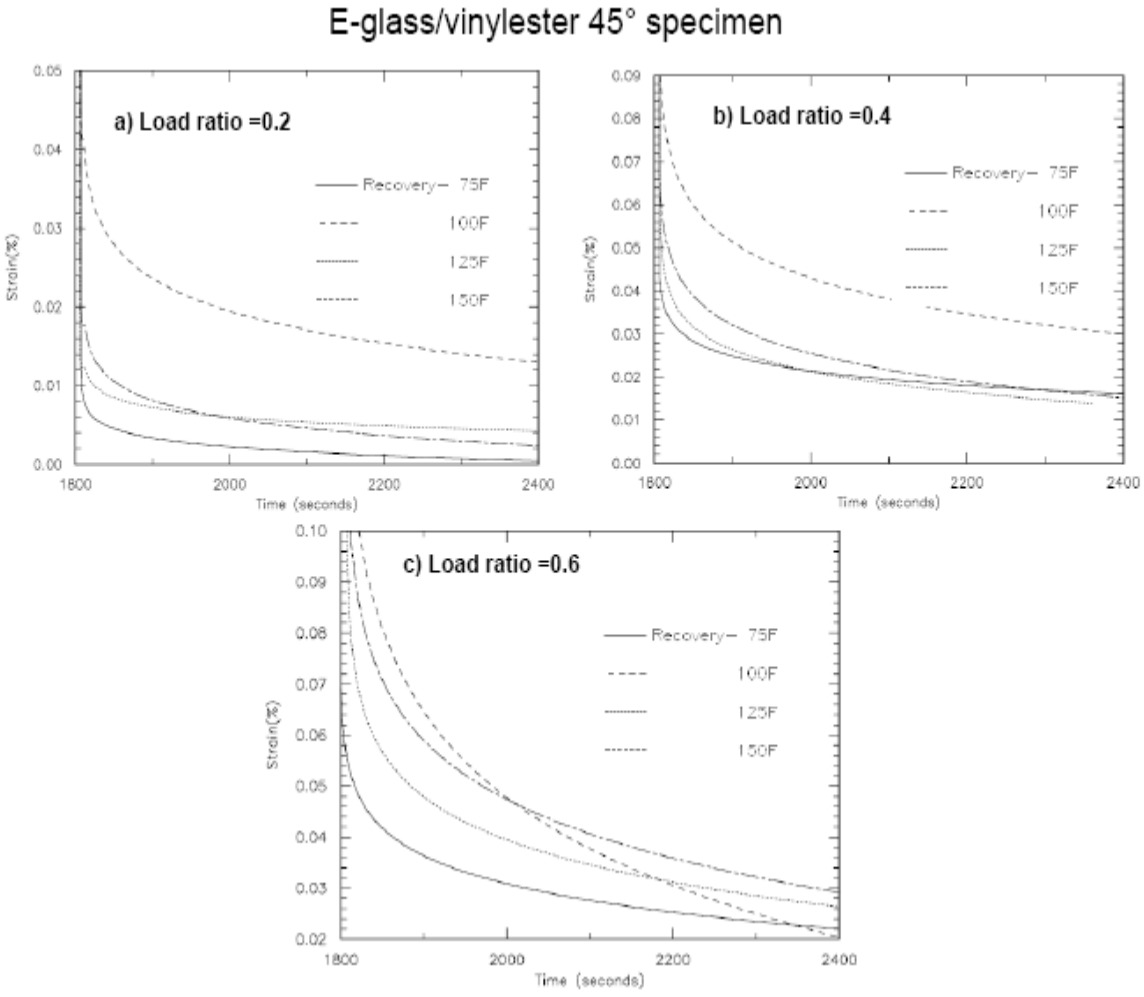


**Figure A-1 Recovery curves for 45° off-axis E-glass/vinylester specimens under load various ratios.**

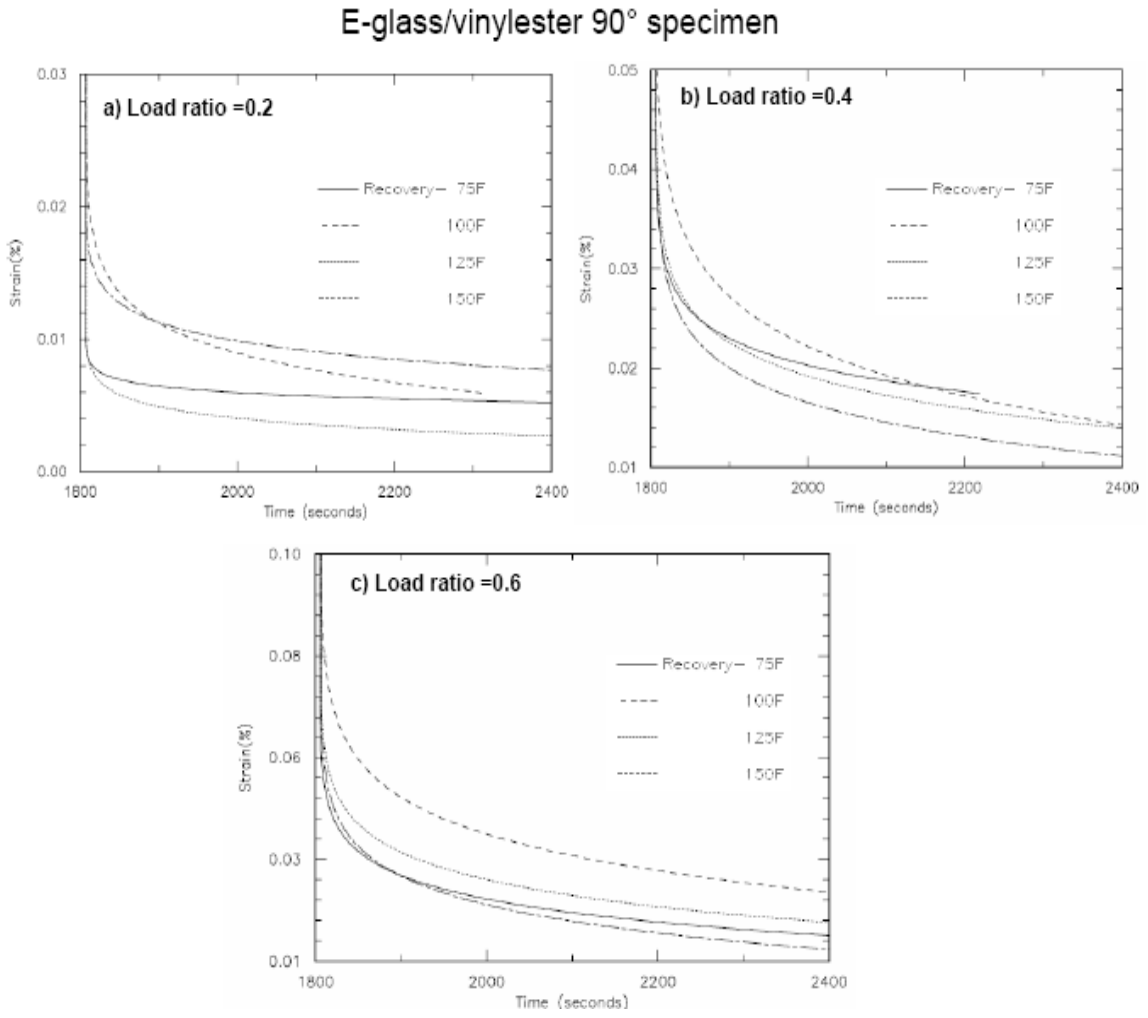


**Figure A-2 Recovery curves for transverse E-glass/vinylester specimens under various load ratios and temperatures.**

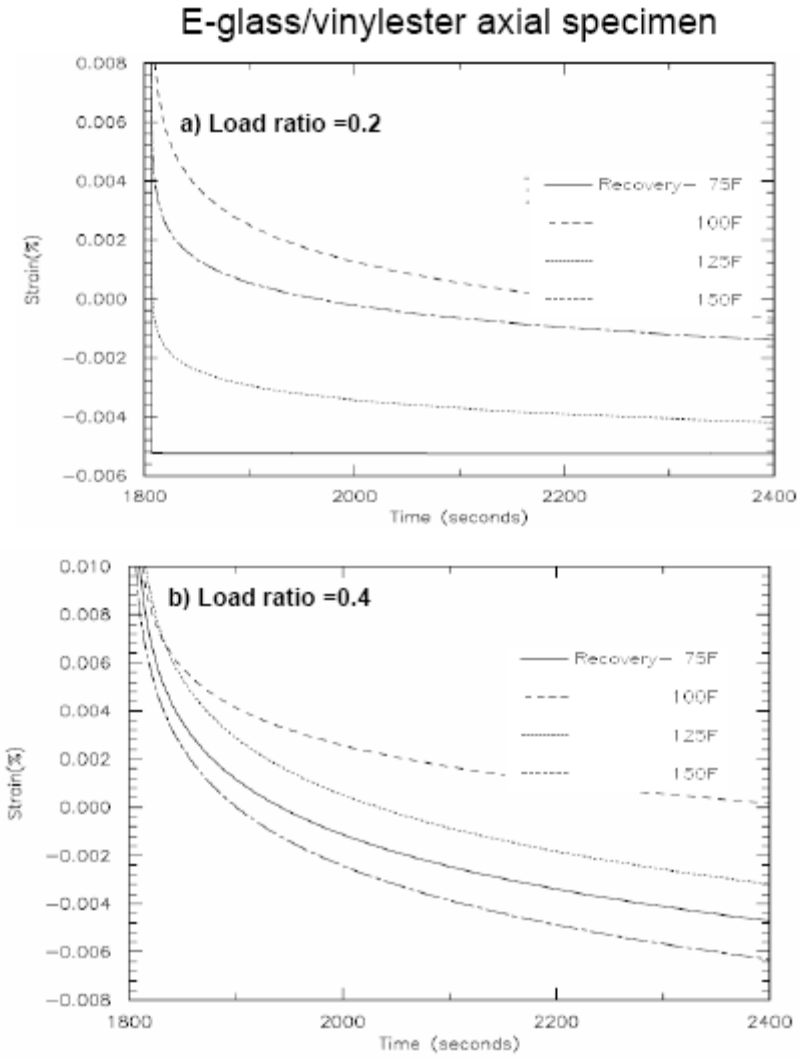


**Figure A-3 Recovery curve for E-glass/vinylester axial specimens under load ratio a) 0.2 and b) 0.4 and temperatures 75°F- 100°F.**

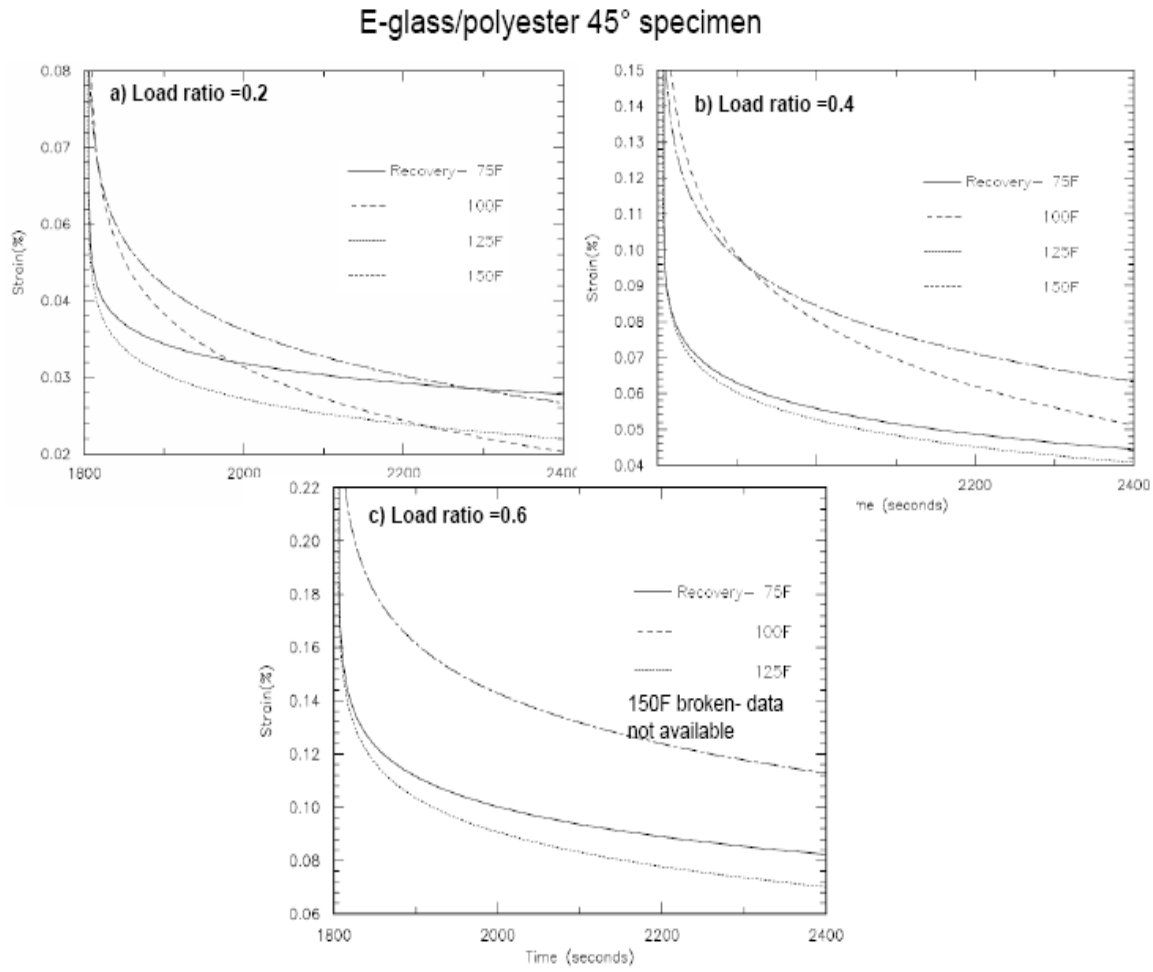


**Figure A-4 Recovery curves for 45° off-axis E-glass/polyester specimens under various load ratios and temperatures.**

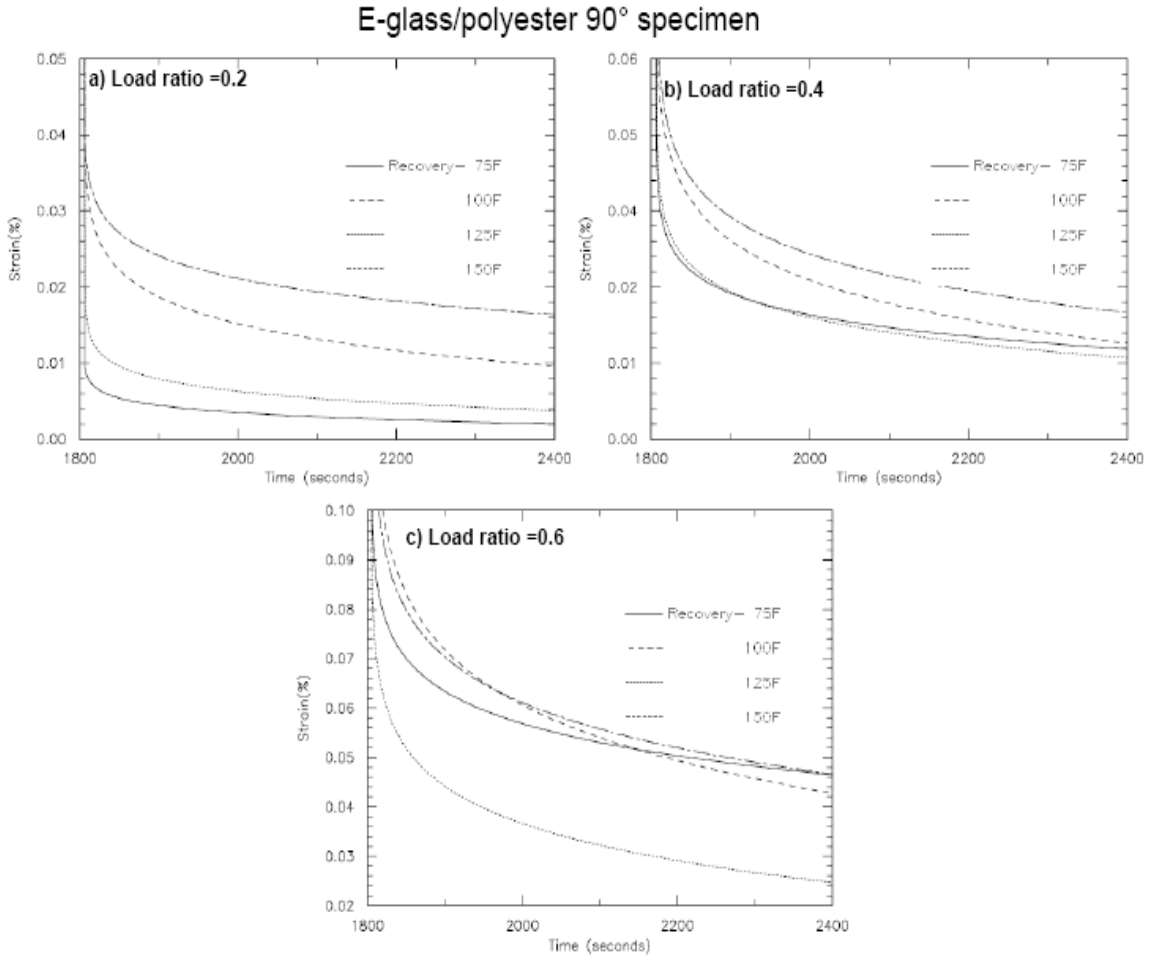


**Figure A-5 Recovery curves for transverse E-glass/vinylester specimens under various load ratios and temperatures.**

# APPENDIX B

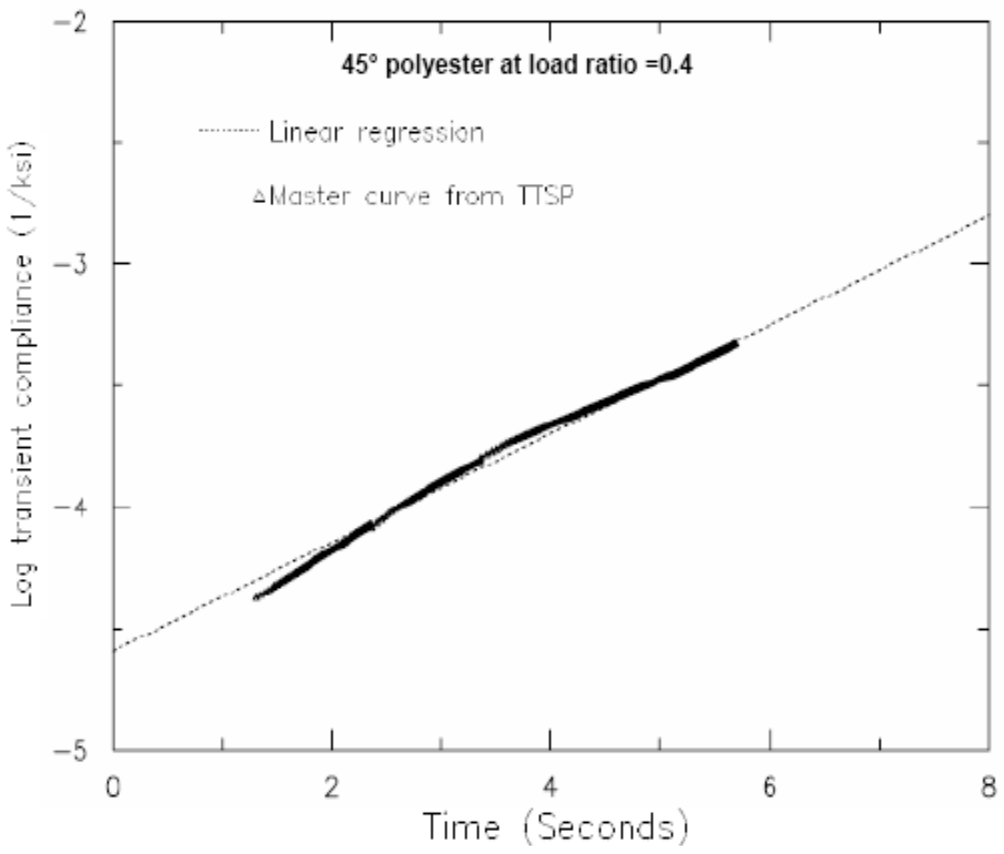


**Figure B-1 Master curve by time-temperature shifting for 45° off-axis E glass/polyester specimen under load ratio 0.4**

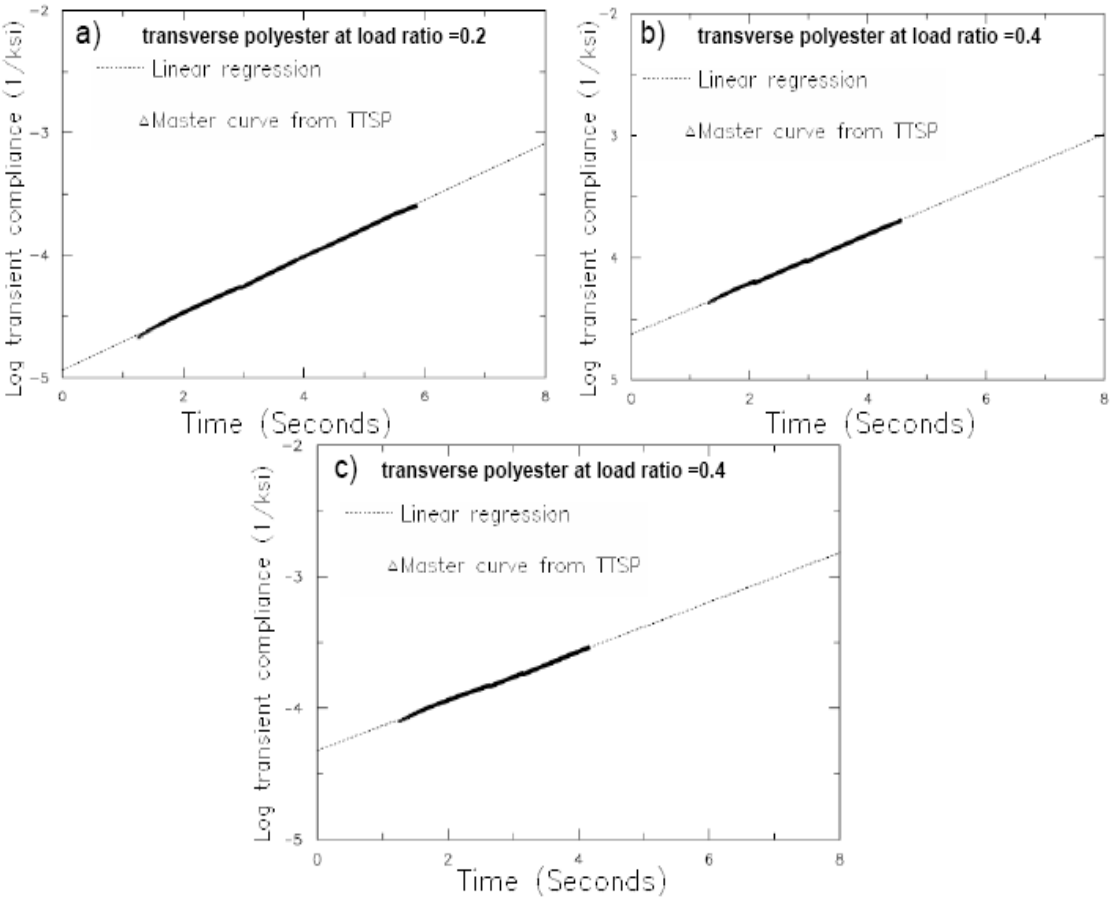


**Figure B-2 Master curve by time-temperature shifting for transverse polyester specimens under load ratio 0.2-0.6**

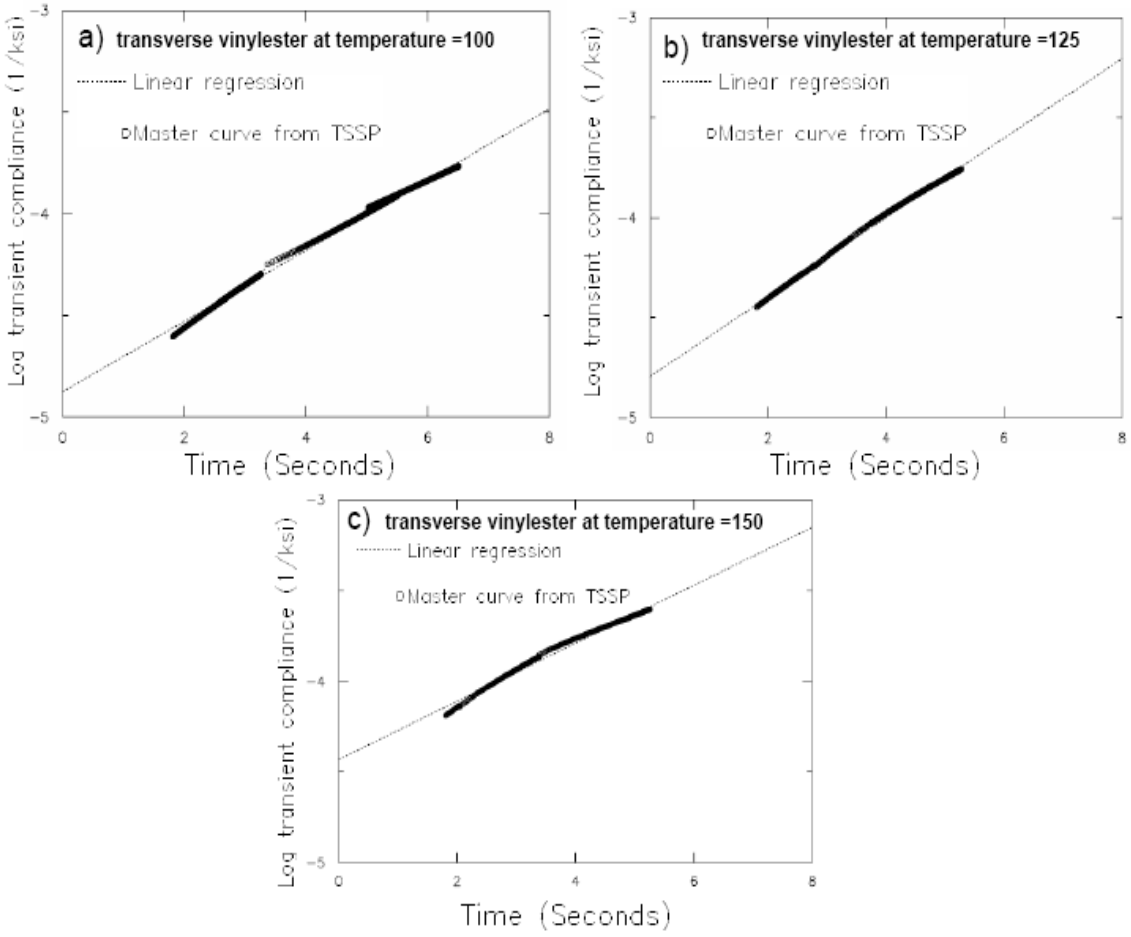


**Figure B-3 Master curve by time-stress shifting for E-glass/ vinylester specimens under various temperatures (100-150°F).**

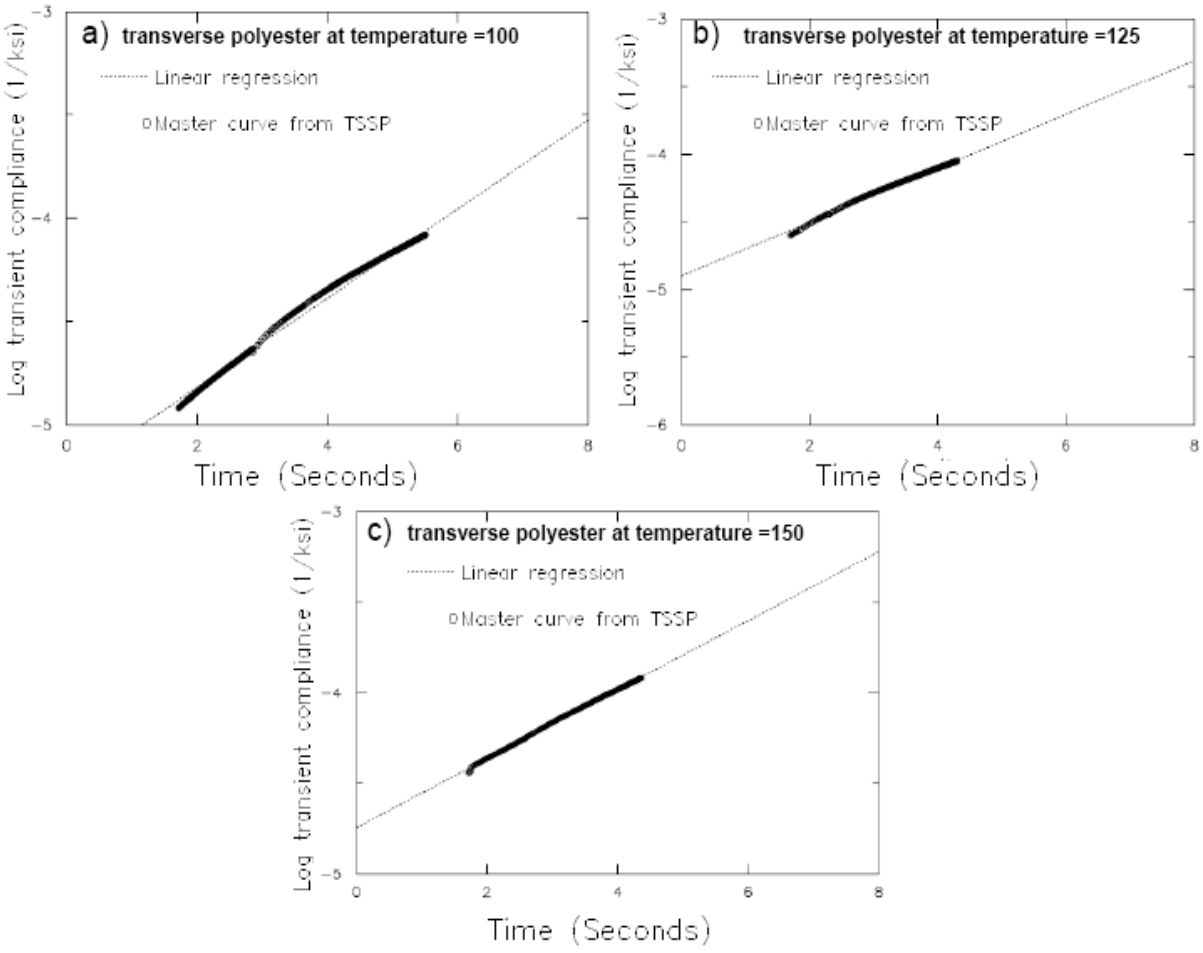


**Figure B-4 Master curve by time-stress shifting for E-glass/polyester specimens under various temperatures (100-150°F).**

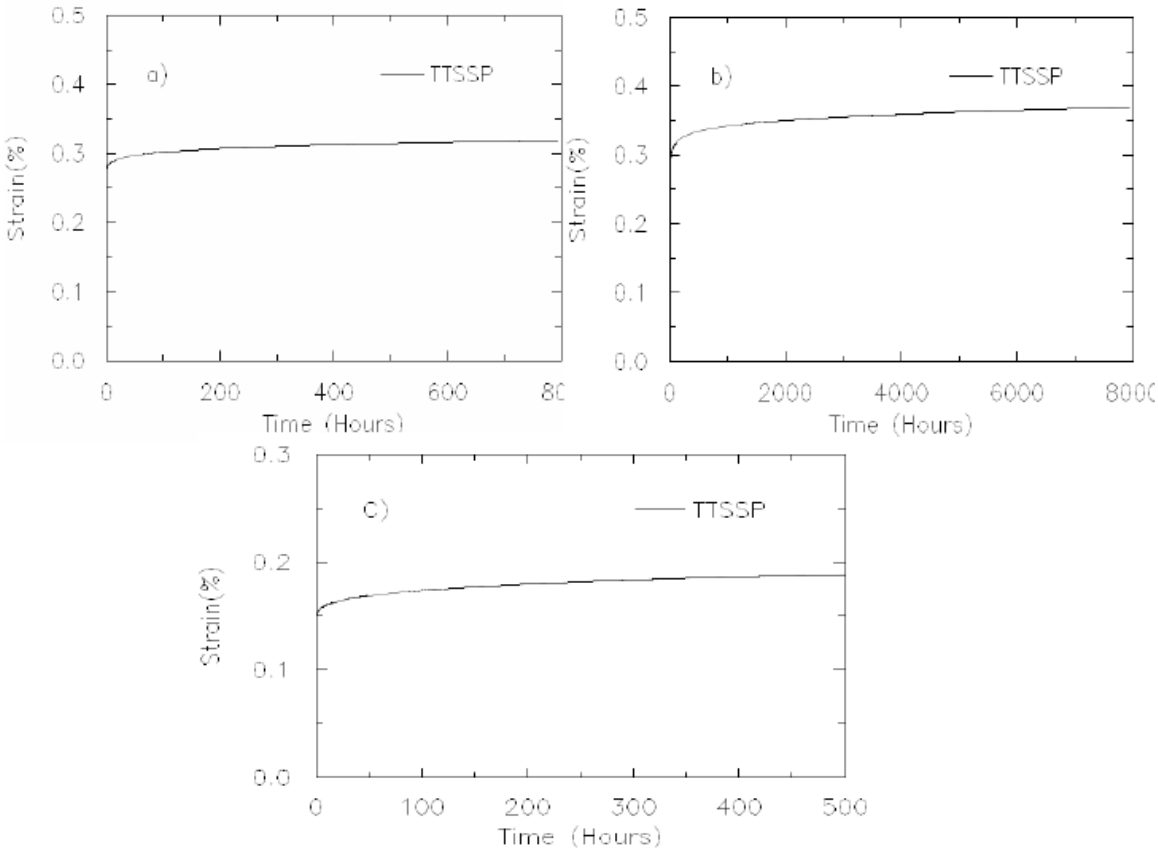


**Figure B-5 Creep strain response through time-temperature and stress shifting for the a) transverse b) 45° off-axis E-glass/vinylester specimens and c) the transverse E-glass/polyester specimen under reference temperature (75°F) and stress level 0.2.**

# VITA

Name: Aravind R. Nair

Address: KGWS-57, Vivekananda Nagar, Golf Links Road, Kowdiar
Trivandrum, Kerala, India, 695041

Email Address: arnair@neo.tamu.edu

Education: B.E, Hindustan College of Engineering, University of Madras, India, 2004
M.S, Dept. of Mechanical Engineering, Texas A&M University, College Station, Texas, 2006